UNIVERSITA' DEGLI STUDI DI PADOVA

DIPARTIMENTO DI ASTRONOMIA

Dottorato di Ricerca in Astronomia
Ciclo XIX

Investigating the Nature of Ultraluminous X-ray Sources through X-ray and Optical data

Coordinatore: Prof. Giampaolo Piotto
Supervisori: Ch.mo Prof. Alberto Franceschini
              Dott. Luca Zampieri
              Prof. Roberto Turolla

Dottorando: PAOLA MUCCIARELLI

31 Luglio 2008

UNIVERSITY OF PADOVA
ASTRONOMY DEPARTMENT

PhD in Astronomy
Cycle XIX

Investigating the Nature of Ultraluminous X-ray Sources through X-ray and Optical data

PhD Coordinator: Prof. Giampaolo Piotto
Supervisors: Prof. Alberto Franceschini
Dott. Luca Zampieri
Prof. Roberto Turolla

Candidate: PAOLA MUCCIARELLI

July 31st, 2008

A Morgan, la mia piccola candela standard,
che ha dato la giusta misura al mio universo.

RIASSUNTO (ITALIAN ABSTRACT)

Fin nelle sue prime fasi, l'osservazione dell'Universo nei raggi X ci ha riservato numerose sorprese e risultati inaspettati. Una delle scoperte più avvincenti è stata l'esistenza di sorgenti puntiformi che emettono luminosità comprese tra quella di buchi neri di massa stellare in accrescimento (fino a $\sim 10^{38}$ erg s^{-1}) e quella di buchi neri super-massivi ($\gtrsim 10^{42}$ erg s^{-1}). Un certo numero di sorgenti con luminosità maggiori di 10^{39} erg s^{-1} sono state rivelate dal satellite *Einstein* (Clark et al., 1978; Long & van Speybroeck, 1983; Fabbiano, 1989). A queste sorgenti ci si riferisce oggi come a "sorgenti X ultraluminose" (*Ultraluminous X-ray sources*, ULXs). Assumendo che l'emissione X abbia origine da accrescimento su un oggetto compatto e che tali sorgenti emettano isotropicamente al loro limite di Eddington, i valori della massa del buco nero (*black hole*, BH) centrale, ottenuti dal flusso osservato, cadono nell'intervallo 100-1000 $M_\odot$ (Fabbiano & Trinchieri, 1987). In questo caso l'oggetto compatto in questi sistemi sarebbe un buco nero di massa intermedia (*Intermediate Mass Black Holes*, IMBHs, Colbert & Mushotzky 1999). Ovviamente non c'è *a priori* nessun motivo per cui queste sorgenti debbano emettere isotropicamente. Per questo motivo in letteratura sono stati proposti modelli alternativi all'esistenza di IMBHs. Le proprietà di molte ULXs possono essere spiegate assumendo che la loro emissione sia collimata oppure dominata dalla presenza di getti relativistici. In questo caso, le ULXs ospiterebbero un BH di massa stellare e sarebbero quindi simili ai microquasar Galattici.

Una prima definizione di ULX può essere la seguente: le ULXs sono sorgenti puntiformi in galassie vicine, non coincidenti con il centro della galassia ospite, con una lumnosità in banda X che eccede la luminosità di Eddington per un BH di 10 $M_\odot$. Cataloghi di ULXs selezionate seguendo questa definizione osservativa hanno il problema di contaminazione dovuta ad identificazioni spurie (e.g. resti di supernova, ammassi globulari e nuclei galattici attivi). Questo problema può essere risolto attraverso l'analisi dello spettro X e della variabilità, ma soprattutto dall'identificazione della controparte ottica.

L'insieme delle proprietà delle ULXs suggerisce chiaramente che si tratta di sistemi binari in accrescimento, che imitano il comportamento di binarie X Galattiche

(*Galactic X-ray binaries, XRBs*).

Recenti osservazioni ottenute con i satelliti *Chandra* ed *XMM-Newton* mostrano che lo spettro delle ULXs ha una struttura complessa. Numerose ULXs, con una buona statistica di conteggi, mostrano uno spettro a due componenti, simile a quello osservato nelle XRBs Galattiche (componente termica di bassa energia + coda ad alta energia). La bassa temperatura (0.1-0.3 keV) delle componete termica osservata in varie sorgenti è stata interpretata come ulteriore indicazione della presenza di un IMBH. Tuttavia, anche particolari parametrizzazioni di modelli di emissione Comptonizzata sembrano in grado di descrivere l'intero spettro delle ULXs. In varie ULXs è stata inoltre osservata curvatura nello spettro ad alte energie, sopra i 2 keV, associata alla presenza di una corona di materiale otticamente spesso. L'osservazione di variabilità spettrale insieme alle variazioni del flusso in banda X ricorda, con qualche differenza, le transizioni di stato osservate nelle XRBs Galattiche.

Numerose ULXs mostrano variabilità su diversi tempi scala. In parecchie ULXs con osservazioni in banda X multiple è stata osservata variabilità irregolare su tempi scala di mesi, mentre non è raro che il flusso vari anche durante una stessa osservazione. Inoltre, alcune ULXs sono transienti. Recentemente è stata osservata una modulazione di 62 giorni nella curva di luce della ULX M82 X-1. Questa modulazione è stata interpretata come periodo orbitale del sistema binario, confermando in modo diretto la binarietà di almeno alcune ULXs.

Le proprietà temporali in banda X possono essere usate per arricchire la nostra conoscenza delle ULXs. Le strutture più evidenti presenti nello spettro di potenza di sistemi in accrescimento sono le oscillazioni quasi periodiche (QPO). L'identificazione del tipo di QPO osservato può avvenire tramite il confronto con le proprietà dei QPOs nelle XRBs. La massa del BH può quindi essere stimata scalando i valori di riferimento delle XRBs. Fino ad oggi soltanto in due ULXs, M82 X-1 e NGC 5408 X-1, sono stati osservati tali QPOs. In entrambi i casi la massa stimata del BH eccede alcune decine di masse solari.

La scoperta di controparti ottiche stellari conferma ulteriormente la binarietà delle ULXs. Osservazioni X/ottiche ottenute con i satelliti *Chandra* ed *HST* hanno consentito un notevole balzo in avanti nell'identificazione delle controparti ottiche, grazie alla loro ottima risoluzione spaziale. La maggior parte delle ULXs si trova in galassie con attiva formazione stellare. Attualmente solo 4 delle controparti ottiche identificate sono stelle singole. Queste controparti ottiche hanno proprietà consistenti con quelle di stelle giovani e massicce, in particolare di tipo spettrale O e B. La presenza di ULXs in galassie ellittiche è ancora materia di discussione. Tuttavia due ULXs sono state associate con ammassi globulari in ellittiche e recentemente è stata identificata una ULX nella galassia ellittica NGC 3379.

Alcune ULXs sono inoltre coincidenti con nebulose ottiche in emissione giovani e molto estese. Alcune ULXs sono associate con controparti radio estese.

Anche se la maggior parte delle ULXs potrebbe essere la coda di grande massa ed alta luminosità delle XRBs (con BHs di massa fino ad alcune decine di masse solari, Gilfanov et al., 2004), almeno le sorgenti più luminose potrebbero invece rappresentare sistemi atipici che ospitano BH di massa dell'ordine di 100 $M_{\odot}$. Nonostante le ULXs siano state studiate approfonditamente negli ultimi anni, la comprensione di queste

sorgenti è tutt'altro che soddisfacente. È ancora di fondamentale importanza studiare a fondo le singole sorgenti per fare luce sulla natura dell'intera classe di oggetti.

Al momento attuale NGC 1313 X-2 è una delle ULXs meglio studiate. Nella mia Tesi ho analizzato in dettaglio la più lunga osservazione ottenuta con il satellite *XMM-Newton* (quindi con un alto numero di conteggi), utilizzando diversi modelli spettrali. Una buona rappresentazione dello spettro è stata ottenuta con modelli del tipo "componente termica di bassa energia + coda ad alta energia". La temperatura della componente soffice, se interpretata come emissione da un disco in accrescimento, indica una massa del BH di $\approx 60 f^4 M_\odot$ (assumendo accrescimento al limite d Eddington), paragonabile al valore della massa ottenuto dal flusso.

Osservazioni ottiche del campo di NGC 1313 X-2 ci hanno fornito informazioni fondamentali. Abbiamo prima identificato la controparte ottica di NGC 1313 X-2 su un'immagine presa con il telescopio ESO 3.6m. Successivamente, immagini dei telescopi VLT e *HST* ci hanno permesso di risolvere la controparte in due distinti oggetti, C1 e C2, dentro il cerchio di errore di *Chandra* (Zampieri et al., 2004; Mucciarelli et al., 2005). I colori e le magnitudini osservati sono consistenti per C1 con una stella O9-B0 di sequenza principale, mentre per C2 con una supergigante G4 di classe Ib. Le due possibili controparti hanno entrambe proprietà consistenti con stelle massicce ($\sim 10 - 20 M_\odot$) in NGC 1313. Indipendentemente dalla reale controparte della ULXs, NGC 1313 X-2 è un *high mass X-ray binary*, una XRB con compagna di grande massa.

Abbiamo inoltre utilizzato osservazioni quasi simultanee ottenute con i telescopi *XMM-Newton*, *HST* e VLT (Mucciarelli et al., 2007). Alla fine di Dicembre 2003 la sorgente ha sperimentato un breve ma intenso aumento di luminosità, raggiungendo il valore 10^{40} erg s^{-1}. Contemporaneamente il flusso ottico non ha mostrato variazioni pronunciate. Dall'analisi della curva di luce in banda X ed ottica, abbiamo trovato che i dati disponibili sono consistenti con i due seguenti scenari:

controparte C1 : L'oggetto C1 è la controparte più probabile. Il nostro modello indica che in questo caso NGC 1313 X-2 è una binaria X formata da un IMBH ed una stella massiccia di sequenza principale che riempie il suo lobo di Roche. Considerando un BH di $\sim 120 M_\odot$, come risulta in caso di emissione isotropa, la massa della compagna cade nell'intervallo $10 - 18 M_\odot$.

controparte C2 : In questo caso il sistema binario è formato da una stella massiccia supergigante e da un BH di massa stellare con emissione collimata.

M82 X-1 è una delle ULXs più luminose ed è la prima sorgente di questo tipo in cui è stato osservato un QPO. La nostra analisi di dati *XMM-Newton* e *RXTE* ci ha permesso di restringere l'intervallo di massa del BH presente in questa ULX (Mucciarelli et al., 2006).

Particolare attenzione è stata fatta nell'analizzare lo spettro *XMM-Newton* di M82 X-1, sottraendo la contaminazione dovuta al contributo della galassia ospite (ottenuto dall'analisi di dati *Chandra*) e mascherando alcune delle vicine sorgenti puntiformi. Abbiamo evidenziato che nello spettro *XMM-Newton* della ULX è presente

una componente termica di bassa temperatura. Assumendo che questa componente sia dovuta ad emissione da un disco di accrescimento standard, si ottiene un intervallo per la massa del BH di $M_{BH} \approx [200 - 2000] f^4 \, M_\odot$.

La massima luminosità raggiunta da M82 X-1 è $L \sim 2 \times 10^{41}$ erg s^{-1} (ad una distanza di 3.9 Mpc). Assumendo che al massimo la sorgente emetta al limite di Eddington, possiamo stimare una massa per il BH intorno al valore $M_{BH} \sim 1500 M_\odot$. È importante osservare che l'alta luminosità di questa sorgente è difficilmente spiegabile in termini di modelli alternativi che prevedano emissione non isotropa.

Lo spettro di potenza delle osservazioni *XMM-Newton* mostra un QPO variabile. QPOs sono stati rilevati anche in 7 osservazioni *RXTE*. Le proprietà del QPO (rms, variabilità e fattore di qualità) e del rumore nello spettro di potenza suggeriscono una associazione del QPO osservato in M82 X-1 con quelli di tipo C osservati nelle XRBs (Mucciarelli et al., 2006). Assumendo che la frequenza scali inversamente alla massa, le frequenze osservate (50-166 mHz) indicano un valore di M_{BH} nell'intervallo 10-1000 $M_\odot$.

Varie argomentazioni sono state proposte per ridurre l'incertezza sulla determinazione della massa dell'oggetto compatto in M82 X-1, in particolar modo la correlazione tra le proprietà spettrali e temporali osservate. La massa del BH in M82 X-1 potrebbe essere intorno alle centinaia di masse solari.

Osservazioni in varie bande suggeriscono che le ULXs non siano una popolazione uniforme di sorgenti. Una parte significativa mostra proprietà simili a quelle di binarie Galattiche in accrescimento. Riuscire a discriminare tra sistemi che ospitano un BH di massa stellare oppure un IMBH è una sfida avvincente, ma fino ad oggi sono state trovate solo evidenze marginali a supporto di entrambe le possibilità. Non vi è ancora una prova definitiva sull'esistenza degli IMBHs.

Il lavoro svolto per la mia Tesi ci ha permesso di mettere dei limiti significativi alla massa del BH in due ULXs ben studiate. Tuttavia sviluppi cruciali in questo campo possono venire solo da dettagliate osservazioni spettroscopiche della controparte ottica della ULX, come nel caso di NGC 1313 X-2. L'identificazione di righe in emissione ed/o in assorbimento negli spettri ottici di queste stelle potrebbero fornire la *misura dinamica della funzione di massa del sistema binario della ULX ed, eventualmente, la massa del BH*.

ABSTRACT

Since the early days of X-ray astronomy observations have brought us numerous surprises and unexpected results. One of the most challenging discoveries is the existence of point-like sources that emit at luminosities intermediate between those of accreting Stellar Mass Black Holes (up to $\sim 10^{38}$ erg s^{-1}) and Super Massive Black Holes ($\gtrsim 10^{42}$ erg s^{-1}). Several X-ray sources with luminosities in excess of 10^{39} erg s^{-1} were early revealed by *Einstein* (Clark et al., 1978; Long & van Speybroeck, 1983; Fabbiano, 1989), and they are now commonly referred as to Ultraluminous X-ray sources (ULXs). If we assume that the X-ray emission comes from accretion on to a compact object and that these sources emit isotropically at the Eddington limit, then masses in the range 100-1000 $M_\odot$ are inferred for the central Black Hole (BH) from the observed flux (Fabbiano & Trinchieri, 1987). In this case the remnants in these systems would be Intermediate Mass Black Holes (IMBHs, Colbert & Mushotzky 1999). Clearly, there are no *a priori* reasons for which these sources need to emit isotropically, so alternative explanations for them have been proposed in the literature. It has been proposed that many of the ULX properties can be explained assuming that they do not emit isotropically or are dominated by emission from a relativistic jet. In this case, they may harbor stellar mass BHs and may be similar to Galactic microquasars.

A definition at a glance of ULXs could be the following: *ULXs are off-nuclear, point-like sources in nearby galaxies with X-ray luminosity in excess of the Eddington luminosity for a 10 $M_\odot$ BH.* Catalogs of ULXs selected applying this "phenomenological" definition suffer the major problem of contamination from spurious identifications (e.g. supernova remnants, globular clusters, young stellar clusters and active galactic nuclei). Spectral and variability analyses or the identification of an optical counterpart may help to solve this problem.

The overall X-ray properties of ULXs strongly suggest that these sources are accreting binary systems, that echo the behavior of Galactic X-ray binaries (XRBs).

Recent observations performed with the *Chandra* and *XMM-Newton* satellites show a complex structure in the X-ray spectrum. A great number of ULXs, with sufficiently good statistics, show a two-component spectrum, similar to that observed in Galactic XRBs (soft thermal component + hard tail). The low temperature (0.1-0.3 keV)

of the soft component observed in several sources has been interpreted as evidence for the presence of a IMBH. However, also different parametric implementations of Comptonization models appear to be able to account for the whole X-ray spectrum of ULXs. Spectral curvature in the high energy part of the spectrum, above 2 keV, has been reported in a number of ULXs and correlated to the presence of an optically thick corona. The detection of spectral variability along with X-ray flux variations echoes, with some differences, the state transitions observed in Galactic BH candidates.

A number of ULXs seems to exhibit variability at different levels. Irregular variability in the X-ray flux on timescales of months is observed in several ULXs with multiple observations. It is not uncommon that ULXs show variability during a single observation. Transient behavior was also detected in some ULXs. The recent detection of a 62 days modulation in the light curve of the ULX M82 X-1, interpreted as the orbital period of the system, has provided direct confirmation of the binary nature of at least some ULXs.

Also the X-ray timing properties can be used to improve our understanding of ULXs. The most evident feature in the power density spectrum of accreting systems is the presence of QPOs, quasi-periodic variability in the X-ray flux. Comparing the properties of the QPOs detected in the power density spectrum of ULXs with that of the QPOs in Galactic XRBs can lead to the identification of the QPO type. Then scaling arguments can be used to estimate the BH mass. Up to now only two objects have been found to show features in their PDS (M82 X-1 and NGC 5408 X-1). Both indicate a BH mass in excess of few tens solar masses.

Also the detection of stellar counterparts in the optical supports the binarity of ULXs. A significant step forward in the identification of optical counterparts was performed through *Chandra*/*HST* observations because of their good spatial resolution. The great majority of ULXs are hosted preferentially in star-forming galaxies. Currently there are only 4 optical counterpart identified with single stars. These optical counterparts have properties consistent with those of early young, massive stars, in particular O or B stars. The presence of ULXs in early-type galaxies is still matter of debate. However two identifications of ULXs with globular clusters have been reported and a ULX in the elliptical NGC 3379 was recently identified.

Furthermore, several ULXs are coincident with young and very extended emission nebulae and a few of them also with extended radio counterparts.

The majority of ULXs may be the high mass, high luminosity tail of ordinary X-ray binary systems (with BH mass up to few tens of solar masses, Gilfanov et al., 2004), but at least the most luminous sources may well be unusual binaries with a BH mass of at least 100 $M_\odot$. Although ULXs were extensively studied in the past years, our understanding of these sources is far from being satisfactory. It is of fundamental importance to investigate in detail individual sources in order to shed light on the properties of the entire ULX class.

At present NGC 1313 X-2 is one of the best studied ULXs. In my Thesis I present a detailed analysis of the longest *XMM-Newton* observation with the best counting statistics, exploring a number of different spectral models. Good fits can be obtained with models of the type "soft thermal component + hard tail". The temperature of

the soft thermal component, if interpreted as emission from an accretion disk, implies $M_{BH} \approx 60 f^4 \, M_\odot$ for Eddington limited accretion (where f is the color correction factor), comparable to the mass estimated from the flux.

Crucial information have been obtained also from the analysis of optical observations. We first identified the optical counterpart of NGC 1313 X-2 on an ESO 3.6m image. VLT and *HST* images of the field of NGC 1313 X-2 allowed us to resolve the counterpart in two distinct objects, named C1 and C2, inside the *Chandra* error box (Zampieri et al., 2004; Mucciarelli et al., 2005). We found that both colors and magnitudes are consistent only with a O9-B0 main sequence star for C1, while for C2 they are consistent with a G4 supergiant of type Ib. The two candidate counterparts show properties consistent with massive stars ($\sim 10 - 20 M_\odot$) in NGC 1313. Irrespectively of which of the two objects the actual counterpart is, this implies that NGC 1313 X-2 is a high mass X-ray binary.

We also analyzed quasi-simultaneous observations of NGC 1313 X-2 obtained with *XMM-Newton*, *HST* and VLT (Mucciarelli et al., 2007). At the end of December 2003 the source experienced a short, but quite intense flare, reaching a maximum luminosity of 10^{40} erg s^{-1}. At the same time, the optical flux of both counterparts did not show pronounced variations. From an analysis of the X-ray and optical light curves we found that the available data are consistent with the following scenarios:

counterpart C1 : This object is the more likely counterpart. Our model indicates that in this case NGC 1313 X-2 is an IMBH X-ray binary with a relatively massive main sequence donor which fills its Roche lobe. Taking a black hole mass of $\sim 120 M_\odot$, as required in order to account for the observed X-ray flux in terms of isotropic emission, the donor mass is in the range $10 - 18 M_\odot$.

counterpart C2 : In this case the source is a binary formed by a late type, massive supergiant and a stellar mass black hole with beamed X-ray emission.

M82 X-1 is one of the most luminous ULXs and is the first source in which a QPO was detected. Our analysis of *XMM-Newton* and *RXTE* observations gives useful constraints for the mass of the BH hosted in this ULX (Mucciarelli et al., 2006).

We carefully analyzed the *XMM-Newton* spectrum subtracting the contribution of the galaxy emission (modeled using *Chandra* data) and masking some of the nearby point-like sources. We found that a very soft thermal component is present in the *XMM-Newton* spectrum of M82 X-1. Modeling it with a standard accretion disk would imply a black hole mass in the range $M_{BH} \approx [200 - 2000] f^4 \, M_\odot$.

The highest recorded luminosity emitted by M82 X-1 is $L \sim 2 \times 10^{41}$ erg s^{-1} (at a distance of 3.9 Mpc). Making the assumption that, at maximum, the source emits at the Eddington limit, we can derive a rough estimate of the BH mass, $M_{BH} \sim 1500 M_\odot$. It is worth noticing that the high luminosity of this source is not easily explained invoking alternative anisotropic models.

The power density spectrum of the *XMM-Newton* observations show a variable QPO. The QPO was also found in 7 archival *RXTE* observations. As far as the properties of the QPO are concerned, the similarities in fractional rms, variability,

quality value, and underlying noise strongly suggest an association between the QPO in M82 X-1 and the low-frequency, type-C QPOs observed in BHCs (Mucciarelli et al., 2006). Scaling the frequency inversely to the BH mass, the observed QPO frequency range (from 50 to 166 mHz) would yield M_{BH} anywhere in the interval 10 to 1000 $M_\odot$. Some arguments have been proposed to reduce the uncertainty on the determination of the mass of the compact object in M82 X-1, using in particular the correlation between the spectral and timing properties observed in BHCs. It is tempting to conclude that a likely value for the mass of M82 X-1 may be a few hundreds solar masses.

The available X-ray and multiwavelength observations suggest that ULXs are a composite population, a significant fraction of which shows the properties of galactic accreting binaries. Discriminating between a binary system hosting a solar mass BH and one with an IMBH is an extremely challenging task. Marginal evidences supporting both these conclusions have been found but up to now there is still no definitive proof of the existence of IMBHs.

My Thesis work allowed us to place significant constrains to the BH mass of two well studied ULXs. However, a crucial development in this field will only come from the detailed spectroscopic observations of ULX optical counterparts, as the one of NGC 1313 X-2. The identification of emission and/or absorption lines in the optical spectra of these stars held the promise to provide *dynamical measurement of the mass function of ULX binary systems and, eventually, of the black hole mass.*

CONTENTS

LIST OF FIGURES

LIST OF TABLES

CHAPTER 1

INTRODUCTION

1.1 A short historical overview

The *Einstein* satellite: the beginning

Although bright, pointlike sources, hosted in external galaxies, were already detected with the *UHURU* and *HEAO-1* satellites (e.g. Giacconi et al., 1972; Wood et al., 1984), only the sensitivity and spatial resolution (few arcminutes) of the *Einstein* observatory (*HEAO-2*, Giacconi et al., 1979) permitted a significant step forward in this field. Known X-ray pointlike sources observed in our Galaxy and in the Local Group galaxies, as M 31 and M 33, were observed at luminosities not higher than few times the Eddington limit for a neutron star (1.3×10^{38}erg s^{-1}). *The discovery in nearby galaxies of very bright sources, with emission up to few times 10^{39} erg s^{-1}, if they are located at the distance of the host galaxy (Long & van Speybroeck, 1983; Fabbiano, 1989), was the first step in the study of the sources, now commonly referred as to Ultraluminous X-ray sources (ULXs).* After considering the distance uncertainties and the chance coincidence probability (that confirmed the association of such sources with the host galaxies), Long & van Speybroeck (1983) pointed-out that such objects maintain an average luminosity in excess of the Eddington limit for neutron stars at least for the exposure times of the *Einstein* pointings.

One of the sources analyzed in this Thesis, the ULX NGC 1313 X-2, was among the first objects observed. A pioneering work in this field is that of Fabbiano & Trinchieri (1987) where an analysis of the *Einstein*-IPC (Imaging Proportional Counter) data of a sample of 13 spiral galaxies was presented. At least 6 of those galaxies are now known to host ULXs. Some of them were confused with the nuclei of the host galaxy, due to the limited spatial resolution of the IPC instrument (e.g the ULX NGC 1313 X-1). In Figure 1.1 two of those galaxies are shown. Fabbiano & Trinchieri (1987) pointed out that if these sources are isolated bright binary systems, "their X-ray luminosity could be largely in excess of the Eddington limit for a $1M_\odot$ object, suggesting the presence of massive black holes" or super-Eddington accretion.

Although the hypothesis that ULXs may contain Intermediate Mass Black Holes
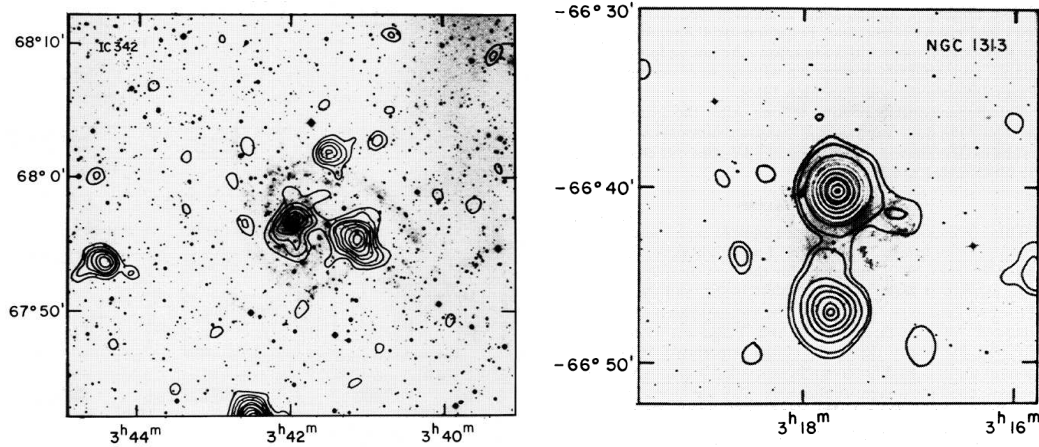
Figure 1.1: Isodensity *Einstein*-IPC contour of IC 342 (*left panel*) and NGC 1313 (*right panel*), from Fabbiano & Trinchieri (1987). In both galaxies off nuclear point-like X-ray sources, later identified as ULXs, are present.

(IMBHs; Colbert & Mushotzky 1999; Miller et al. 2003; Patruno et al. 2006) is certainly exciting, alternative explanations for ULXs were also proposed, as e.g. complex emission regions hosting sources not exceeding 10^{38}erg s^{-1} clustered together in a small volume (Fabbiano & Trinchieri, 1987). From this first sample of few tens of ULXs observed with the *Einstein* satellite, it was already clear that the contamination from Supernovae (Canizares et al. 1982, see also Swartz et al. 2004 for more recent data), foreground/background sources and spurious detections (Palumbo et al. 1981; see also Foschini et al. 2002b; Masetti et al. 2003) was important. Despite this, the variability of some sources and their association with the spiral arms of the host galaxies contributed to keep alive the scenario of truly single systems with a massive black hole.

ROSAT and *ASCA* data: ULX catalogs and spectra

In 1990 the *ROSAT* satellite (ROentgen SATellite) was launched and X-ray images with a better spatial resolution (about $\sim 10-20''$ for the HRI, High Resolution Imager, instrument) could be taken. Thanks to this, the number of discovered ULXs started to increase and the first ULX catalogs were produced (Colbert & Mushotzky 1999; Roberts & Warwick 2000; Colbert & Ptak 2002 and more recently Liu & Bregman 2005). A number of sources identified with the nuclear emission of the host galaxy, at higher spatial resolution appeared to be off-nuclear sources. An example is reported in Figure 1.2: Colbert et al. (1995) pointed out that the central *Einstein* source in NGC 1313 was actually located at $1'$ off the nucleus. The *ROSAT* observations had the important merit to show that ULXs are quite common objects in the nearby Universe and are present in up to half of the sampled galaxies, both spirals, ellipticals and irregulars (Colbert & Ptak, 2002; Liu & Bregman, 2005).

The progress made in this field thanks to the *ASCA* satellite (Advanced Satellite for Cosmology and Astrophysics) is mainly due to its wide spectral coverage and sen-
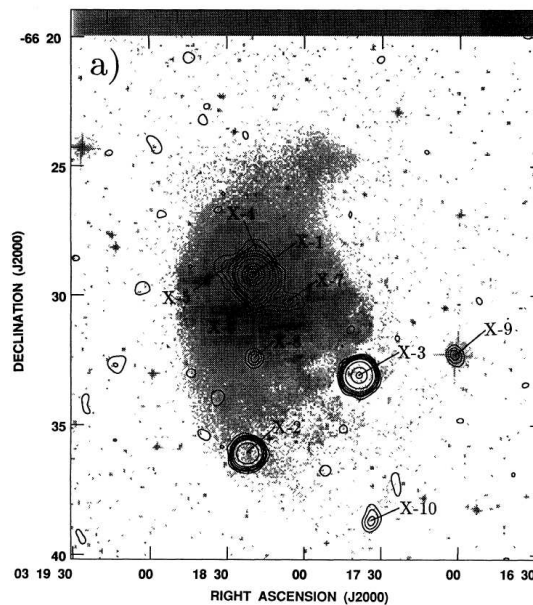
Figure 1.2: *ROSAT*-PSPC contours superposed on the digitized Sky Survey ESO B band image of the entire galaxy NGC 1313 (from Colbert et al. 1995).

sitivity. *ASCA* spectra of ULXs were usually modeled with a soft thermal component describing the emission from an accretion disk (see Figure 1.3, Mizuno et al., 1999). The temperatures of the inner accretion disk, derived from these fits, were expected to be very low if the compact remnant of the system is an IMBH. *ASCA* spectra gave temperatures too high for IMBH ($kT \sim 1.1 - 1.8 keV$, Mizuno et al. 1999; Colbert & Mushotzky 1999; Makishima et al. 2000), even higher than those observed in Galactic X-ray binaries ("too hot a disk problem" Makishima et al., 2000). To maintain an IMBH at the center of ULXs some authors proposed a rotating Kerr black hole (Mizuno et al., 1999; Makishima et al., 2000; Ebisawa et al., 2001), but also systems hosting a stellar mass black holes started to be proposed. In this case ULXs are simply not emitting isotropically (King et al., 2001; King, 2002; King & Pounds, 2003) or are dominated by emission from a relativistic jet (Körding et al., 2002; Georganopoulos et al., 2002; Kaaret et al., 2003). Another possibility is that they are truly emitting above the Eddington limit for $10 M_\odot$, e.g. because accretion proceeds through a slim disk (Abramowicz et al., 1988; Watarai et al., 2001; Ebisawa et al., 2003; Kawaguchi, 2003).

XMM-Newton and *Chandra*: the modern era

The so called "too hot a disk" problem has now been surpassed thanks to the recent observations taken with modern era satellites, such as *XMM-Newton* and *Chandra*. In the last few years a huge progress was made in the study of ULXs thanks to the new instruments with better spatial resolution ($4''$ and $1''$, for *XMM-Newton* and *Chandra* respectively), wider bandwidth ($\sim$ 0.2-10.0 keV) and huge collecting areas on board these satellites.

First of all ULX spectra with high counting statistics show a very wide range of
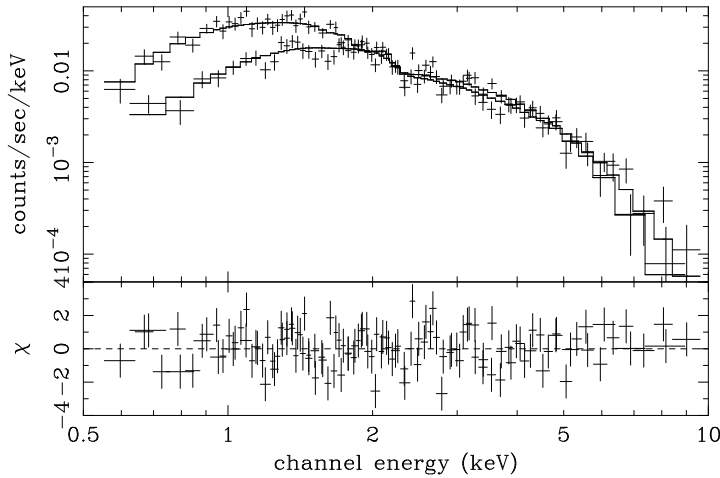
Figure 1.3: The SIS and GIS spectra of NGC 4565, dominated by two ULXs. The histogram shows the best fit model (a single thermal component) and the crosses represent the observed spectra (from Mizuno et al. 1999).

behaviors previously ignored, that often require complex modeling. In several cases the ULX spectra can be well reproduced by a multicolor disk black body plus a power law, although the temperature of the multicolor disk component is often much lower than that observed in *ASCA* data of ULXs and in Galactic X-ray binaries (e.g. Miller et al. 2003, 2004; Feng & Kaaret 2005, see also Figure 1.4). For the brightest ULXs, a possible curvature above 2-3 keV has been recently reported and more sophisticated spectral models appear to give better agreement with observations (Roberts et al., 2006; Stobbart et al., 2006). The possibility that the observed soft component truly arises in the accretion disk is also under debate and alternative models have been recently proposed (e.g. the warm absorber of Gonçalves & Soria 2006).

ULXs show spectral variability (also observed by ASCA) that, along with X-ray flux variations, is reminiscent of the state transitions observed in Galactic X-ray binaries. These sources, however, exhibit some anomalies with respect to their Galactic cousins (Kubota et al., 2001b; Roberts et al., 2002; Fabbiano et al., 2003b). Furthermore, the X-ray variability on month/year timescales observed in many ULXs is similar to that observed in Galactic X-ray binaries (see e.g. La Parola et al. 2001; Colbert & Ptak 2002; Swartz et al. 2004; Zampieri et al. 2004). The recent detection of a 62 days modulation in the light curve of M 82 X-1, interpreted as the orbital period of the system, has provided a direct confirmation of the binary nature of at least some ULXs (Figure 1.5; Kaaret et al., 2006a,b).

The available X-ray observations suggest that ULXs are a composite population, a significant fraction of which shows the properties of galactic accreting binaries. ULXs are also studied within the framework of the X-ray source populations of nearby galaxies (e.g. Fabbiano, 2006) through their X-ray luminosity function (XLF). An important result that has been obtained from these studies is the correlation between
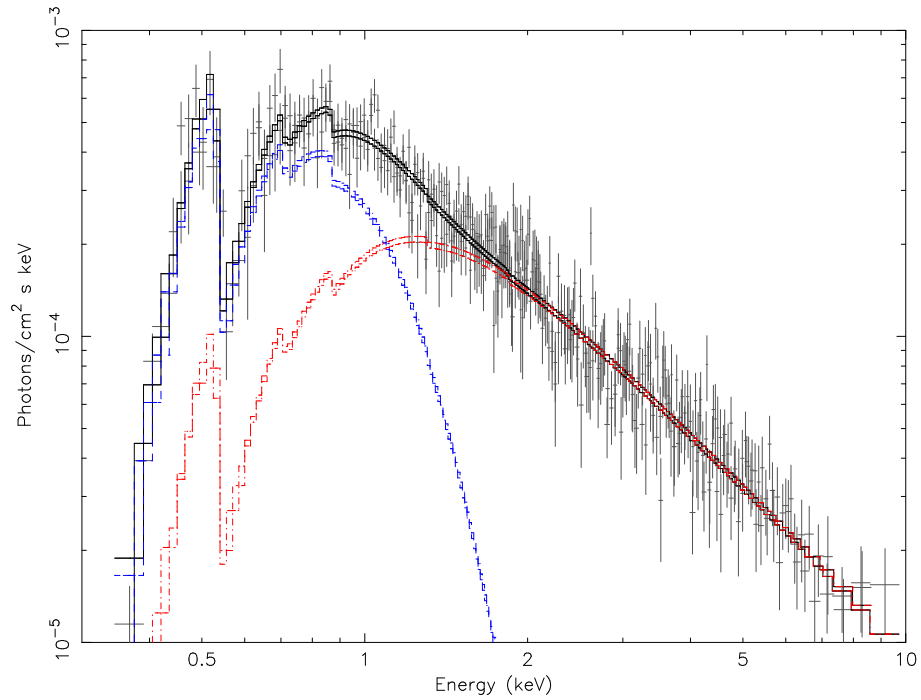
Figure 1.4: The unfolded *XMM-Newton* joint MOS1 and MOS2 spectra of NGC 1313 X-1. The total spectrum, cool ($kT \simeq 150$ eV) disk component, and power-law components are shown with solid, dashed and dotted lines respectively (from Miller et al. 2003).
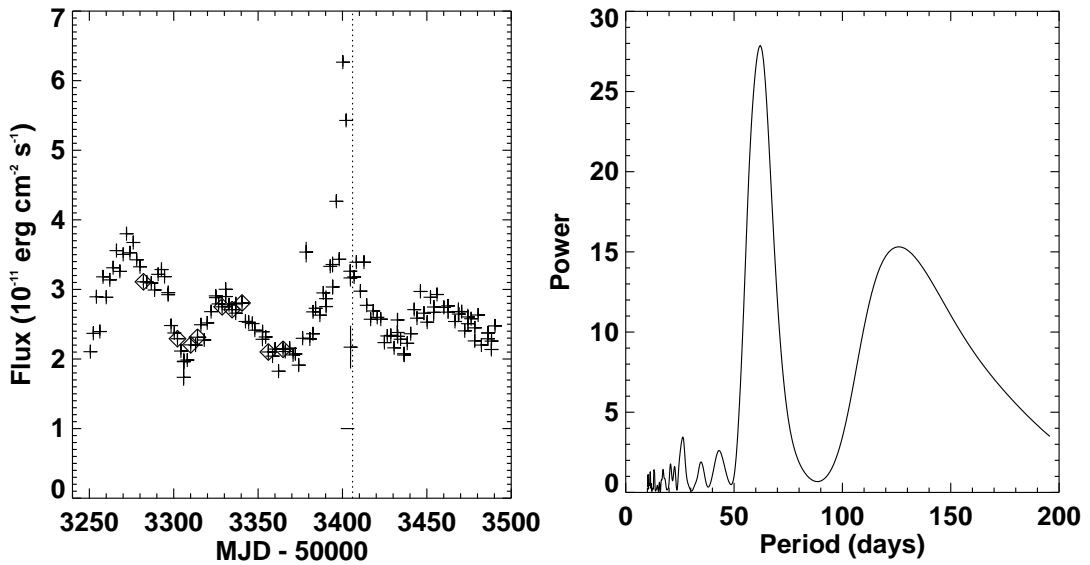
Figure 1.5: (*left*): X-ray light curve (2-10 keV) of M82 obtained with the PCA (Proportional Counter Array) on RXTE (Rossi X-ray Timing Explorer). (*right*): periodogram (Kaaret et al., 2006b). A strong peak in the power spectrum near a period of 62 days is apparent.

the presence of ULXs and the star formation of the host galaxy (e.g. Zezas & Fabbiano, 2002; Swartz et al., 2004; Wolter & Trinchieri, 2004). Recent work suggests that ULXs may represent the high luminosity (and mass) end of the X-ray luminosity function of more usual X-ray binaries (e.g. Gilfanov et al., 2004).
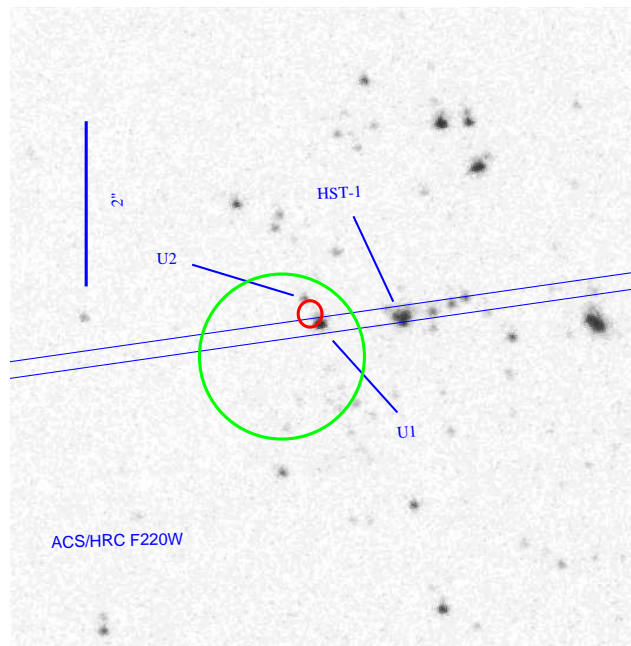
Figure 1.6: The optical counterpart to the ULX in NGC 5204 in an *HST*-ACS (Hubble Space Telescope, Advanced Camera for Surveys) image. The small error ellipses are derived from *Chandra* data (Liu et al., 2004).

The leap to other wavelengths

Multiwavelength observations are an valuable tool to investigate the nature of ULXs. Before *Chandra* the identification of ULX counterparts at other wavelengths was extremely difficult because of the limited spatial resolution of the previous satellites. The sub-arcsecond positional accuracy of *Chandra* permitted a successful cross correlation with the radio and optical bands (e.g. Liu et al., 2002, 2004; Zampieri et al., 2004). Radio emission, when present, gives important clues about the geometry, energetics and lifetime of ULXs (Kaaret et al., 2003; Miller et al., 2005). Optical observations are crucial to identify ULX counterparts and to study the properties of putative ULX binary systems (e.g. Roberts et al. 2001; Goad et al. 2002; Soria et al. 2005; Liu & Mirabel 2005). Up to now only a very small number of ULXs have been convincingly associated with stellar objects of known spectral type (e.g. Liu et al. 2002, 2004; Kaaret et al. 2004; Mucciarelli et al. 2005, 2007, see also Figure 1.6). All these ULXs are hosted in young stellar environments or star-forming regions and their optical counterparts have properties consistent with those of massive stars. Some ULXs are also associated with extended optical emission nebulae (Pakull & Mirioni, 2002; Zampieri et al., 2004; Ramsey et al., 2006; Pakull et al., 2006, see also Section 2.2.2).

1.2   Why are ULXs so interesting?

ULXs are commonly defined as very bright sources, with emission in excess of the Eddington limit for a 10 $M_\odot$ black hole, irregularly variable, hosted in nearby galaxies

and located at an off-nuclear position in the host galaxy (e.g. Colbert & Ptak, 2002; Miller & Colbert, 2004; Swartz et al., 2004; Fabbiano, 2006).

If ULXs host intermediate mass black holes, then they would represent the missing link between the stellar mass black holes, observed in some X-ray binaries in our Galaxy, and the super massive black holes at the center of active galactic nuclei. Stellar mass black holes are theoretically predicted to form at the final stages of stellar evolution, from the core collapse of very massive stars ($\gtrsim 25 M_\odot$, e.g. Woosley & Weaver, 1995; Fryer, 1999). At solar metallicity, mass loss leads to the ejection of most of the stellar envelope and the final remnant mass is typically not larger than 10-20 $M_\odot$ (Heger et al., 2003). How super massive black holes form is still not well established and various scenario were proposed (see e.g. Peterson, 1997; Frank et al., 2002). Direct acquisition of matter from the accretion disk can represent the primary mode for their growth but also other mechanisms, like dynamical interactions or relativistic instabilities (e.g. Begelman et al., 1984), may have an important role.

If ULXs are compact remnants between few tens to $10^4 M_\odot$, then their formation scenario may be totally different. If they really host an IMBH, then how did they form? And how can the binary system be born and the BH fueled? Some theories propose the formation of IMBHs in cosmological epochs (e.g. Niemeyer & Jedamzik, 1999) or in a zero metallicity environment with the first generation of stars (Madau & Rees, 2001). The creation of IMBHs was also predicted to occur at the center of dense stellar clusters (Bahcall & Ostriker, 1975; Lightman & Shapiro, 1977; Quinlan & Shapiro, 1987; Portegies Zwart et al., 1999) and, at the present time, this seems to be a very promising possibility for at least the brightest ULXs (Portegies Zwart et al., 2004). If, on the contrary, the compact remnant in ULXs is a stellar mass black hole, the formation mechanism is analogous to that of Galactic X-ray binaries (King et al., 2001; King, 2002; King & Pounds, 2003). In this case the emission mechanism and/or the geometry of the system account for the apparent super-Eddington emission (King et al., 2001; Körding et al., 2002; Ebisawa et al., 2003).

In order to asses if ULXs host stellar or intermediate mass black holes, it is necessary to measure the mass of the compact object Much of the observational effort to date is focused on this. Along with the high X-ray luminosity, evidence for the presence of an IMBH comes from the cool temperature of the soft spectral component (Miller et al., 2003, 2004; Feng & Kaaret, 2005) and from the low frequency of the quasi-periodic oscillation (QPO), observed at least in one source (M 82 X-1 Strohmayer & Mushotzky, 2003; Fiorito & Titarchuk, 2004; Mucciarelli et al., 2006). In Galactic X-ray binaries both the soft spectral component and the QPOs are associated to the emission of the accretion disk, but in ULXs this hypothesis is still under debate.

Discriminating between a binary system hosting a solar mass BH and one with an IMBH is an extremely challenging task. Marginal evidences supporting both these conclusions have been found but up to now there is still no a definitive proof of the existence (or not) of IMBH. Although X-ray data give fundamental information on the ULX systems, the definitive answer will come from optical observations of the proposed counterparts. The presence of spectral features in emission and/or absorption could definitely constrain the orbital parameters of the system permitting to measure the mass function and give the definitive answer to the existence of IMBHs.

1.3   My work in this context

Despite the significant advancements of the past years, our knowledge of ULXs is still far from being satisfactory and we are still at a stage when observations of single sources can provide invaluable information about the entire class. In this respect, detailed X-ray spectral and timing observations, optical photometry and spectroscopy of the proposed counterparts are of fundamental importance. This is the framework in which my Thesis work is inserted, focusing in particular on the analysis of the X-ray and optical properties of two of the best studied ULXs: NGC 1313 X-2 and M 82 X-1.

The ULX NGC 1313 X-2 (Chapter 3) *HST* and VLT images of the field of NGC 1313 X-2 allowed us to identify two possible counterparts inside the *Chandra* error box (Zampieri et al., 2004; Mucciarelli et al., 2005). The two candidate counterpart show properties consistent with massive stars ($\sim 10 - 20 M_\odot$) in NGC 1313. Irrespectively of which of the two objects the actual counterpart is, this implies that NGC 1313 X-2 is a high mass X-ray binary. From the study of the X-ray light curve and its possible correlation with the optical emission of the two proposed ULX counterparts, we found that the optical/X-ray data are consistent with NGC 1313 X-2 being an early type, main sequence star of approximately $15 M_\odot$ dumping matter through Roche-lobe overflow onto a $\sim 120 M_\odot$ black hole at an orbital separation corresponding to a period of ~ 2 days (Mucciarelli et al., 2007).

The first QPO in an ULX: M 82 X-1 (Chapter 4) M82 X-1 is one of the most luminous ULXs and is the first source in which a QPO was detected (Strohmayer & Mushotzky, 2003). A comparison of the properties of this QPO with those of the various types of QPOs observed in Galactic BHCs strongly suggests an association with the type C, low-frequency QPOs. Estimating the BH mass from independent method (e.g. from the very high luminosity or from the observed QPO frequency range, scaling the frequency inversely to the BH mass) would yield M_{BH} anywhere in the interval few tens to 1000 $M_\odot$ (Mucciarelli et al., 2006).

CHAPTER 2

WHAT WE KNOW ABOUT ULXS

Since the early times, the observation of the X-ray universe has given us numerous surprises and unexpected results. One of the most challenging discoveries is the existence of point-like sources that emit at luminosities intermediate between those of accreting Stellar Mass Black Holes (up to $\sim 10^{38}$ erg s^{-1}) and Super Massive Black Holes ($\gtrsim 10^{42}$ erg s^{-1}, e.g. Long & van Speybroeck 1983; Fabbiano 1989; Colbert & Mushotzky 1999; Roberts & Warwick 2000; Colbert & Ptak 2002). Several X-ray sources with luminosities in excess of 10^{39} erg s^{-1} were early revealed by *Einstein* (Clark et al., 1978; Long & van Speybroeck, 1983; Fabbiano, 1989, 1995). If we assume that the X-ray emission comes from accretion on to a compact object and that these sources emit isotropically at the Eddington limit, then masses in the range 100-1000 $M_\odot$ are inferred for the central BH from the observed flux (e.g. Fabbiano & Trinchieri, 1987; Roberts & Warwick, 2000; Lira et al., 2000; Colbert & Ptak, 2002, , see also Figure 1.1). In this case the remnants in these systems would be Intermediate Mass Black Holes (IMBHs, Colbert & Mushotzky 1999). Clearly, there are no *a priori* reasons for which these sources need to emit isotropically, so alternative explanations for them have been proposed in literature. In the present Chapter I describe the main properties of ULXs as well as the implications that they have for their nature.

2.1 X-ray properties of ULXs

A definition of ULXs at a glance is based on the fact that their luminosities turn out to be higher than what is expected for an accreting system hosting a stellar mass BH (with $M_{BH} \lesssim 10$ M$_\odot$). On the other hand ULXs never reach luminosities $\gtrsim 10^{42}$ erg s^{-1} observed for AGNs that host supermassive BHs (with $M_{BH} \gtrsim 10^6$ M$_\odot$).

Formally this concept is expressed in terms of the Eddington limit, that can be applied to any source powered by accretion. Under the assumption that accretion onto the compact object is steady and spherically symmetrical, there exists a limiting luminosity, L_{Edd}, for which the radiative force becomes equal to the gravitational force

acting on an atom. For fully ionized hydrogen it is:

$$L_{Edd} = \frac{4\pi G M_{BH} m_p}{\sigma_T} \cong 1.3 \times 10^{38} \frac{M_{BH}}{M_\odot} \mathrm{ergs}^{-1} \qquad (2.1)$$

where σ_T is the Thomson cross–section, M_{BH} is the mass of the accreting object (in this case a BH) and m_p the proton mass.

For a BH of 10 $M_\odot$ the Eddington luminosity is 1.3×10^{39} erg s^{-1}. Although different authors use different values for the definition of a ULX, the latter is widely adopted as the known masses of Galactic Black Hole Candidates (BHCs) cluster around ~ 10 $M_\odot$ (Bailyn et al., 1998; McClintock & Remillard, 2006). Very bright ULXs, as M 82 X-1 (see Chapter 4), can easily reach a luminosity higher than 10^{40} erg s^{-1}, but up to now ULXs are never observed to shine at luminosities $\gtrsim 10^{42}$ erg s^{-1}. *Therefore ULXs can be defined as off-nuclear, point-like sources in nearby galaxies with X-ray luminosity in excess of* 10^{39} *erg s^{-1}.*

A number of ULXs seems to exhibit variability at different levels. Irregular variability in the X-ray flux on timescales of months is observed in about half of the *ROSAT* ULXs with multiple observations (Colbert & Ptak, 2002), while about 5-15% of the *Chandra* ULXs show variability during a single observation (Swartz et al., 2004). Transient behavior was also detected in some ULXs (e.g. the ULX in NGC 3628, Strickland et al. 2001, an the one in NGC 628, Soria & Kong 2002). In few cases a periodicity was detected in the X-ray flux (Liu et al., 2002; Fabbiano et al., 2006). The recent detection of a 62 days modulation in the light curve of M 82 X-1, interpreted as the orbital period of the system, has provided direct confirmation of the binary nature of at least some ULXs (Kaaret et al., 2006a,b). Variability on short timescales (1-10s) has also been discovered in the ULX M 82 X-1 (Strohmayer & Mushotzky 2003, see Section 2.1.5 and Chapter 4).

ULXs show composite X-ray spectra, similar to those observed in Galactic XRBs (Roberts & Colbert, 2003; Swartz et al., 2003; Miller et al., 2003; Zampieri et al., 2004; Feng & Kaaret, 2005, among the others). An important X-ray marker of ULXs is the very soft component present in the X-ray spectra of several of them at a temperature of 0.1-0.2 keV (Miller et al., 2003, 2004; Feng & Kaaret, 2005). This is 5-10 times lower than the typical temperature of the soft thermal component observed in Galactic XRBs.

The detection of spectral variability along with X-ray flux variations echoes, with some differences, the state transitions observed in Galactic BH candidates XRBs (e.g. IC 342 ULXs, Kubota et al. 2001b, or M 81 X-9, La Parola et al. 2001). Kubota et al. (2002) argue that ULXs do not really mimics the Low Hard State (LHS) of XRBs but rather a Compton dominated Very High States (VHS). Some ULXs have been observed to behave in the opposite way, showing a high/hard-low/soft dichotomy (e.g. M 51 X-7, Liu et al. 2002, four ULXs in the "Antennae" galaxies, Fabbiano et al. 2003b, NGC 1313 X-2, Zampieri et al. 2004).

2.1.1 Contamination of the ULX sample

Catalog of ULXs suffer of the major problem of contamination from spurious identifications. Sources that could reach luminosities in the range of ULXs are Supernova Remnants (SNRs, see e.g. SN 1993J, among the others in Bregman et al. 2003, SN 1988Z in Fabian & Terlevich 1996 and SN 1995N in Zampieri et al. 2005), Globular Clusters (GCs), Young Stellar Clusters (YSCs, e.g. Fabbiano & Trinchieri 1987) and AGNs (Foschini et al. 2002b; Masetti et al. 2003, see also Section 2.4).

In Supernovae (SNe) X-ray emission may arise usually few years after the explosion, when the ejecta interact with the CircumStellar Medium (CSM). The violent collision of the supernova ejecta with the dense surrounding gas released by the massive progenitor star in a previous evolutionary stage originates high energy emission. The interaction generates forward and reverse shock waves which bound the shocked wind and ejecta. In the "standard" model (Chevalier & Fransson, 1994, 2003) the forward shock produces a hot shell ($\sim 10^9$ K), while the reverse shock produces a denser, cooler ($\sim 10^7$ K) shell with much higher emission measure. The pressure and temperature behind the shocks are sufficiently high that the post-shock ejecta and circumstellar material (CSM) may become powerful X-ray emitters. At the same time synchrotron radiation is generated by electrons accelerated up to relativistic energies at the shock front.

GCs host a number of neutron star LMXBs, binary systems in which a weakly magnetized neutron star (NS) accretes material from a low mass companion star ($M_* \lesssim 1 M_\odot$). These X-ray binaries are usually associated with old stellar populations. In GCs the number density of such sources per unit mass is two order of magnitudes greater than in our Galaxy. This is probably due to the fact that in the dense environment of GCs tidal capture of a companion by the compact object may be favored. As LMXBs can reach luminosities of 10^{36-38} erg s^{-1}, an unresolved GC hosting few tens of LMXBs could be mistakenly identified with a rather bright ULX of 10^{39} erg s^{-1} (e.g. Fabbiano & Trinchieri, 1987).

YSCs may also host X-ray binaries usually associated to a young companion. As in GCs, the presence of several unresolved binaries in a YSCs could be misleadingly interpreted as a single ULX.

The contamination of ULXs from SNe can be easily removed. In some cases the positional coincidence with known optical SNe is a straightforward method to identify such objects. Furthermore, the X-ray spectrum of interacting SNe has a characteristic shape with prominent X-ray emission lines. Depending on the spectral resolution, it is possible also to discriminate two components at different temperatures generated by the forward and revers shocks (e.g. Schlegel et al., 2000; Zampieri et al., 2005). Moreover, SNe do not show the irregular variability in the X-ray flux typical of XRB systems.

In the case of clusters, variability alone may not be sufficient to rule out an association because of the possibility of strong variability of single objects. In this case a combined flux/spectra variability that mimics the spectral transitions of Galactic XRBs (see Kubota et al., 2001b; Zezas & Fabbiano, 2002) and/or high resolution X-ray observations, could be used to identify the source as a single binary system.

AGNs are a more problematic source of contamination. They could easily emit at a luminosity greater than 10^{41} erg s^{-1}. As they are powered by accretion onto a compact -supermassive- object, the properties of their X-ray emission are similar to those of XRBs and ULXs. Variability on long time scales (months, years) could be similar to what expected for ULXs. X-ray spectra of AGNs also show multiple components, a soft excess and a power law. From the X-ray emission alone, it is not easy to discriminate ULXs from background AGNs. Up to now spurious AGN identifications were discovered through the study of their optical counterparts. In these cases the optical spectra showed the presence of emission lines redshifted at the recession velocity of their host galaxies (Foschini et al., 2002b; Masetti et al., 2003; Clark et al., 2005).

2.1.2   A concise view of the ULX models

The overall X-ray properties of ULXs briefly summarized above, in particular the correlated flux/spectral variability, are strongly suggestive of a XRB origin. Using the Eddington limit as a rough estimate of the mass of the accreting object, ULX host remnants have masses greater than 10 M$_{\odot}$, clearly in the range of IMBHs. Moreover, assuming that the temperature of the soft component detected in several ULXs is related to the characteristic temperature of a standard accretion disk, it is possible to derive an independent order of magnitude estimate of the BH mass $\gtrsim 100 M_{\odot}$, in the range of IMBHs.

However, *a priori* there is no need for these objects to be spherically symmetric nor stationary, so alternative explanations were invoked in literature to explain their luminosities. The most obvious explanation to circumvent the Eddington limit is the presence of some kind of beaming, geometrical as suggested by King et al. (2001) or induced by the presence of relativistic jets (Körding et al., 2002; Kaaret et al., 2003). Moreover, some ULXs could truly emit above their Eddington limit (e.g. because the accretion proceeds through a slim disk, Watarai et al. 2001; Ebisawa et al. 2003; Kawaguchi 2003). In all these cases ULXs may be more similar to Galactic BH binaries and may harbor stellar mass BHs (see Section 2.1.4).

The IMBH interpretation offers a direct explanation of the very high luminosity and the low disk temperature of ULXs (e.g. Miller et al. 2004) and it is also supported by the link of ULXs with very massive OB stars association (e.g. Roberts et al., Goad et al., Z04). Furthermore, several ULXs are coincident with uniformly X-ray irradiated emission nebulae and few of them also with extended radio counterparts.

As it is clear from this brief introduction, the issue of the nature of ULXs is still open and a number of viable models, that I will discuss in detail later in this Chapter, have proposed in the past years. Here a concise list of all the ULX model is given.

IMBH (Colbert & Mushotzky, 1999; Miller et al., 2003, 2004): a companion star accretes material onto an intermediate mass BH. The high mass of the BH is consistent with isotropic emission and no super-Eddington accretion is required. The IMBH interpretation offers a direct explanation of *both* the very high luminosity *and* low disk temperature of ULXs (e.g. Miller et al. 2004). Also

the association with very massive OB stars (e.g. Roberts et al., Goad et al., Z04) is not inconsistent with this interpretation as, if the ULX is born in such an environment, the mass function of the parent stellar association is likely to be top-heavy. Furthermore, the association with uniformly X-ray irradiated emission nebulae and extended radio counterparts suggests a rather isotropic illumination of the surrounding interstellar medium by the ULX. All these aspects will be discussed in more detail in Sections 2.2 and 2.3.

Geometrical and/or relativistic funneling : in geometrical funneling (King et al., 2001; King, 2002) a stellar mass BH accretes material from a companion during the thermal timescale mass transfer phase. Geometrical funneling of the emission in the direction of the observer is required. Higher beaming factors than those provided by the previous model may be reached in the relativistically beamed disk/jet model, similar to the galactic Microquasar model (Körding et al., 2002; Georganopoulos et al., 2002; Kaaret et al., 2003; Begelman et al., 2006). In both cases the BH mass required is $\lesssim 10 M_\odot$. The beamed XRB interpretation is supported by the fact that the statistical properties of ULXs appear to be indistinguishable from those of less luminous X-ray sources in the same galaxy fields (Swartz et al., 2004, , see also Section 2.4). Also the correlation of ULXs with active star forming regions (association with massive stars, presence of emission nebulae, correlation with the far-IR luminosity in spirals) has been taken as evidence in favor of this interpretation. This interpretation is supported mainly by the X-ray spectrum and multiwavelength spectral energy distribution of one source, the ULX NGC 5408 X-1 (Kaaret et al., 2003). However, the beamed XRB interpretation can not explain why several ULXs show a very high luminosity and, at the same time, a very low temperature of the accretion disk. This fact is not consistent with the behavior of Galactic BH XRBs where high luminosities are associated to high disk temperatures ($kT \sim 1$ keV). Also the extended radio emission around some ULXs (e.g. Holmberg II X-1; Miller et al. 2005) is not in agreement with the beamed interpretation.

Super-Eddington accretion via a slim disk (Ebisawa et al., 2003): if the disk accretes at rates larger than the Eddington rate, it is dominated by advection in its inner part. Then the disk becomes thicker and super-Eddington luminosities ($\lesssim 10 \ L_{Edd}$) are reached also for accretion onto a stellar mass BH. This model was successfully applied at the ULX M 33 X-8 by Foschini et al. (2004), but do not give satisfactory results on ULXs that shows very soft components.

Super-Eddington accretion via photon-bubble instabilities (Begelman, 2002): accretion onto a stellar mass BH could be super-Eddington also if photon bubble instabilities in the accretion disk permit to the radiation to escape, exceeding the Eddington limit.

Maximally rotating Kerr BH (Makishima et al., 2000): a Kerr rotating BH was invoked to explain ULX spectra showing a hot soft component (e.g. in the case of *ASCA* data in Makishima et al., 2000). However, such high temperatures

were the consequence of the fact that, because of the low statistics, the early *ASCA* spectra were fitted with single thermal models, usually a MultiColor Disk (MCD) component. The *XMM-Newton* spectra of some ULX (e.g. M 33 X-8, Foschini et al. 2004, a ULX in NGC 2276, Davis & Mushotzky 2004) still require a 'hot' disk component, but for a large number of ULXs high quality *XMM-Newton* and *Chandra* spectra are fitted with more sophisticated spectral models with no evidence for such high temperatures.

Wandering IMBH model (Krolik, 2004): an isolated IMBH, moving rapidly in its host galaxy, may be able to accrete material from a dense interstellar medium, typically molecular clouds, at accretion rates sufficiently high to explain the observed luminosity.

2.1.3   X-ray energy spectrum

The first energy spectra obtained with the *ASCA* and *ROSAT* satellites could be fitted with single component models, as an absorbed power law, a thermal black-body (BB) or a disk black-body (DISKBB) model (Makishima et al., 2000; Foschini et al., 2002a). The PL model usually overestimates the absorbing column density to mimic the soft break. Conversely a fit with a thermal soft component alone gives values of the temperature as high as that observed in stellar mass XRBs ("too hot a disk" problem, Makishima et al. 2000 and Table 2.1). The low sensitivity and spectral resolution of the *ASCA* and *ROSAT* satellites did not permit to discriminate more complex spectral shapes.

More recent observations performed with the *Chandra* and *XMM-Newton* satellites indicate a more complex structure in the X-ray spectrum of ULXs . A great number of ULXs, with sufficiently good statistics, show a two-component spectrum (Miller et al., 2003, 2004; Feng & Kaaret, 2005).

At present, the available data indicate the existence of three types of spectral behaviors (Feng & Kaaret, 2005):

1. hot, optically thin thermal spectra, fitted with a MEKAL model (e.g. Schlegel et al., 2000);

2. typical BHC-like spectra, often fitted with a low temperature (0.1-0.4 keV) MCD + power law (PL) components (Miller et al., 2003; Zampieri et al., 2004). The MCD emission represents emission from an accretion disk, while the PL mimics the action of unsaturated Comptonization from a hot corona;

3. spectra with a curvature at high energies, fitted with a high temperature (1-1.5 keV) MCD + PL model (e.g. Foschini et al., 2004) or a Comptonization model (Kubota et al., 2002; Roberts et al., 2006; Stobbart et al., 2006).

The low temperature of the soft thermal component observed in several sources showing typical BHC-like spectra has been interpreted as evidence for the presence of a IMBH (e.g. Miller et al., 2003, 2004), as discussed thoroughly below. However, more recently a number of authors tried to use different spectral models with the purpose to provide physically consistent explanations for the emission of these sources.

Reference	Model	Characteristic
Makishima et al. (2000)	MCD	emission from a standard accretion disk $kT \sim 1 - 2$keV insufficient statistics of $ASCA$ data, "too hot a disk" problem
Foschini et al. (2002a)	BB or PL	$kT = 0.5 - 0.9$keV, $\Gamma = 1.1 - 2.3$ similar to XRBs in the hard or soft state
Miller et al. (2003, 2004)	MCD+PL	emission from a standard accretion disk with $kT \sim 0.1 - 0.2$keV + optically thin, comptonized corona $M_{BH} \gtrsim 100 M_\odot$ (from T and norm.)
Kubota et al. (2002)	thcomp	Comptonized, opt. thick accretion disk $kT \sim 1$keV associated to a VHS $M_{BH} \gtrsim 30 M_\odot$ (from L_{disk} vs. T)
Foschini et al. (2004)	MCD+ cut-offPL	$kT = 1.2$keV ($M_{BH} \sim 12 M_\odot$) orientation and anisotropy effects
Stobbart et al. (2006)	DISKBB+EQPAIR	similarly to Kubota et al. (2002). Comptonized, opt. thick corona + cool disk around a stellar mass BH
Roberts et al. (2006)	COMPTT	as Stobbart et al. (2006) associated to a VHS (as in XTE J1550-564)
Gonçalves & Soria (2006)	TABS+TEMI (their model)	optically thick, thermal wind, as in the warm absorber model of AGNs

Table 2.1: Summary X-ray spectral models of ULXs.

Different parametric implementation of Comptonization models appear able to account for the whole X-ray spectrum of ULXs. Using *ASCA* data, Kubota et al. (2002) suggest that the observed spectra are associated with a strongly Comptonized optically thick accretion disk. A similar behavior is also observed in Galactic BHCs in the so-called VHS (Kubota et al., 2001a). From their model, they estimate BH masses in the interval 30-250 $M_{\odot}$. Spectral curvature in the high energy part of the spectrum, above 2 keV, has been reported in a number of ULXs (e.g. Holmberg IX X-1, Dewangan et al. 2006, M 82 X-1, Agrawal & Misra 2006) and correlated to the presence of an optically thick corona. Stobbart et al. (2006) applied a Comptonization model to a sample of 13 ULXs with high statistics finding that it gives a good fit. Roberts et al. (2006) suggests that ULXs are stellar mass BH binaries in a strong VHS (like that observed in XTE J1550-564; Kubota & Done 2004) characterized by a cool disk and a thick corona. This model implies high mass transfer rates but does not requires a IMBH.

It has also been suggested that the very soft X-ray spectral components observed in ULXs with typical BHC-like spectra may be produced by optically thick, thermal winds (King & Pounds, 2003; Gonçalves & Soria, 2006), similarly to what proposed for Super-Soft ULXs (e.g. M 101 X-1, Mukai et al. 2003; a ULX in the Antennae, Fabbiano et al. 2003a).

A summary of the models is presented in Table 2.1.

The soft thermal component

As mentioned above, one of the hypothesis about the origin of the soft component is that it comes from a standard optically thick accretion disk around a BH, although this interpretation is controversial.

The last stable orbit around a BH is at $3\,\gamma\,r_s$, where $r_s \equiv 2GM_{BH}/c^2 \equiv 2\,r_g$ is the Schwarzschild radius, r_g the gravitational radius and γ a constant that varies according to the adopted metric ($\gamma = 1$ for a Schwarzschild BH). Values $\gamma \gtrsim 1$ may actually mimic possible variations in the values of the inner disk radius. Neglecting general relativistic corrections, the radial dependence of the "effective" temperature of a standard, optically thick accretion disk may be written as (Shakura & Sunyaev, 1973):

$$T_{eff}(r) = \left\{ \frac{3GM_{BH}\dot{M}}{8\pi\sigma r^3} \left[1 - \left(\frac{r_{in}}{r} \right)^{1/2} \right] \right\}^{1/4} = T_* \left\{ \left(\frac{r_{in}}{r} \right)^3 \left[1 - \left(\frac{r_{in}}{r} \right)^{1/2} \right] \right\}^{1/4} \quad (2.2)$$

where:

$$T_* = \left(\frac{3GM_{BH}\dot{M}}{8\pi\sigma r_{in}^3} \right)^{1/4}. \quad (2.3)$$

Here $\dot{M}$ is the accretion rate, σ the Stefan-Boltzmann and G the gravitational constant. The effective temperature is zero at $r = r_{in}$, peaks at $r \approx (49/36)\,r_{in} \approx 8\,\gamma\,r_g$ where $T_{max} = 0.488\,T_*$, and decreases with a dependence $\propto r^{-3/4}$ outwards.

In the inner part of the optically thick accretion disk, the electron scattering opacity is dominant, and the hotter disk atmosphere distorts the emergent spectrum. As a

consequence the local spectrum from each ring of the disk can be approximated by the "diluted black body", $(T_{eff}/T_{col})^4 \, B(E, T_{col})^1$, where $B(E, T_{col})$ is the Planck function with color temperature T_{col} $(> T_{eff})$. The ratio of the color temperature to the effective temperature, the color correction factor $f = T_{col}/T_{eff}$, is approximately constant along the disk radius ($f \sim 1.6 - 1.7$, Shimura & Takahara, 1995; Zampieri et al., 2001).

The standard Shakura & Sunyaev accretion disk is a starting point to describe X-ray spectra of XRBs, but in many cases a successful physical description was obtained with a simpler mathematical approximation called the multi-color disk black body (MCD) model (Mitsuda et al., 1984). Also in this model the emission from the accretion disk is assumed to be a superposition of rings emitting locally a black body spectrum at different temperatures, up to a certain maximum value T_{in} that occurs near the innermost disk boundary. However, the radial dependence of the local disk temperature $T(r)$ is simplified as

$$T(r) = T_{in} \left(\frac{R_{in}}{r} \right)^{-3/4} \quad , \tag{2.4}$$

where here R_{in} and T_{in} are independent model parameters, the apparent inner disk radius and the disk temperature at R_{in}, respectively. The MCD formalism is known to give a reasonable approximation of the disk emission, as found in the case of Nova Muscae (Mineshige et al., 1994). T_{in} may be identified with the maximum disk color temperature, while the true inner disk radius r_{in} and apparent radius R_{in} are related (Kubota et al., 1998):

$$r_{in} = \xi \, f^2 \, R_{in} \approx 0.4 \, f^2 \, R_{in} \tag{2.5}$$

where ξ is a correction factor reflecting the fact that the maximum temperature of the MCD (T_{in}) occurs at a radius somewhat larger than R_{in}. The flux is proportional to $R_{in}^2 T_{in}^4$ (Makishima et al., 2000).

If the soft component inferred from the MCD+PL fit of ULXs with BHC-like spectra represents the emission of an accretion disk, then the temperature and normalization of the MCD component can be used to obtain a rough estimate of the BH mass, to be compared with that obtained from independent methods. The effective temperature of a standard accretion disk as a function of radius is given by Equation 2.2. If T_{in} is identified with the maximum disk color temperature, then $T_{in} = 0.488 \, T_* \simeq (1/\alpha) \, T_*$, with $\alpha \sim 2$.

From Equation 2.3:

$$\alpha T_{in} = \left(\frac{3GM_{BH}\dot{M}}{8\pi\sigma r_{in}^3} \right)^{1/4} , \tag{2.6}$$

and hence

$$\frac{M_{BH}}{M_\odot} = \left(\frac{\dot{M}c^2}{L_{Edd}} \right) \frac{f^4}{\gamma^3} \left(\frac{\alpha T_{in}}{1.5 \times 10^7 \, \mathrm{K}} \right)^{-4} , \tag{2.7}$$

---

[1] T_{eff} and T_{col} are two different temperature. Fitting the spectrum with a Planck function gives the color temperature T_{col}. The effective temperature, T_{eff} is the temperature of a BB emitting the same total flux.

where $\dot{M}c^2 = L_X/\eta$ and $\eta \approx 0.1$ is the accretion efficiency.

Also the normalization of the MCD component can be used to estimate the black hole mass (Miller et al., 2003). The normalization is given by

$$K = \left(\frac{R_{in}/\text{km}}{D/10\,\text{kpc}} \right)^2 cos\,i \qquad (2.8)$$

where D is the distance to the source and i the inclination angle of the disk with respect to the observer. Then if we assume that $r_{in} = 3\,\gamma\,r_s$ and using Equation 2.5, we obtain:

$$M_{BH} = \xi \frac{f^2}{\gamma} \left(\frac{K}{cos\,i} \right)^{1/2} \left(\frac{D}{10\,\text{kpc}} \right) (8.86)^{-1} M_\odot, \qquad (2.9)$$

from which it is possible to derive a lower limit for the BH mass.

The γ factor can assume values higher than unity, implying that the inner disk radius is farther out than the innermost stable circular orbit.

Given the strong dependence of M_{BH} on the model parameters, any uncertainty in the accretion physics and radiative transfer may induce significant errors in the resulting value of M_{BH}. So, the inferred spectroscopic measurement of the BH mass should be taken simply as an order of magnitude estimate. In this spirit, Equation 2.7 and 2.9 will be used throughout this Thesis to estimate the BH mass.

The hard tail

As shown by Galactic XRBs in the Low/Hard State (LHS) or Intermediate State (IS), the X-ray spectrum of ULXs shows a high energy PL component, comparable to the soft component emission. In XRBs this component has typical values of the photon index $\Gamma \simeq 1.5$-1.8 and a cut-off at ~ 50-200 keV. The power law is produced by Comptonization of the disk emission by a hot medium (corona). In ULXs this component is always present, with $\Gamma \gtrsim 1.7$. The flux of the PL component in ULXs is usually comparable or greater than that of the soft component (see e.g. Table 3.8 in Chapter 3).

2.1.4 Alternative models of ULXs

The first and most obvious criticism to the isotropic emission of such ultraluminous sources is the need of a mass greater than 100 $M_\odot$, a high value if compared to the mass of BHCs in our Galaxy. While it is plausible that individual ULXs could harbor such massive BHs, some scientists retain that unbeamed models for ULXs have to invoke to explain a class of too extremely massive compact object. As an example the "Antennae" galaxy contain up to 9 ULXs (Fabbiano et al., 2003b). Although such an high number of IMBH could have some difficulties to be explained from the point of view of their formation scenario, conversely, if we assume that the observed sources are beamed towards our line of sight, their total number could increase at least by a factor 4. Such a large number of microquasar-like sources in the "Antennae" example is usually explained with the presence of a major merger between the two galaxies that form the system that it is a not negligible factor for the formation of those kind of

binaries. At the same time is well known that also the formation of ULXs is triggered in interacting and star-forming regions. Here in the following I describe the main beamed model invoked to explain the existence of ULXs.

Geometrical funneling

The simplest candidate mechanism to avoid such high BH masses is geometrical funneling of the X-ray emission. This mean that the X-ray flux can emerge only in particular directions. For example a thick disc with a central funnel (for which the optical depth is lower only over a restricted range of solid angles), may allow very large apparent luminosities for standard BH masses. Assuming a beaming factor b ($b = \Omega/4\pi$, where Ω is the solid angle subtended by the funnel), if we define L_{iso} as the apparent isotropic X-ray luminosity of the source the "true" luminosity is:

$$L = bL_{iso} = 10^{40} \ bL_{40} \ \text{erg s}^{-1} \qquad (2.10)$$

where $L_{40} = L_{iso}/10^{40}$ erg s^{-1}. The minimum BH mass, assuming that the source does not exceed the Eddington limit, becomes:

$$M_{BH} \gtrsim 10^2 \ bL_{40}M_{\odot}. \qquad (2.11)$$

Therefore a beaming factor $b \sim 0.1$ decreases the estimated BH mass to $M_{BH} \gtrsim 10M_{\odot}$, in agreement with the values found for Galactic X-ray binaries (see (McClintock & Remillard, 2006)). The corresponding opening angle θ_0 of the funnel is given by:

$$4\pi b = \int_0^{2\pi} \int_0^{\theta_0} sin\theta \ d\theta \ d\phi = 2\pi(1 - cos\theta_0), \qquad (2.12)$$

that, for a beaming factor $b \sim 0.1$, gives $\sim 37°$.

As the luminosity is close to the Eddington limit, large values of the accretion rate are needed. King et al. (2001) propose that such beamed ULXs pass through a short-lived phase, common in the evolution of a large class of X-ray binaries, characterized by episodes of thermal-timescale mass transfer. In this phase the mass transfer rate become highly super-Eddington. The short X-ray lifetime of this phase ($\sim 10^5$yr) is balanced by the high birthrate, at least in the case of HMXB, of approximately few times 10^{-5}/yr. This mechanism seems to explain naturally also the association of ULXs with young stellar populations, as they would descend in this case from HMXB.

The "microquasar" model

The beaming factor ($b \sim 0.1$) invoked by King et al. (2001) is difficult to achieve with pure disk models. Some XRBs could be explained by a coupled disk/jet model, whose emission would naturally be relativistically beamed. Observations of BH candidate XRBs provide evidence of powerful collimated outflows when they are in the low/hard state (LHS, low luminosity/ hard X-ray spectrum, see Belloni et al. (2000)). In this state the X-ray spectrum is characterized by a power law component and a small (or no) thermal component. Only few XRBs have resolved jets in radio images, but a

number of both persistent and transient XRBs (e.g. Cyg X-1, GX 339-4, GS 2023+30, etc., see Fender (2001)) in the LHS reveals the presence of jets in broadband radio spectra with a flat-to-inverted synchrotron shape, as the signature emission of jets in AGNs.

A common scenario for the LHS and then the presence of jets in XRBs (Markoff et al., 2001; Körding et al., 2002) is that the outer part of the accretion disk consists of a standard optically thick disk (Shakura & Sunyaev, 1973) down to a transition radius $r_{tr} \sim 10^{2-3} r_s$ where the accretion flow turns into an optically thin advection dominated accretion flow (ADAF). The inner ADAF flow is hot and radiatively inefficient so that near relativistic electrons were injected in the jets with high energies allowed by the low inverse Compton cooling. Conversely, in the high/soft state, the cooling increases and the jet may disappear (Markoff et al., 2001).

Mirabel & Rodríguez (1999) pointed out that a number of nearby galaxies could host microquasar like objects with relativistically beamed jets pointed towards us. Körding et al. (2002) compared the X-ray luminosity function of nearby galaxies with two different population synthesis model: X-ray point sources with relativistic beaming in the first case and with isotropic emission in the second. They found that both models could explain the data (BHs with masses $\lesssim 10 M_\odot$ with relativistic jets or a distribution of IMBHs with masses up to $1000 M_\odot$).

In this respect the detection of radio emission in ULXs could be of great importance to discriminate between the beamed and unbeamed models. Up to now only a few sources were observed in radio, unfortunately without conclusive answers (see Section 2.3 for more details).

Super-Eddington luminosities via photon-bubble instabilities

Another model of ULXs that does not require the presence of a IMBH is that of Begelman (2002). In this model the emission is truly super-Eddington: the presence of photon bubble instability in a radiation pressure dominated magnetized accretion disk permits to the radiation to exceed the Eddington limit.

In luminous homogeneous accretion disks, the inner regions are radiation pressure dominated (Shakura & Sunyaev, 1973). If the luminosity approaches the Eddington limit for the central mass, the disk must be inflated to a thickness of the order of its radius. At the same time magnetized, radiation pressure dominated atmospheres tend to develop inhomogeneities on scales much smaller then the radiation pressure scale height (e.g. the disk scale height h) as a result of the nonlinear development of photon bubble instabilities. In this mechanism, gravity squeezes the radiation out of overdense regions, while the magnetic field enhances the overdensity by preventing the gas from spreading sideways. Thanks to the presence of such strong inhomogeneities the disk become "leaky" and the radiation is allowed to escape at a rate higher that that predicted by standard accretion disk theory, preventing the disk itself to become thick. The disk scale height is then smaller than that of the same disk without inhomogeneities, so the disk can remain geometrically thin even if the flux approaches or exceeds the Eddington limit. Also catastrophic mass loss, expected from the upper layer of the disk approaching Eddington luminosities, can be prevented by the presence

of inhomogeneities.

The model of Begelman (2002) predicts that the escaping flux can exceed the Eddington luminosity by a factor up to ∼10 for stellar mass BHs and to ∼100 for super massive BHs (e.g. AGNs). These values reflect a weak dependence of this process on the BH mass. ULXs with $L \gtrsim 10 L_{Edd}$ may be explained also in terms of such super-Eddington fluxes around stellar mass BHs without invoking IMBHs. As for the model of King et al. (2001), also in this case a very large accretion rate $\dot{M}$ is required and ULXs have to be short lived, since objects accreting at such high rates would double their mass in a few $\times 10^6$ yr. Furthermore the existence of very bright ULXs such as M 82 X-1 (Chapter 4) that exceed their stellar mass BH Eddington limit of a factor ~ 100, unexplained within the framework of the present model.

A model for very high accretion rates: the slim disk

At mass accretion rates comparable or greater than that corresponding to the Eddington limit ($\dot{M} \gtrsim L_{Edd}/c^2$) the accretion disk theory has another branch of stable optically thick solutions, the optically thick ADAF (Advection Dominated Accretion Flow) disks or slim disks (Abramowicz et al., 1988). With respect to the standard accretion disk (Shakura & Sunyaev, 1973) where all the gravitational energy is released locally as thermal radiation, in this model part of it is carried inward through radial advection. The slim disk is geometrically thick and hotter than the standard disk. In fact, at high accretion rates the basics assumptions and approximations of the standard disk break down. For example, the radial pressure is no longer negligible in the momentum equation and the advection term cannot be omitted in the energy equation.

The slim disk can reach luminosities up to ~ 10 times the Eddington limit of the system. From a qualitatively point of view, the local radiation pressure cannot exceed the vertical radiation force:

$$F(r) \lesssim \frac{cGM_{BH}}{kr^2} \frac{h/2}{r} \tag{2.13}$$

where $F(r)$ is the energy flux, r the disk radius, h the disk scale height. Hence, integrating on the disk surface:

$$L_{disk} \equiv 2 \int_{r_{in}}^{r_{out}} 2\pi r F(r) \, dr \lesssim \frac{4\pi cGM}{\kappa} \int_{r_{in}}^{r_{out}} \frac{h}{r^2} dr \approx L_{Edd} \left(\frac{h}{r}\right) \ln\left(\frac{r_{out}}{r_{in}}\right) \tag{2.14}$$

with r_{in} and r_{out} are inner and outer disk radius (with $ln(r_{in}/r_{out}) \approx 10$). While in a standard disk, that is geometrically thin and for which $h/r \lesssim 0.1$, the disk luminosity is lower than L_{Edd}, in the slim disk, in which $h/r \approx 1$, the luminosity may approach $\sim 10 \, L_{Edd}$. The slim disk luminosity cannot exceed $10 \, L_{Edd}$ because as the mass accretion rate exceeds the critical rate L_{Edd}/c^2, the energy conversion efficiency decreases due to advection. Then the disk luminosity is no longer proportional to the mass accretion rate, but saturates at $\sim 10 \, L_{Edd}$.

The slim disk has two characteristic properties. The first affects the radial dependence of the effective temperature. If we express this dependence as $T_{eff} \propto r^{-p}$

("*p*-free disk"), then, as advection progressively dominates and the mass accretion rate increases, the exponent p decrease from 0.75 to 0.5, flattening the slope of the temperature profile. The second is that, as in the previous cases, the very large accretion rate required to support the slim disk increases the temperature of the disk. This effect is enhanced also by the fact that the innermost radius of the disk can be closer to the BH than the last stable orbit (Mineshige & Watarai, 2005).

2.1.5   X-ray power density spectrum

Also the X-ray timing properties can be used to improve our understanding on ULXs. As Galactic XRBs show different timing features associated with their states, ULXs are expected to behave similarly, being binary systems. The most evident feature in the power density spectrum (PDS) of accreting systems is the presence of QPOs, quasi-periodic variability in the X-ray flux.

QPOs provide the highest frequencies observed in accreting systems hosting a compact object. Whatever their physical nature, they are likely to originate in the inner regions of accretion disks around BHs and are expected to be produced also in AGNs and ULXs. However, in the case of AGN the frequencies involved are much smaller because of the frequency dependence from the compact object mass (Lachowicz et al., 2006). The keplerian frequency for the motion an object of mass M at radius r_k is given by

$$\nu_k = \frac{1}{2\pi} \left(\frac{GM}{r_k^3} \right)^{1/2}. \tag{2.15}$$

where r_k is the last stable orbit around a Schwarzschild BH, $6GM/c^2$. We obtain an inverse relation of the frequency with the mass:

$$\nu_k \approx \frac{1}{2\pi} \frac{c^3}{6^{3/2}GM} \propto \frac{1}{M}. \tag{2.16}$$

Accretion onto a $\sim 10\ M_\odot$ BH has a characteristic Keplerian frequency of ~ 200 Hz. Higher masses may then produce rapid variability at lower frequencies, ~ 20 Hz for $M_{BH} \sim 100\ M_\odot$ and ~ 2 mHz for $M_{BH} \sim 10^6\ M_\odot$. As the Keplerian frequency scales inversely to the BH mass, it is not unreasonable to assume that the observed frequency of any QPO varies in the same way, whatever their origin.

An important issue is of course the possible identification of QPOs in ULXs with one of the QPO types observed in the X-ray light curves of stellar-mass BHCs. These QPOs can be broadly divided into three classes:

(a) *very low frequencies QPOs* : QPOs at very low frequencies (<0.02 Hz), probably associated to oscillations and instabilities in the accretion disk (see Morgan et al. 1997; Belloni et al. 1997, 2000);

(b) *Low-Frequency (LF) QPOs* : LF QPOs, with typical frequencies between 0.1 and 10 Hz, probably connected to similar oscillations in neutron star systems (see e.g. Belloni et al. 2002; Remillard et al. 2002b; van der Klis 2006; Casella et al. 2005), over whose origin there is no consensus; in Black Hole Candidates (BHCs)

3 main different types of LF QPOs have been identified (Casella et al. 2005, and references therein);

(c) *"hecto-Hertz" QPOs* : "hecto-Hertz" QPOs, with a typical frequency of 100-300 Hz, in two cases observed to appear in pairs (Strohmayer, 2001a,b). It is currently unclear whether these QPOs show a constant frequency for each source (see Homan et al. 2001; Remillard et al. 2002a), and whether they do appear in pairs obeying particular frequency ratios (see Remillard et al. 2002a).

For ULXs with QPOs, this provide an independent method to estimate the mass of the central remnant. The properties of the QPOs (frequency, rms, quality factor, variability) and of the underlying noise (break frequency, shape, intensity) can be compared with the properties of the QPO types described above. Once the QPO type is identified univocally, then scaling arguments can be used to estimate the BH mass.

Up to now very few objects have been found to show features in their PDS. The best case is the very bright ULXs M 82 X-1. Strohmayer & Mushotzky (2003) first detected a QPO at 54 mHz in the PDS of *XMM-Newton* observations of the source. We also extensively studied the timing properties of this ULX and our results are reported in Chapter 4. The identification of this QPO, also present in *RXTE* and more recent *XMM-Newton* observations, with a type C QPO in BHCs lead us to estimate a BH mass between a few tens to one thousand solar masses.

Recently other two identification have been reported. Strohmayer et al. (2007) found a 20 mHz QPO in the 0.2-5 keV X-ray flux of the ULX NGC 5408 X-1, suggesting a connection with the very-high states of Galactic systems.

2.2 Optical observations: counterparts and environment

The optical band may give a fundamental contribution to the interpretation of ULXs through the identification and study of their optical counterparts. The determination of their spectral type can constrained the binary type and then its evolutionary history. The spectroscopy, where possible, of the ULX companion may enable the measurement of the radial velocity profile, leading to a direct estimate of the BH mass and then to definitively discriminate between the intermediate and the stellar mass BH interpretation of ULXs. Moreover the environment provides information on the progenitor of ULXs (i.e. young or old population) and on the condition required for their formation and occurrence, as low metallicity or high star formation rates. Last but not least, the association of some ULXs with optical emission nebulae enable us to investigate their formation scenarios and to determine the energetics of the system.

2.2.1   Optical counterparts of ULXs

Optical observations are crucial to identify ULX counterparts and clean up the sample from the contamination of known X-ray sources. Some ULXs were identified with background AGNs through optical follow-up spectroscopy (see Section 2.1.1). Up to now only a very small number of ULXs have been convincingly associated with stellar objects (e.g. Liu et al., 2002, 2004; Kaaret et al., 2004; Zampieri et al., 2004; Mucciarelli et al., 2005, see below).

A significant steps forward in the identification of optical counterparts of ULXs were performed by the X-rays/optical *Chandra*/*HST* observations because of their good spatial resolution. Pre-*Chandra* positions of ULXs, mainly from *ROSAT* and *XMM-Newton* observations, suffer of significant positional errors ($6''$ and $4''$ at $2\,\sigma$ for *ROSAT*-HRI and *XMM* EPIC MOS respectively). Consequently a large number of stars may fall in their error circles, especially when ULXs are associated with crowded star-forming regions and/or have weak optical counterparts. *Chandra* improved the situation but the identification is still difficult. Two illustrative examples are NGC 1313 X-2 and NGC 5204 X-1. In the first case the ROSAT position suggested a relatively bright source as the counterpart of NGC 1313 X-2 (Stocke et al., 1995). The *Chandra* aspect position ruled out such source and allowed the identification of a nearby weaker counterpart. Finally, only VLT and *HST* observations resolved the counterpart in two distinct objects, a early type main sequence and a G-K supergiant (see Chapter 3). Goad et al. (2002) analyzed an *HST* image of the field of NGC 5204 X-1. Unfortunately, the size of the *Chandra* error circle includes some potential counterparts. Measuring the magnitudes and colors of these objects, Goad et al. (2002) identify them with a F supergiant plus a few early type supergiants and a small and young stellar cluster. However, the interpretation is not univocal.

The situation can be significantly improved if objects with known optical, X-ray and possibly radio positions can be identified in the ULX field. In this case, the relative optical/X-ray astrometry can made more accurate using these sources. Unfortunately, the number of cases where this has been possible is small. Usually the *Chandra* and *HST* fields have a low number of overlapping sources. Liu et al. (2002) used the interacting SN 1993J to align the *HST* and *Chandra* images of M81. They obtained relative astrometry accurate to $0.2''$ and identified a unique optical counterpart to the ULX NGC 3031 X-11. Zampieri et al. (2004) exploited the presence of SN 1978 K in NGC 1313 for relative astrometry to identify the counterpart of the ULX X-2 (Section 3.3). When multiple associations are possible multiwavelength observations of field objects can be used to point out the actual counterpart of the ULX as done from Liu et al. (2004). They were able to pinpoint a unique counterpart to the NGC 5204 X-1 among the three found by Goad et al. (2002) (see above). The fact that ULXs are often associated with optical emission nebulae (see below, Section 2.2.2) can also be exploited to obtain a unique counterpart identification without recurring to highly accurate relative astrometry.

Once identified the ULX counterparts, optical spectroscopy enables detailed analysis of their properties. First of all, the identification with a background AGN is easy if the spectrum shows redshifted emission lines. The potential of the spectral analysis

is not limited to the identification of the optical counterpart and its properties, but may give fundamental information on the ULX binary system:

- the presence of emission lines in the spectrum not usually seen in stars, are the signature of reprocessed emission from an X-ray illuminated accretion disk. They can also be used to confirm the identification of the companion;

- the detection of shifts in the position of spectral lines from the optical companion raises the exciting possibility to obtain a radial velocity curve and therefore a dynamical measurement of the compact object mass.

The latter point is of fundamental importance in order to resolve the debate on stellar mass BHs versus IMBHs. Although the evidence coming from X-ray data alone is not conclusive, the detection of shifts in the emission/absorption lines will permits to measure the mass function of these systems and the masses of their compact remnant.

The presence of an optical emission nebula associated with the ULX may cause some difficulties in pinpointing the (permitted) lines produced by X-ray reprocessing on the disk and companion surfaces because of the contamination from the nebula, especially in the case of a complex morphology.

Optical counterparts of ULXs in star-forming regions or association of massive stars

The great majority of ULXs are hosted preferentially in star-forming galaxies. Currently there are only 4 optical counterpart identified with single stars (Liu et al., 2002, 2004; Kaaret et al., 2004; Mucciarelli et al., 2005, 2007, see also Figure 2.1). Despite the quite small number, a significant trend appears to emerge from this sample. The optical counterparts have properties consistent with those of early young, massive stars, in particular O or B stars. In these systems X-ray reprocessed emission, from both the disk and the star itself, may contribute to the optical light, so that care must be taken in interpreting the spectral type (see Section 3.4.8 in which we describe a model of the reprocessed emission and its application to the X-rays/optical data of NGC 1313 X-2).

ULXs preferentially occur in starburst galaxies and the most luminous ULXs are often found near sites of active star formation (Zezas & Fabbiano, 2002). Starburst galaxies are the natural location of such regions. In starburst, a substantial fraction of young stars are found in "super star clusters" (SSC, luminous, compact clusters containing up to $10^6 M_\odot$ of stars within a radius of a few parsecs). Portegies Zwart et al. (2004) found that stellar encounters in such dense clusters may lead to enhanced production of binaries, in particular binaries containing compact objects.

Kaaret et al. (2004) studied the spatial correlation between the X-ray population (including ULXs) and stars clusters of the three starburst galaxies M 82, NGC 1569 and NGC 5253. The position of the X-ray sources are well correlated with the SSCs, but have significant offsets from them. Furthermore, the X-ray sources preferentially occur close to clusters and there is a lack of very bright sources at large displacements from the clusters. Because the super star clusters are very good tracers of current star

formation activity, the good positional correlation of X-ray sources with SSC indicates that the X-ray sources are young objects associated with current star formation. This may suggest that the X-ray sources and the ULXs in particular could be produced via dynamical interactions in the SSCs (Portegies Zwart et al., 2004). The offset of the X-ray sources from the SSCs could be explained in terms of ejection of the X-ray binary through dynamical interactions within the clusters. The absence of luminous sources (L> 10^{38} erg s^{-1}) at large displacements imply first that the switch-on (capture of the companion and start of the accretion phase) of these ULXs occurs promptly after the creation of the binary without significant delay and second that the X-ray emitting lifetime of the sources has to be limited.
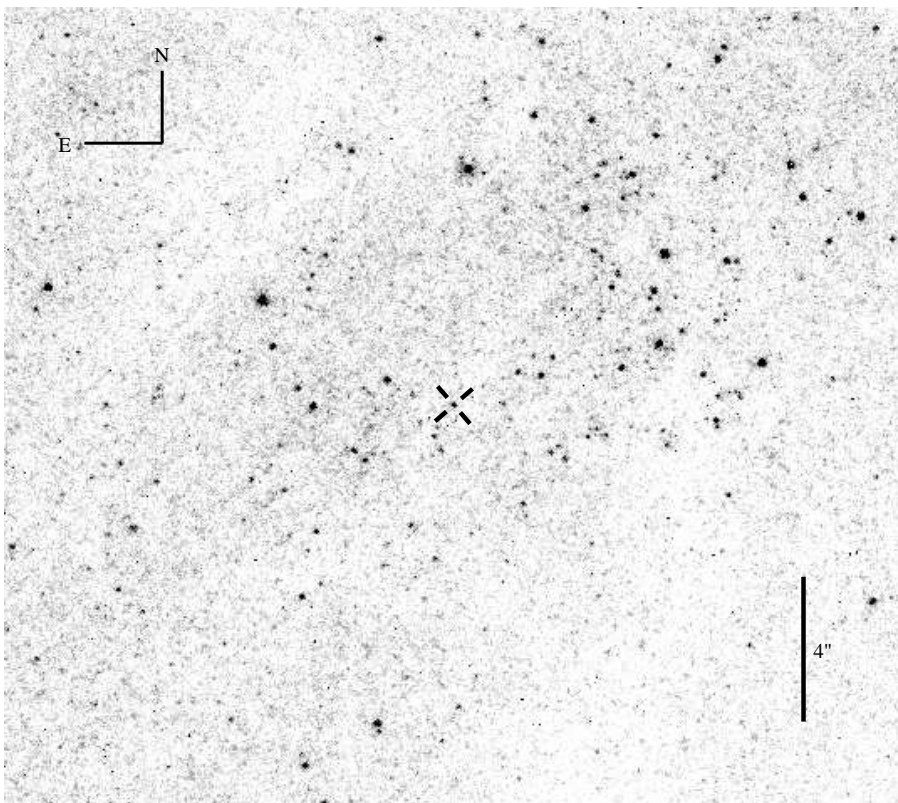
Figure 2.1: The optical counterpart of NGC 3031 X-11 and its environments. The counterpart is indicated by a cross. Its absolute magnitude and colors correspond to those of an O8V star (Liu et al., 2002).

Optical counterpart of ULXs in elliptical galaxies

The presence of ULXs in early-type galaxies in which there is no active star formation and the stellar population is old (Pop.I), is still matter of debate. Irwin et al. (2004) showed that the numbers of very bright X-ray sources in early-type galaxies (L$\gtrsim$ 2×10^{39} erg s^{-1}) are consistent with the expected number of foreground/background sources, mainly AGNs. However, it is worth noticing that ULXs identified with QSOs (Foschini et al., 2002b; Masetti et al., 2003) lie far away from the central part of the

host galaxy, improving the probability of serendipitous coincidence.

Despite the claim that there are no ULXs in ellipticals, however two identifications of ULXs with globular clusters have been reported: one in NGC 1399 (Angelini et al., 2001) and the other in NGC 4565 (Wu et al., 2002). The isotropic X-ray luminosities of these ULXs can be as high as than few $\times$ 10^{39} erg s^{-1}, in the lower range of those exhibited by ULXs. However, this emission could be also produced by the summed output from several different objects (e.g. LMXBs of the cluster). Moreover, the elliptical galaxy NGC 720 also hosts a population of 9 ULXs, three of which associated to GCs (Jeltema et al., 2003). However, the high number of objects and the spatial arc-like distribution are peculiar and it has been suggested that they are remnants of a hidden young stellar population associated to a possible recent merger event. More recently also a ULX in NGC 3379 has been reported by Fabbiano et al. (2006).

For the ULXs in GCs, the presence of IMBHs may be attributed to the effects of dynamical interactions in a dense stellar environment, in a similar way to the case described above for SSCs. Such BHs may remain within the clusters and later capture a star to become active again at the current epoch (Portegies Zwart & McMillan, 2002). However, because of the old stellar population of elliptical galaxies, the host ULXs may also be LMXBs with beamed emission (see Section 2.1.4). King (2002) suggest that they may be soft X-ray transients in outburst, as recently reported by Fabbiano et al. (2006) for the ULX in NGC 3379.

2.2.2   Nebulae around ULXs

A significant fraction of unobscured ULXs are surrounded by optical emission nebulae. It is not unlikely that all ULXs are associated to such structures, considering that many of them are seen in edge-on galaxy and in strongly absorbed regions. These ULX Nebulae (ULXNe) are typically young ($\sim$ 1 Myr) and very extended (few hundreds parsecs in diameter) and show both low and high ionization emission lines. Therefore the gas must be either photoionized by the X-tray emission or be shock-ionized in the expanding bubbles. The nebulae have kinematic ages of some million years and appear to be directly linked to the highly energetic formation process of the compact ULX or being inflated by ongoing stellar wind/jet activity. Relatively compact X-ray ionized nebulae can be used to independently infer the ULX luminosities, and thus exclude possible beaming effects into our line of sight. Larger bubble-like nebulae reach several hundred parsec diameters and provide important information on the formation of the associated ULX.

A pioneering work in this respect is the optical survey of ULXNe presented by Pakull & Mirioni (2002). The narrow band images shown in Figure 2.2 represent some of the most spectacular ULXNe. A comprehensive list of the observed ULXNe with their peculiarities is reported in Table 2.2 at the end of this Section.

More in detail the nebulae identified to date show some interesting similarities. At least in one case (see below) the effects of the X-ray source ionization allowed to independently estimate the measure of the ionizing luminosity. Most of the ULXNe show the presence in the outer region of strong [SII] and [OI] emission lines and of
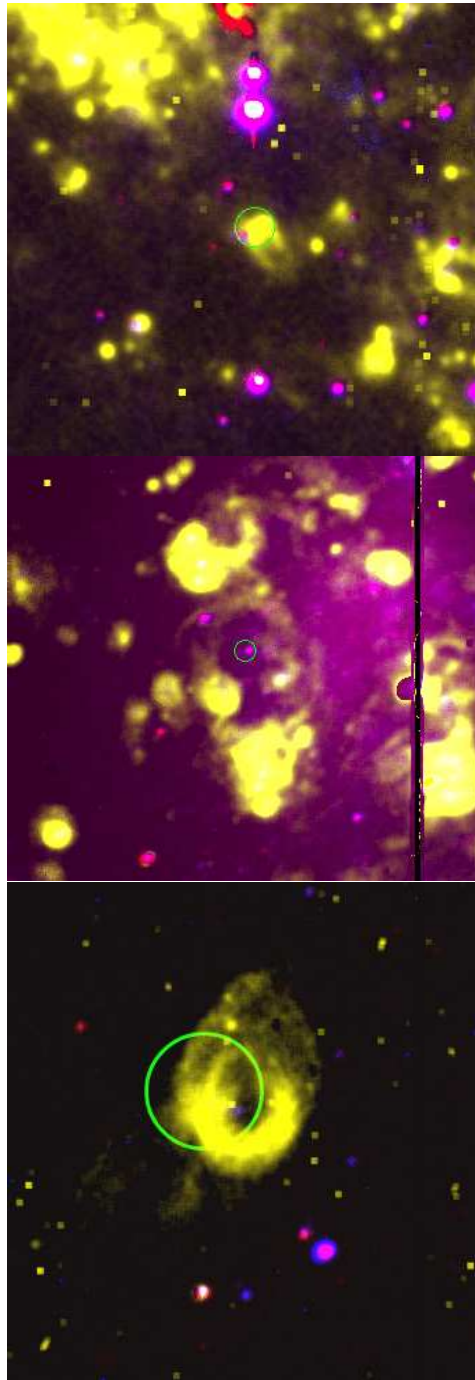
Figure 2.2: *Top*: the field of the ULX IC 342 X-1 with the "Tooth" nebula (220 pc diameter). The *ROSAT* error circle is shown. *Center*: the field around the ULX NGC 5204 X-1 contains many H II regions and a striking ring-like structure (360 pc diameter) centered on the X-ray source. The circle is the *Chandra* position. *Bottom*: the barrel shaped nebula (250 pc diameter) surrounding M 81 X-9 in the dwarf galaxy companion Holmberg IX. The HRI error circle includes a small group of faint blue stars possibly associated with the ULX. All the images represent H_α band in yellow, B in blue and R in magenta. From Pakull & Mirioni (2002).

supersonic expansion speeds of 80 to 250 km s^{-1} (from the H$_\alpha$ width). This suggests that the nebula is shock-heated rather than photoionized. In analogy with standard SNRs, a natural explanation of the formation of ULXNe is in terms of expanding shells of material powered by initial explosions. From the observed properties it is possible to estimate the kinetic energy involved. If the ULXNe is formed in an explosive event with kinetic energy E_o and assuming conservation of energy:

$$E_o \approx 1.99 \times 10^{52} \text{erg} \left(\frac{R}{100 \text{ pc}} \right)^3 \left(\frac{v}{100 \text{ km s}^{-1}} \right)^2 n, \qquad (2.17)$$

$$\frac{t}{10^6 \text{ yr}} \approx 0.4 \left(\frac{R}{100 \text{ pc}} \right) \left(\frac{v}{100 \text{ km s}^{-1}} \right)^{-1} \qquad (2.18)$$

where R is the shell radius, v its expansion velocity, n the interstellar particle density and t the age. The same calculation can be performed assuming that the origin of the bubble is inflation from a wind/jet mechanism. In this case the mechanical energy L_w is:

$$L_w \approx 3.8 \times 10^{39} \text{erg} \left(\frac{R}{100 \text{ pc}} \right)^2 \left(\frac{v}{100 \text{ km s}^{-1}} \right)^3 n, \qquad (2.19)$$

$$\frac{t}{10^6 \text{ yr}} \approx 0.6 \left(\frac{R}{100 \text{ pc}} \right) \left(\frac{v}{100 \text{ km s}^{-1}} \right)^{-1} \qquad (2.20)$$

Typical ages of ULXNe are of the order of 10^6 yr with densities in the range of 0.1-1.0 cm^{-3}. Given also their high radii of the order of few hundreds parsecs, the previous formulae result in very large energy requirements for such objects, of the order of $\sim 10^{52-53}$ erg in the SNR scenario and $\sim 10^{39-40}$ erg s^{-1} in the case of wind/jet inflation. Such energies may be provided by hypernovae or multiple SN explosions, but they could also be lower by 1-2 orders of magnitude if the explosion occurred in a low density region or in a clumpy ISM.

Irrespectively of their formation, the observed emission of the nebulae may be sustained by photoionization of the ULXs themselves. If the X-ray emission ionizes the nebula, then the atoms produce line emission from high excitation states. The main difference of X-ray ionized nebulae (XINs) with respect to more conventional HII regions is the absence of sharp transitions between ionized and neutral plasma at the outer boundary, like in a Strömgren sphere. This happens because the X-rays are not very efficiently absorbed and creates an extended warm weakly ionized zone at an electron temperature of $\sim 10^4$ K, in which neutral atoms can be collisionally excited. Then the hallmarks of XINs are emission lines from highly ionized gas (e.g. HeII λ 4686 A) close to the ionizing source and from forbidden transitions of neutral elements like [OI] λ 6300 A in the extended outskirts.

The BH calorimeter of Kaaret et al. (2004)

If we assume that a nebula is powered by photoionization, it is possible to measure the total energy output of the ULX, enabling us to finally understand if the X-ray emission is beamed or not along our line of sight.

ULX	Nature	References	Description
IC 342 X-1	nebula	$a; b$	Tooth-shaped nebula, diameter 220 pc, SNR-like emission line ratios (Figure 2.2)
Ho II X-1	XIN	$a; b$	Foot-shaped nebula, heel diameter 34 pc (Figure 2.2), high excitation [OIII]
M 51 X-7	nebula	b	cluster with offset nebular emission
M 81 X-6	nebula	c	Barrel-shaped nebula (MF 22 and MF 23), enhanced [SII]/H$_\alpha$ ratio
M 81 X-9/Ho IX X-1	bubble	a, b	Barrel-shaped nebula LH 9/10, diameter 200×400 pc, high line ratios (Figure 2.2)
M 101 P098	nebula	b	High excitation [OIII], elongated shape 35×140 pc
NGC 1313 X-1	nebula	a	Diameter 240 pc, with high [OI]/H$_\alpha$ ratio extended for 800 pc
NGC 1313 X-2	bubble	$a; d$	Complex structure (see Section 3.3.1 and 3.4.5), diameter 400 pc
NGC 4559 X-7	Hɪɪ	a	—
NGC 5204 X-1	bubble	a	Diameter 360 pc (Figure 2.3)
NGC 6946 X-1	nebula	b	Peculiar nebula MF 16 photoionized by an ultraviolet source, 20×34 pc
NGC 7331 X-1	Hɪɪ	b	Hɪɪ region associated with a young star cluster

a: 1=Pakull & Mirioni (2002);

b: 1=Abolmasov et al. (2007);

c: 1=Pakull & Mirioni (2003);

d: 1=Zampieri et al. (2004); Mucciarelli et al. (2005);

Table 2.2: ULXs in nearby galaxies known to be associated with optical nebulae. A brief description of the emission and references are also given.
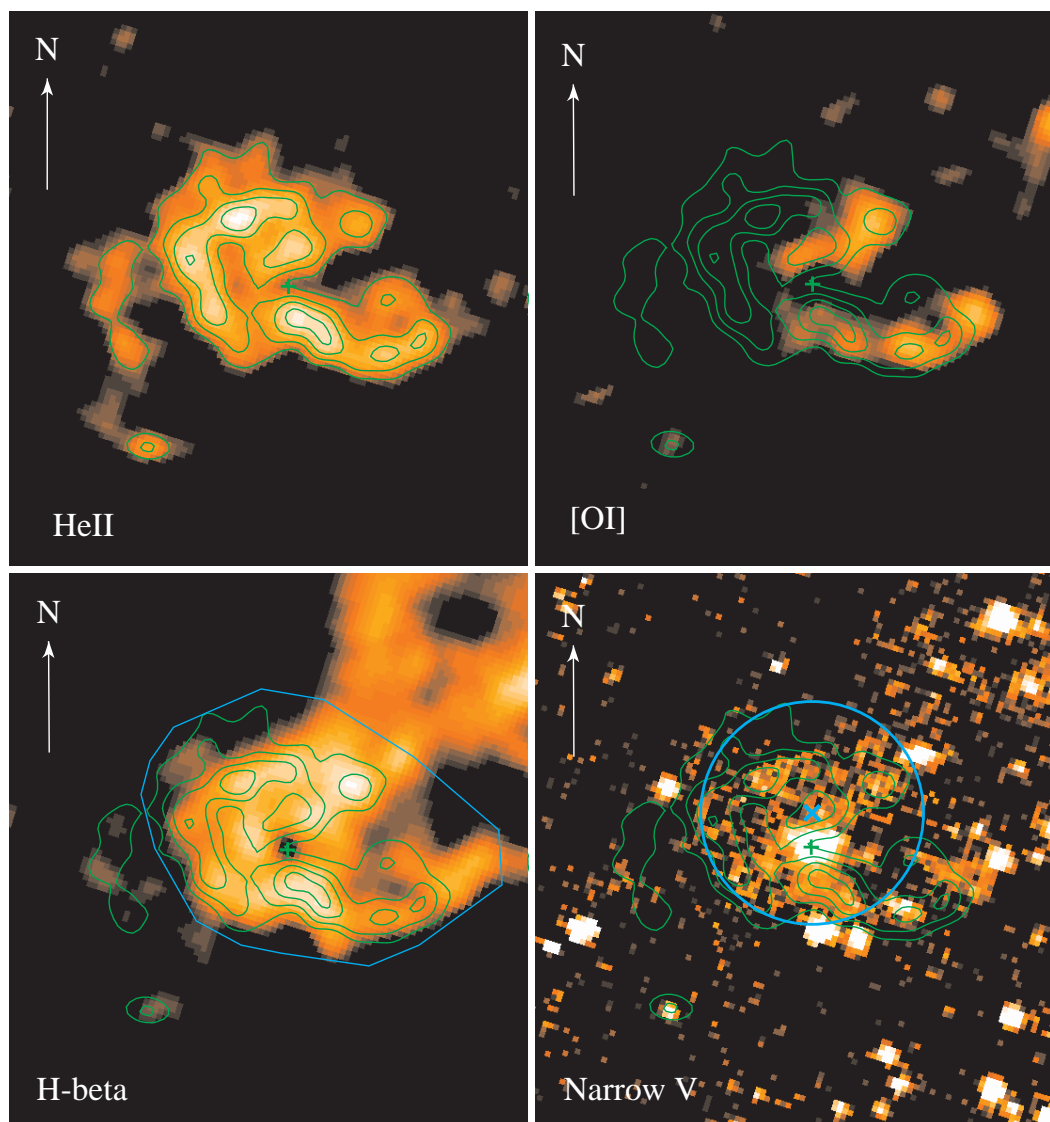
Figure 2.3: False color images of the continuum subtracted line emission of the nebula associated to Holmberg II X-1 from Kaaret et al. (2004), for HeII, Hβ, and [OI] and for the narrow V-band continuum. In each image, the arrow points Northward and has a length of 1″ (15 pc), the green cross marks the position of the bright star within the nebula, and the green curves are contours of the HeII emission. The cyan circle and 'X' in the narrow-V image denote the best *Chandra* position for the ULX and the relative *Chandra*/*HST* error circle with the associated optical counterpart.

A particularly useful emission line in XINs is the λ 4686 A from the fully ionized He. This line acts like a photon counter: at most one HeII is produced for each X-ray in the range from 54 eV (the ionization threshold of He) to about 300 eV. This implies that the HeII emission is proportional to the ionizing luminosity.

A template case in this respect is an ULX hosted in Holmberg II, source X-1 (Pakull & Mirioni, 2002; Kaaret et al., 2004). Although the morphology of the whole nebula associated with Holmberg II X-1 is rather complex (the "Foot" nebula of Figure 2.3), the HeII nebular emission comes mainly from the "Heel" and it is likely isotropic. The suggestion that the nebula is photoionized is also confirmed by the

H$_\beta$ and [OI] behavior. The total HeII luminosity inferred from *HST* data is 2.7 $\times$ 10^{36} erg s^{-1}. The X-ray spectrum from *XMM-Newton*, fitted with a Comptonization model and extrapolated to the 54-300 eV interval, was used as an input to model the photoionization and to check if it could produce the observed He II line luminosity. The estimated X-ray luminosity is at least 4-6 $\times$ 10^{39} erg s^{-1}, in agreement with the inferred isotropic luminosity of the source. The minimum BH mass estimated applying the Eddington limit is then 25 $M_\odot$, establishing this source as truly ultraluminous.

2.3 Radio observations

In the search for counterparts in other wavelength bands it is natural to look also in the radio domain. The radio data have excellent angular resolution and sensitivity and contain unique diagnostics for understanding the nature of the sources. Moreover radio wavelengths do not suffer of extinction by the interstellar medium.

Under the assumption that the radio emission is powered by the same source that produce the X-ray emission, then the radio morphology may help understanding whether or not relativistic jets or beaming are present in ULXs, possibly discriminating between the stellar and intermediate mass BH scenarios. In general, three different cases are possible:

- unresolved, *compact luminous radio cores* at the position of ULXs: this is consistent with beaming towards us (as in the case of microblazars) and has been observed in the ULX NGC 5408 X-1 (see below and Kaaret et al., 2003);

- resolved *extended emission*: this morphology rules out beamed emission, favoring the IMBH scenario. The coincidence with the optical morphology of emission nebulae strengthens this interpretation, as in the case of Holmberg II X-1 (Miller et al., 2005);

- *resolved jets or double radio, jet morphology* with typical quasar or radio galaxy appearance: this supports the idea that the source is a background AGN, especially for objects located at peripheral galactic location (Sánchez-Sutil et al., 2006).

As their nearest cousins, XRBs in the Very High State (VHS), also ULXs are expected to be *radio transients*. Radio flares are observed nearby the bright ULX M 82 X-1 (Körding et al., 2005). Also radio fluxes and spectral indices can be used to evaluate the emission mechanism and the energetic and lifetime of the source.

Kaaret et al. (2003) observed the ULX NGC 5408 X-1 in two radio bands, 4.8 (see Figure 2.4) and 8.64 GHz, detecting a compact core in coincidence with the ULX only in the first band. The radio spectral index derived from the flux at 4.8 GHz and the upper limit at 8.64 GHz is $\alpha > 1$ (where the flux is $S_\nu \propto \nu^{-\alpha}$, Miller et al. 2005). The radio, optical and X-ray properties of the ULXs are consistent with a binary system, in particular with beamed emission of a relativistic jet from a stellar mass BH.
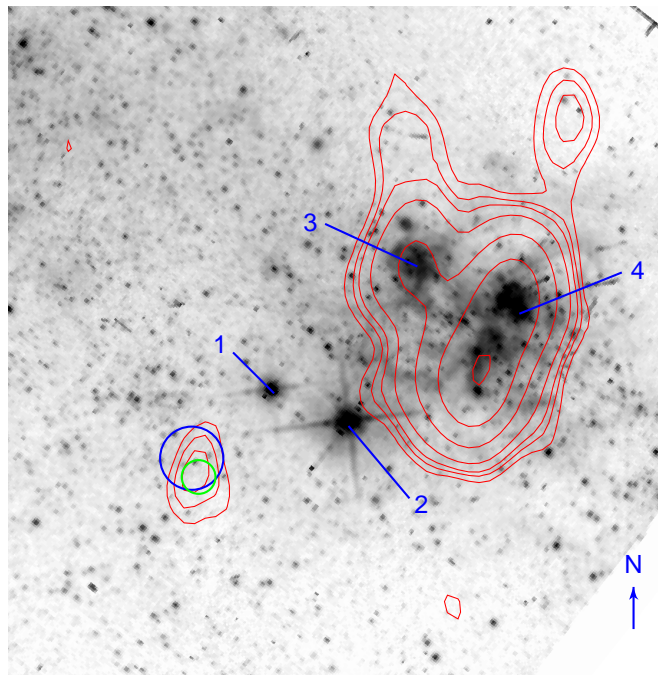
Figure 2.4: *HST* F606W filter image of NGC 5408 X-1 from Kaaret et al. (2003) with the ATCA 4.8 GHz radio contours (red), the error circles of the *Chandra* (blue) and ATCA (green) positions, and the main surrounding star formation regions (blue).
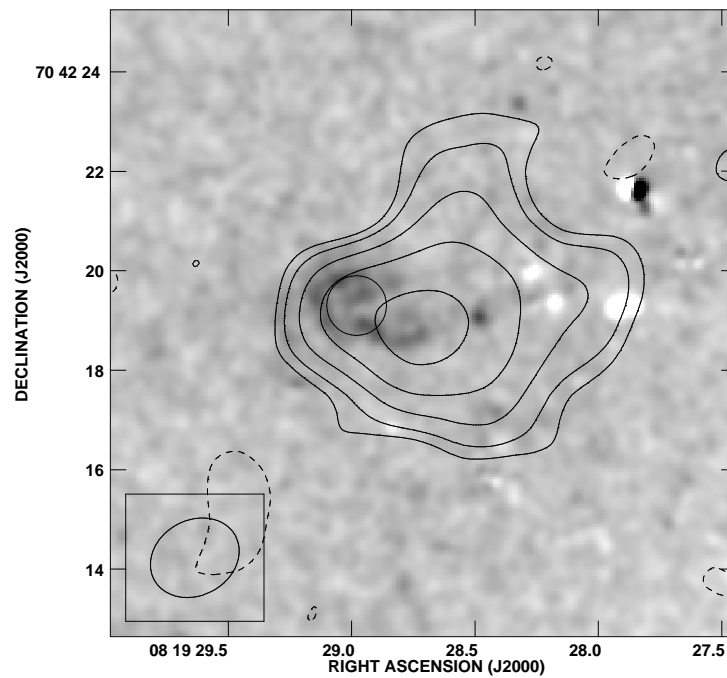
Figure 2.5: 1.4 GHz contours of the radio source coincident with Holmberg II X-1, overlaid on the He II image. The *Chandra* position is indicated by a circle (positional uncertainty of 0.7″, from Miller et al. 2005.

ULX	nature	reference
Ho II X-1	extended emission	Miller et al. (2005); Mushotzky (2004)
NGC 3877 X-1	extended emission (possible LLAGN)	Miller et al. (2005); Mushotzky (2004)
NGC 3877 X-2	SN 1998S	Miller et al. (2005)
NGC 4314 X-1, X-3	very large radio emission (more than few SNR)	Mushotzky (2004)
NGC 4631	four aligned components (background radio gal.)	Miller et al. (2005); Mushotzky (2004)
NGC 4736 ULX-1	strong radio emission in coincidence with a LLAGN	Körding et al. (2005)
NGC 7424 ULX-2	off-set bright unresolved radio source (SNR or jet)	Soria et al. (2006)
M 82 X-1	off-set SNR and off-set flares	Körding et al. (2005)
NGC 5408 X-1	compact core consistent with beaming	Kaaret et al. (2003)

Table 2.3: Known radio counterparts of ULXs.

The opposite case is represented by the radio emission associated with the ULX Holmberg II X-1 that is diffuse and extended with a size of $3'' \times 2''$ ($\sim 60 \times 40$ pc at the distance of the host galaxy). Miller et al. (2005) compared optical, X-rays and radio data ruling out an association with either a H II region or a SNR (see Figure 2.5 for a comparison of the optical nebular emission and the radio flux). The spectral index derived from the fluxes at 1.4 and 4.86 GHz is α=0.27±0.36. For both bremsstrahlung and synchrotron emission, the source lifetime is 10^8 yr. The radio to X-rays flux ratio is about 6×10^{-6}, consistent with the values observed in microquasar-like sources. The radio nebula in Holmberg II X-1 has the same extension as the optical nebula reported in Section 2.2.2. The extended radio emission and the properties of the optical nebula support the interpretation that this ULX is one of the best candidates for a true IMBH binary.

To date, the number of cases in which radio counterparts of ULXs has been detected is not sufficient to establish statistically robust conclusions. In Table 2.3 we report the detection of radio emissions associated with ULXs and their main characteristics. Only recently cross correlation between ULX and radio catalogs starts to appear in the literature (Mushotzky, 2004; Sánchez-Sutil et al., 2006).

Interesting the number of radio counterparts to ULXs may lead to a significant boost in our understanding of these sources.

2.4 Statistical properties from X-rays catalogs of ULXs

Studies on the statistical properties of ULXs rely mainly on *ROSAT* HRI (Colbert & Ptak 2002; Liu et al. 2005) and *Chandra* (Swartz et al., 2004) observations for accurate celestial positions.

In the *Chandra* survey by Swartz et al. (2004), a total of 154 ULXs out to 3400 sources were detected (about 5%) in a total of 82 galaxies. Among these ULXs, 57 are hosted in elliptical galaxies and 97 in spirals with an average value of ~ 2 sources per galaxy. Power-law X-ray spectral fits show that the spectral indices of ULXs have a Gaussian distribution with $< \Gamma >= 1.9 - 2.0$, similar to that of non-ULXs sources. Also the location in their host galaxies and the spatial distribution of ULXs are similar to that of less luminous X-ray field sources. There is evidence of a correlation between the luminosity function of ULXs and the morphological type of the host galaxies. More luminous ULXs tend to occur preferentially in spiral galaxies: 2 sources out of 3 have $L > 2 \times 10^{39}$ erg s^{-1}, while only 1 out of 3 ULXs in ellipticals are this luminous. There exists also a strong correlation between the ULXs properties and the host galaxy far-IR luminosity in spirals. About 14% (5%) of the ULXs are slightly (significantly) variable during an observation.

From the available observations, ULXs turn out to be a composite population. Swartz et al. (2004) found that a large fraction ($\sim 25\%$) are, in fact, background AGNs. The contamination is stronger in ellipticals (44% of the sources, to be compared with a 14% in spirals). Another source of contamination are supernovae interacting with the circumstellar medium, ~ 22 % of the total (e.g. SN 1978K, SN 1993J). A

contamination from very soft, thermal sources (similar to Galactic Super-Soft Sources, e.g. Di Stefano & Kong 2003) is also present. Finally, it has been suggested that some ULXs may be young, Crab-like pulsars, powered by rotation (Perna & Stella, 2004). However, for the majority of ULXs, the X-ray variability (on hours, months, years timescale), spectra and correlated luminosity/spectral variability are strongly suggestive of accreting binaries.

2.5   X-ray binary source populations and ULXs

The X-ray binary source populations in nearby galaxies is an important component of the X-ray emission of galaxies (see e.g. Fabbiano, 2006). In this respect, our Galaxy provides us with a well studied and representative sample that can be used to interpret X-ray observations of external galaxies (e.g. Grimm et al., 2002; Gilfanov, 2004). At luminosities greater than 10^{37} erg s^{-1}, both LMXBs and HMXBs are present, but also young SNRs may be expected to contribute. LMXBs are an old population of accreting compact objects with a low mass companion and an estimated life-time of $\sim 10^{8-9}$ yr. HMXBs are younger compact accreting systems and a shorter life-time of $\sim 10^{6-7}$ yr. They are born as massive binary systems where the more massive star already evolved off the main sequence and exploded as a SN.

An important tool to study the global properties of these populations is their X-ray Luminosity Function (XLF), i.e. the number distribution of sources as a function of their X-ray luminosity, both in the differential or cumulative form. Although the first studies in this area started already with the *Einstein* survey of normal galaxies (Fabbiano, 1989; Fabbiano et al., 1992), the sensitive sub-arcsecond *Chandra* observations, complemented with *XMM-Newton* data, led to a significant step forward (Sarazin et al., 2000; Soria & Wu, 2003). In this studies, contamination of the sample and variability of the X-ray sources have to be taken into account. The completeness of the sample may affect the estimate of the XLF as well as the low statistics, at low energy because of the cut in sensitivity of the present satellites and at high energy because of the true paucity of bright sources.

As they are associated with old populations, it is easier to study the global properties of LMXBs in early-type galaxies (E and S0), where the contamination form younger X-ray sources, HMXBs and SNRs, is expected to be small or absent. In E and S0 galaxies, populations of several tens to hundreds sources have been detected. The X-ray colors and spectra of these sources are consistent with those of LMXBs, except for a few Super-Soft Sources (SSS). Irwin et al. (2003) investigated a sample of 15 nearby early-type galaxies with *Chandra* and found that only few sources with luminosities of $1-2 \times 10^{39}$ erg s^{-1} are present in 10 galaxies of the sample.

XLFs are usually fitted with a PL taking into account for the possible presence of breaks, but their presence is still under debate. Recently Kim & Fabbiano (2004) compute the *Chandra* XLFs of a sample of 14 early-type galaxies. The composite differential XLF shows a slope of 1.8±0.2 up to a luminosity of $\sim 5\times \sim 10^{38}$ erg s^{-1}, then steepens (with an index 2.8±0.6). A cut-off may be present at luminosities greater than $\sim 10^{39}$ erg s^{-1}. The steepen at high luminosity indicates a lack of

very bright sources in early-type galaxies. Gilfanov (2004) essentially confirmed these findings. Although the high luminosity XLF is somewhat steeper, they found a cut-off at a similar luminosity.

The XLF of late-type galaxies, both spirals and irregulars, is a more complicated matter. The association of HMXBs with the young stellar population of galaxies is well known and they are expected to dominate the X-ray emission of star forming galaxies (Helfand & Moran 2001; see also the review Fabbiano 2006). As they are marker of recent star formation (see above), their number correlates with the galaxy star formation rate (SFR) and their number in each galaxy varies from few tens to more than hundreds of sources. In normal galaxies their contribution can be smaller, due to the less intense SFR and the mixed presence of older stellar populations. The complexity of the X-ray source populations in spiral galaxies shadows their stellar population and evolution. Consequently the XLF of late-type galaxies is the sum of contributions of various X-ray populations of different ages (and metallicity, e.g. M 31, Kaaret 2002; Kong et al. 2002, M33, Grimm et al. 2005, M 51, Terashima & Wilson 2004, M 81, Swartz et al. 2003, M 83, Soria & Wu 2003, etc.). Taking M 81 as an example (Swartz et al., 2003), disk sources show flatter XLF than that of the bulge. The XLFs relative to the arms is instead very flat, indicating a massive presence of young, high luminosity sources. The XLF itself becomes steeper at higher distances from the spiral arms.

A similar work to the one performed for early-type galaxy by Kim & Fabbiano (2004), was performed by Grimm et al. (2003) on a sample of 10 star-forming galaxies observed with *Chandra*. Their data were broadly consistent with the existence of a universal XLF of HMXBs with a slope of ~ 0.6, a cut-off at a luminosity of $\sim$ few $\times 10^{40}$ erg s^{-1} and a normalization proportional to the star formation rate. Nevertheless a number of more complex behaviors are also observed (also other SFR-dependent effects are present). Consistent results were found by other authors. In general, the HMXB XLF is flatter than that of LMXBs, implying that young HMXB populations contain on average a larger fraction of very luminous sources than the old LMXB populations.

This problematic is directly connected with the issue of where ULXs stand from the point of view of X-ray source populations. From a sample of 13 galaxies, Humphrey et al. (2003) deduced a strong connection between the number of ULXs in each galaxy and its 60 μm emission and no relation with the mass of the galaxy. The Swartz et al. (2004) *Chandra* catalog of ULXs indicated the association of ULXs with young stellar populations, in particular in merging and colliding galaxies. Clear examples of ULXs-SFR correlation are found in the "Antennae" (Zezas & Fabbiano, 2002) and in the "Cartwheel" (Wolter & Trinchieri, 2004) galaxy, both merging systems, very rich in ULXs.

A comprehensive study of 299 ULXs from literature shows that the brightest ULXs ($L_X \gtrsim 10^{40}$ erg s^{-1}) can be found in both star-forming galaxies and in the halo of early-type galaxies (Liu & Mirabel, 2005). In the latter the number of ULXs seems to correlate with the galaxy mass. As mentioned above, Grimm et al. (2003) found that there exists a universal luminosity function of X-ray binaries (applicable to several different galaxies) where the normalization is proportional to the star-formation rate

of the galaxy. Galaxies which are active in star formation tend to have more luminous binaries with a maximum cut-off luminosity of $\sim 10^{40}$ erg s^{-1}. Gilfanov et al. (2004) analyzed the HMXB XLF of the Milky Way, Magellanic Clouds and nearby starburst galaxies, and in particular the high luminosity tail, where ULXs are expected to reside. Their XLF shows a smooth, single slope PL shape in a broad luminosity range, $10^{36-40.5}$ erg s^{-1}. As suggested also by Miller & Colbert (2004), ULXs with luminosities of $\sim 10^{39-40}$ erg s^{-1} may be black holes having a few tens of solar masses and representing the high luminosity end of this distribution. ULX frequency and luminosity distributions should be a smooth extension towards higher luminosities of that of "ordinary" stellar mass XRBs, emerging from the standard stellar evolution sequence. Although some of the ULXs might be indeed rare and exotic objects, Gilfanov et al. (2004) indicate that majority of them can represent the high mass, high $\dot{M}$ tail of the HMXB population.

As they are not linked with recent episodes of star formation, the origin of ULXs in ellipticals is still unclear. Irwin et al. (2004) suggest that sources dimmer than $1 - 2 \times 10^{39}$ erg s^{-1} are truly associated with the host galaxies (with properties consistent with Galactic XRBs). Sources brighter than 2×10^{39} erg s^{-1} are consistent with the expected number and spatial distribution of background AGNs.

In conclusion, ULXs are clearly linked to the star-forming population (e.g. Matsushita et al., 2000) but their presence in early-type galaxies is still under debates (Irwin et al., 2004; Fabbiano et al., 2006).

Unfortunately, up to date the study of XLFs does not allows to discriminate between the two main models of ULXs, isotropically emitting IMBHs or beamed stellar mass BHs. Both models agree with the observed high-luminosity XLFs (see Krolik (2004) for IMBHs and Körding et al. (2002) for jets model).

2.6 Formation scenarios

The major problem of the IMBH scenario for ULXs is the issue about the formation of such massive objects. Black holes in the $10^2 - 10^4\,M_\odot$ mass range are more massive than the most massive stars that are forming in the current universe through standard evolutionary channels. Main-sequence stars can have a maximum mass of $\sim 60 M_\odot$ (Schwarzschild & Härm 1959, but this upper limit is still uncertain), and the final black hole mass could be theoretically as large as its progenitor beyond $40\,M_\odot$ (Fryer, 1999). Stars more massive than $\sim 200\,M_\odot$ are unlikely to form in the current universe, and even if they do then mass losses due to winds and pulsations will reduce significantly the mass of any remnant BHs (e.g. Fryer 1999). The most massive stellar black hole in our Galaxy is GRS 1915+40 and has a mass of $\sim 14 M_\odot$ (Greiner et al., 2001), but also massive stars have been observed (e.g. the Pistol star, with an initial mass $\sim 200 M_\odot$, Figer et al. 1998).

Formation of IMBH in the early-Universe

An hypothesis on the formation of IMBHs is that they either formed at some earlier time, or have accumulated most of their mass since birth, or both (see the review of

Miller & Colbert, 2004).

An exotic possibility came from cosmological models that suggests some class of BHs to form prior to big bang nucleosynthesis (Jedamzik, 1997; Niemeyer & Jedamzik, 1999).

A more promising early-Universe origin for massive black holes is the first generation of stars. By definition, the Population III stars evolved in an environment with negligible metallicity, $\lesssim 10^{-5} Z_\odot$ (e.g. Abel et al. 1998; Schneider et al. 2002). In such an environment, metal line cooling is absent and hence the temperature of molecular clouds was higher than it is in the current universe. As the Jeans mass scales as $T^{3/2}$, thus the initial mass of stars may be significantly larger for Population III stars than it is currently. Moreover, at zero-metallicity, winds and pulsations are negligible (e.g., Fryer, Woosley, & Heger 2001), so a star loses a little of its mass during its evolution. A star with an initial mass between $100\,M_\odot$ and $250\,M_\odot$ is believed to disrupt itself completely via a pair instability that leads to explosive oxygen burning without leaving a remnant (e.g. Barkat, Rakavy, & Sack 1967; Heger & Woosley 2002), but above $250\,M_\odot$ the star is not disrupted and instead is likely to collapse directly to a massive BH, without an explosion.

Madau & Rees (2001) suggest that there may be $\sim 10^3 - 10^4$ such BHs per galaxy but they are expected to be isolated (only accreting from the interstellar medium) and then undetectable. However, in an active star formation environment with many massive young star clusters, isolated black holes could be captured gravitationally. They would then sink to the center of the clusters, where they could acquire a stellar companion and become active as X-ray sources (see also Islam, Taylor, & Silk 2003).

Following the formation scenario suggested by Madau & Rees (2001) for Population III stars, in environments at metallicity lower than solar massive stars may also form in the current epochs.

Formation of IMBH in dense environments

In dense clusters a BH could grow by merger with stars or compact remnants. This mechanism involves hardening of a binary by three-body interactions, with the possibility of a merger due to gravitational radiation. However, the kick experienced by the binary (Heggie 1975) can espell it from the core of a typical globular cluster (Webbink 1985) before the binary can merge. This would prevent substantial growth of a BH. Indeed, Sigurdsson & Hernquist (1993) and Portegies Zwart & McMillan (2002) find that three-body interactions of $10\,M_\odot$ black holes lead to ejection of the binary almost always in globular clusters and inevitably in young, less contracted, stellar clusters. If, however, the initial mass of the black hole is larger than $10\,M_\odot$, it might be able to stay in the cluster long enough to grow significantly (Miller & Hamilton 2002a, Taniguchi et al. 2000). Portegies Zwart et al. (2004) suggest that dynamical friction leads to the massive stars sinking rapidly to the center of the cluster, where they participate in a runaway collision. This produces a star of $\sim 800 - 3000\,M_\odot$, which ultimately collapses to a black hole of intermediate mass. Through numerical simulation of two different cluster they argue that, the larger is the cluster radius, the longer is the mass segregation timescale, making this process less efficient.

CHAPTER 3

A BRIGHT ULX IN NGC 1313

The spiral galaxy NGC 1313 hosts three bright ULXs: the brightest NGC 1313 X-1, NGC 1313 X-2 and the interacting supernova SN 1978K. All the three sources are well studied in X-rays. In the optical SN 1978K was identified with the supernova in 1993 and NGC 1313 X-1 is located in the inner part of the galaxy, too crowded to identify a counterpart univocally. NGC 1313 X-2 is a prototypical ULX with an identified optical counterpart and, although a firm conclusion was still not reached on the nature of the compact object, it is one of the best understood source of this kind.

3.1 X-ray observations of NGC 1313

Since the beginning of the '80s, the field of NGC 1313 was extensively observed by almost all the X-ray satellites. The first observation was performed by *Einstein* with the IPC instrument in 1980. The galaxy was then pointed several times by *ROSAT* (PSPC and HRI) between 1991 and 1998 (Stocke et al., 1995; Colbert et al., 1995; Miller et al., 1998; Schlegel et al., 2000), and by *ASCA* (SIS and GIS) in 1993 and 1995 (Petre et al., 1994; Makishima et al., 2000). Between 2000 and 2004 the field was observed repeatedly by *XMM-Newton* (Miller et al., 2003; Zampieri et al., 2004; Dewangan et al., 2005). The most recent observations consist in a series of short exposures to assess the variability of the ULXs in the field. Also the *Chandra* observatory pointed NGC 1313 several times. We used a 2002 *Chandra* ACIS-S pointing to derive an accurate X-ray position for NGC 1313 X-2. The *Chandra* observation began on 13 Oct 2002 and had a duration of 19.9 ks. The primary goal of the observation was to study sources near the center of the galaxy, but the aim-point was adjusted to also place the tree brightest sources on the S3 chip of the ACIS-I. In Table 3.1 we list all the X-ray observations used in the present analysis.

Observatory	Obs. Id.	Date	Exposure	GTI[a]	Filter
Einstein-HRC	7044	1980-01-02	7775 s	–	–
ROSAT-PSPC	RP600045N00	1991-05-10	10976 s	–	–
ASCA-GIS	60028000	1993-07-12	33344 s	–	–
ASCA-SIS	60028000	1993-07-12	27840 s	–	–
ROSAT-HRI	RH400065N00	1992-04-18 to 05-24	5438 s	–	–
ROSAT-PSPC	RP600504N00	1993-11-05	15161 s	–	–
ROSAT-HRI	RH600505N00	1994-06-23 to 07-16	22621 s	–	–
ROSAT-HRI	RH500403N00	1995-01-31 to 02-10	13621 s	–	–
ROSAT-HRI	RH500404N00	1995-02-02 to 11	27352 s	–	–
ROSAT-HRI	RH600505A01	1995-04-12 to 20	20412 s	–	–
ROSAT-HRI	RH500403A01	1995-05-10 to 06-22	31383 s	–	–
ROSAT-HRI	RH500404A01	1995-05-09 to 06-21	19102 s	–	–
ASCA-GIS	93010000	1995-11-29	42912 s	–	–
ASCA-SIS	93010000	1995-11-29	35808 s	–	–
ROSAT-HRI	RH500492N00	1997-09-30 to 08-10	23001 s	–	–
ROSAT-HRI	RH500499N00	1998-03-21 to 04-20	24226 s	–	–
XMM-EPIC	0106860101	2000-10-17	31637 s	20600 s	Medium
Chandra-ACIS	2950	2002-10-13	20160 s	19900 s	
XMM-EPIC	0150280101	2003-11-25	8365 s	1087 s	Thin
XMM-EPIC	0150280201	2003-12-09	5620 s	0 s	Thin
XMM-EPIC	0150280301	2003-12-21	10334 s	8272 s	Thin
XMM-EPIC	0150280401	2003-12-23	14094 s	3600 s	Thin
XMM-EPIC	0150280501	2003-12-25	15282 s	1668 s	Thin
XMM-EPIC	0150280701	2003-12-27	16666 s	0 s	Thin
XMM-EPIC	0150280601	2004-01-08	14756 s	7696 s	Thin
XMM-EPIC	0150281101	2004-01-16	7034 s	4208 s	Thin

[a] Good Time Intervals in which the total off-source count rate above 10 keV is < 1.0 counts s^{-1}

Table 3.1: Observation log of all the X-ray pointings of NGC 1313 considered in the present analysis.

3.2   NGC 1313 X-2 in X-rays

Because of its X-ray variability, high (isotropic) luminosity and presence of a soft X-ray spectral component NGC 1313 X-2 is a prototypical ULX (see Miller et al., 2003; Zampieri et al., 2004; Turolla et al., 2004, and references therein). Its luminosity, $L_X \sim 10^{40}$erg s^{-1} in the 0.2-10.0 keV band, makes this source a good candidate for harboring an IMBH ($M \gtrsim 100 M_\odot$).

NGC 1313 X-2 was one of the first ULXs to be discovered by *Einstein* and it is certainly one of the best studied. Originally included in the *Einstein* Extended Medium Sensitivity Survey as MS 0317.7-6647, it is located $\sim 6'$ south of the nucleus of NGC 1313. Stocke et al. (1995) investigated the nature of MS 0317.7-6647 on the basis of X-ray, optical and radio observations. They identified also a possible optical counterpart and concluded that the source could be either a Galactic isolated neutron star or a binary containing a massive BH in NGC 1313. Spectral fits to *ROSAT* PSPC data (Stocke et al., 1995; Colbert et al., 1995; Miller et al., 1998) yielded results consistent with many single component models. *ASCA* observations (Petre et al., 1994; Makishima et al., 2000) are described successfully by a multi-color disk black body (MCD) model, representing thermal emission from a standard, optically

thick accretion disk around a BH. Recent analysis of high resolution energy spectra taken with *XMM-Newton* (Miller et al., 2003; Zampieri et al., 2004), indicates that two spectral components, soft and hard, are required to fit the spectrum of NGC 1313 X-2 and that the temperature of the soft component yields $M_{BH} \gtrsim 90 M_\odot$. NGC 1313 X-2 is inserted in a sample of 13 ULXs with high quality *XMM-Newton* spectra by Stobbart et al. (2006). Their study confirms the failure of simple models in fitting the spectra of high statistics ULXs, for which two component models provide better results. The Authors also pointed out that a number of these sources shows evidence of curvature in the high energy tail. Anyways, their best fit to NGC 1313 X-2 spectrum is a MCD plus power law model, with no evidence of curvature.

A detailed analysis of the X-ray properties of NGC 1313 X-2 is presented in the following sections.

3.2.1 X-ray astrometry

The position of NGC 1313 X-2 was previously determined with the *ROSAT* HRI (Stocke et al. 1995; Schlegel et al. 2000) and *XMM* EPIC-MOS (Miller et al., 2003). Typical 1σ error boxes for the two instruments are $\sim 3''$ for *ROSAT* HRI and $\sim 2''$ for *XMM* EPIC-MOS. The *ROSAT* and *XMM-Newton* positions and corresponding error boxes are reported in Table 3.2.

An accurate determination of the X-ray position of NCG 1313 X-2 was obtained from the 2002 *Chandra* pointing, using the *Chandra* aspect solution. Chandra data were extracted from the S3 chip on the ACIS-I and subjected to standard processing and event screening. No strong background flares were found, so the entire observation was used. Because the source is $5'$ off axis, the point spread function was fitted with an ellipsoidal Gaussian ($1.9''$ along the major axis and $1.1''$ along the minor axis at 2σ, rms values). Also, the pixel with the highest number of counts is offset by $0.8''$ from the center of the fitted ellipse. Taking these uncertainties into account, we conservatively estimate a positional error of $0.7''$ (1σ). The final *Chandra* position is: α = 03h 18m 22.27s$\pm$0.12s, δ = -66^0 36' 03.8''$\pm$0.7''.

In order to check the accuracy of the *Chandra* aspect solution, we exploited the presence in the field of view of a quite peculiar supernova, SN 1978K, that shows powerful radio and X-ray emission produced by the interaction of the ejecta with the circumstellar material. The *Chandra* position of SN 1978K is α = 03h 17m 38.69s, δ = -66^0 33' 03.6'' (J2000), within $0.46''$ from the accurate ($0.1''$) radio position of Ryder et al. (1993). This is consistent with the expected *Chandra* aspect accuracy. Recently Liu et al. (2007) determine the position of NGC 1313 X-2 in a different *Chandra* ACIS-I exposure. Their measure is also reported in Table 3.2 for comparison.

3.2.2 X-ray spectrum and light curve

The first detailed spectral analysis of NGC 1313 X-2 was performed on the longer *XMM-Newton* exposure taken in 2000 (Obs.Id. 0106860101, see Table 3.1). We analyzed the *XMM* EPIC data from both the MOS and pn cameras (operated with the medium filter). Both reduction procedures `epchain` and `epproc` were used to

extract the data obtaining similar results, differing typically by a few percents. Data screening, region selection and event extraction were performed using standard software (XMM-SAS v. 7.0.0). An analysis of the MOS and pn light curves shows that solar flares are present in both datasets. They were filtered out using the standard criterion (total off-source count rate above 10 keV < 0.35 counts s^{-1} for MOS and < 1.0 counts s^{-1} for pn). The clean exposure is ∼20 ks for the pn camera and ∼25 ks for the MOS. We extracted the source counts from a circle of 40″ and 30″ for the MOS and pn cameras, respectively, centered on the source position. The proximity of the source to one of the CCD edges in the EPIC MOS data requires some care. We eliminated the area of a box aligned and superimposed to the CCD boundary to avoid contamination from bad pixels close to the source. The background was selected from a circle of 60″ in a nearby source-free region of the same CCD. Ancillary and response files were produced using the appropriate XMMSELECT tasks. Data were grouped to require at least 20 counts per bin for the MOS data and 40 counts per bin for the pn data, and were then analyzed and compared with different models using XSPEC. To minimize the effects of possible relative calibration uncertainties, the fit of the MOS1, MOS2 and pn spectra were performed with an overall normalization constant: the values for the two MOS cameras differ by ∼ 10%, while that of the pn instrument is larger by ∼ 25%. The count rate is 0.08 counts s^{-1} for the MOS cameras and 0.25 counts s^{-1} for the pn.

In order to reconstruct the X-ray variability history of NGC 1313 X-2, we have carefully re-analyzed also the *ROSAT* and *ASCA* observations. Extraction regions for the *ASCA* SIS data were chosen with care to avoid contamination from the CCD edges and SN 1978K. The source counts were extracted from a circle of radius 180″ centered on the source position while the background was selected from a box (270″×600″) in a nearby source free region of the same CCD (subtracting the contamination from SN 1978K present in the same image). Spectra were grouped to require at least 15 counts per bin for the *ROSAT* data and 20 counts per bin for the *ASCA* data.

The results of the spectral analysis are listed in Table 3.3. For *ROSAT* and *ASCA* data there is no need of multiple component models because of the low counting statistics. For these spectra simple one-parameter models are statistically acceptable. When fitted with thermal models, the temperatures are significantly high and comparable with the ones observed in XRBs (see the "too hot a disk" problem in Section 2.1.3): *ROSAT* spectra fitted with a BB model give kT ∼ 0.3 keV, while *ASCA* spectra fitted with a MCD model have kT ∼ 1.2 keV. The high values of the temperature obtained from *ROSAT* and *ASCA* data is a well known problem and it is due to the low sensitivity and spectral resolution of the two satellites and, for ROSAT, also to the narrower bandpass, that did not permit to discriminate more complex spectral shapes (Makishima et al., 2000). Interestingly, comparing data from the first and second epoch *ASCA* observations, the X-ray flux of NGC 1313 X-2 appears to increase with increasing spectral hardness (see Table 3.3). This behavior is similar to that observed in the ULXs of the Antennae galaxy (Fabbiano et al., 2003b) and is opposite to what is usually seen in Galactic BH X-ray binaries (e.g. Cyg X-1).

A significant breakthrough in the spectral analysis of NGC 1313 X-2 has been provided by *XMM-Newton* observations. The observation taken on October 2000 is

Observatory/Instr.	Object[a]	RA[J2000]	DEC[J2000]	Ref.
ROSAT/HRI	NGC 1313 X-2	03 18 22.00±0.50	-66 36 02.3±3.0	Schlegel et al. (2000)
XMM/EPIC-MOS	NGC 1313 X-2	03 18 22.34±0.33	-66 36 03.7±2.0	Miller et al. (2003)
Chandra/ACIS-I	NGC 1313 X-2	03 18 22.18±0.12	-66 36 03.3±0.7	Zampieri et al. (2004)
Chandra/ACIS-I	NGC 1313 X-2	03 18 22.238±0.001	-66 36 03.49±0.01	Liu et al. (2007)
ESO/3.6m	A	03 18 21.97±0.05	-66 36 06.5±0.3	Zampieri et al. (2004)
ESO/3.6m	B	03 18 21.56±0.05	-66 36 00.9±0.3	Zampieri et al. (2004)
ESO/3.6m	C	03 18 22.34±0.05	-66 36 03.7±0.3	Zampieri et al. (2004)
ESO/3.6m	D	03 18 20.96±0.05	-66 36 03.7±0.3	Zampieri et al. (2004)
VLT	A	03 18 21.97±0.05	-66 36 06.4±0.3	Mucciarelli et al. (2005)
VLT	B	03 18 21.57±0.05	-66 36 00.8±0.3	Mucciarelli et al. (2005)
VLT	C1	03 18 22.26±0.05	-66 36 03.3±0.3	Mucciarelli et al. (2005)
VLT	C2	03 18 22.36±0.05	-66 36 03.8±0.3	Mucciarelli et al. (2005)
VLT	D	03 18 20.96±0.05	-66 36 03.6±0.3	Mucciarelli et al. (2005)

[a] See Figure 3.2.

Table 3.2: Positions of NGC 1313 X-2 and other field objects.

the longest *XMM-Newton* exposure of NGC 1313 X-2 analyzed here. The statistics of the spectrum is significantly improved including the EPIC pn data (the pn camera has almost twice more counts than each single MOS instrument). As expected, high statistics spectra can no longer be fitted with single component models. Following what described in Chapter 2, in particular in Section 2.1.3, we applied to NGC 1313 X-2 the various types of spectral models adopted in the literature.

Absorption was taken into account using two distinct components for the Galactic and the intrinsic absorption. The Galactic absorption in the direction of NGC 1313 X-2 is modeled by means of a WABS component with the column density fixed to the value $N_H = 3.93 \times 10^{20}$ cm^{-2} (obtained with the NH FTOOL task). The intrinsic absorption to the source is modeled with a variable TBABS component. An additional multiplicative constant is used to take into account the relative normalization between the pn and MOS cameras.

We performed spectral fitting with a number of models, from the simplest single component to more complex multiple component models. Before showing the results of the fits, I summarize here the main physical properties of these models, referring to Chapter 2, Section 2.1.3, for a more detailed description.

BHC-like semi-phenomenological models

These models were applied in analogy with the spectral behavior observed in Galactic BHCs.

- DISKBB + POWER-LAW (Miller et al. 2003; Zampieri et al. 2004; Stobbart et al. 2006): this is the usual semi-phenomenological model adopted also for Galactic BHCs. This model is a two component model: a soft multicolor disk component (MCD or DISKBB), that represents emission from an accretion disc around a BH, and a power-law hard tail, that represents the effect of a Comptonizing medium. The observed soft temperatures indicate intermediate BH masses, that are consistent with the very high luminosity of these objects, if isotropic emission is assumed.

- DISKPN + POWER-LAW: the DISKPN model in XSPEC is a generalization of the DISKBB model, including corrections for the temperature distribution near the black hole, calculated in a pseudo-Newtonian potential. The inner disk radius can be a free parameter only close to $r = 6R_g$ ($r_g = \frac{GM_{BH}}{c^2}$ is the gravitational radius), otherwise r is strongly correlated with the normalization.

- ST95 + POWER-LAW: this is also a variation of the standard accretion disk spectral model. It takes into account the spectral effects induced by radiation transfer at the disk surface through a hardening factor (Shimura & Takahara, 1995).

Disk-corona models

Also in this case a model usually adopted for BHCs in the low and very high state (VHS) is applied to ULXs (Done & Kubota, 2006).

- DISKBB + COMPTT: the emission is modeled assuming that radiation coming from an accretion disk is comptonized in a hot corona. The Comptonizing corona turns out to be optically thick, as observed in Galactic BHCs in the so-called VHS. Goad et al. (2006) applied this model to Ho II X-1, while Roberts et al. (2006) to NGC 5204 X-1 (with some variations).

AGN-like ionized wind models

In these models the soft excess observed in ULXs is produced by emission from an ionized wind. Winds of this type are believed to be responsible for the soft excess observed in AGNs, at about the same temperature.

- TIME+TABS+TRFL: this model was developed by Gonçalves & Soria (2006) and is not public yet. It represents emission from a relativistically smeared ionized plasma with three possible components, in absorption, emission or reflection. The Authors assumed a primary source of radiation characterized by a power-law spectrum (in the range 10-10^5 keV) that arises close to the BH. A fast moving medium surrounding this primary source (treated in a one dimensional plane parallel geometry) reprocesses the incident light and produces a spectrum that is a combination of reflection from the illuminated side, outward emission from the non-illuminated side of the medium and a transmitted fraction;

- BB + DISKBB: Stobbart et al. (2006) mimic the effects of a wind with a soft black-body component. The warm MCD component has a temperature in the stellar mass BH range.

It is also interesting to mention a not yet public model for ULXs. Begelman et al. (2006) and Fabrika et al. (2006) suggested that ULXs could be object SS 433-like seen face-on. The supercritical accretion disk produces a funnel and a powerful wind the X-ray emission that, seen in a face-on orientation, may reach a luminosity up to $\sim 10^{40} - 10^{41}$ erg s^{-1}.

The results of the spectral fitting are reported in Tables 3.4, 3.5, 3.6 and 3.7.

Single component models do not provide a satisfactory fit of the joint 2000 MOS1, MOS2 and pn spectra, as shown in Table 3.4. An MCD or a DISKPN model gives a reduced χ^2 larger than 2. On the other hand, an absorbed power-law model has $\chi^2_{red} = 1.15$ for 290 *d.o.f.* and it can not be rejected at $> 96\%$ confidence and the TABS model at $> 94\%$. Therefore a simple power-law model is able to reproduce the hard tail of NGC 1313 X-2, that does not appear to show the spectral curvature above ~ 2 keV reported by Stobbart et al. (2006) for other high statistic ULXs. The main problem of these simple models is that they cannot reproduce the curvature of the spectrum at soft energies, where there is evidence of a soft excess below 1 keV.

Two components models provide a significant improvement over single component ones. We found that almost any two-component model of the type "soft thermal + hard tail" gives a good fit to our data. We used a number of different models to describe these two components in different combinations: black body (BB), MCD, DISKPN and ST95 for the soft component, power-law, COMPTT, MCD and THCOMP

(Zdziarski et al., 1996; Życki et al., 1999) for the hard tail. However other spectral models are equally statistically acceptable.

The absorbed MCD plus a power-law is routinely employed for black hole XRBs and previous applications to a number of ULXs, including NGC 1313 X-2 (Miller et al., 2003, 2004; Cropper et al., 2004; Zampieri et al., 2004; Kong & Di Stefano, 2005) gave a satisfactory fit to the data. Figure 3.1 shows the results for a MCD+PL fit. The resulting parameters are $kT = 240^{+50}_{-40}$ eV, $\Gamma = 2.2^{+0.15}_{-0.09}$ and $N_H = 2.40^{+0.92}_{-0.37} \times 10^{21}$ cm^{-2} for the inner disk temperature, photon index and column density, respectively (see Table 3.5) and provide a $\chi^2_{red} = 1.05$ for 288 $d.o.f.$. There are residuals in the fit (mainly in the EPIC pn spectrum) that suggest the possible presence of emission lines. The EPIC pn data provide marginal evidence for the presence of a soft component even at low metallicities. Reducing the abundances of the absorbing gas at 0.5 solar, a simple PL fit of the EPIC pn data has $\chi^2_{red} = 1.24$ (89 $d.o.f.$), while a MCD+power-law fit gives $\chi^2_{red} = 1.15$ (87 $d.o.f.$).

Almost all the models give statistically acceptable fits. More in detail:

MCD+PO   This model provides the best fit among the "soft thermal + hard tail" components model. The soft temperature implies a mass for the BH of $\sim 60 f^4 M_\odot$.

DISKPN+PO   Fits with the DISKPN model indicates that there is degeneracy between the two parameters M_{BH} and R_{in}. IMBHs accreting from a disk with R_{in}=3R$_s$ have spectra with a characteristic temperature similar to that of a stellar mass BH with a disk terminating far away (few tens R$_s$). In conclusion, if we do not make a specific assumption on the value of R_{in}, there is no way to constrain the BH mass.

ST95+PO   For this model no convergence was found for a stellar mass BH. This confirms what found with the DISKPN+PO the previous point, because the inner radius of the disk is fixed at 3R$_s$.

MCD+COMPTT   The best fit is obtained when the temperature of the disk and that of the soft photon input are free to vary independently. In a physically consistent model these two temperatures must be linked, as the disk emission represents the input spectrum for the Comptonizing corona. As the optical depth of the corona is quite large ($\tau \gtrsim 5$), the spectral state is reminiscent of the VHS in BHCs (Kubota et al., 2002; Done & Kubota, 2006). In these assumptions, the apparent low temperature of the disk is consistent with the fact that the innermost hot part is hidden by the corona.

MCD+THCOMP & DISKPN+COMPTT   These models adopt a more accurate description for the disk and/or the Comptonizing corona. All the previous conclusions remain valid.

TABS, TEMI, TRFL   The fit with the models from Gonçalves & Soria (2006) are in some cases statistically acceptable (see Table 3.7). However, it remains to be understood where the power-law input is produced and what powers the relativistic wind.
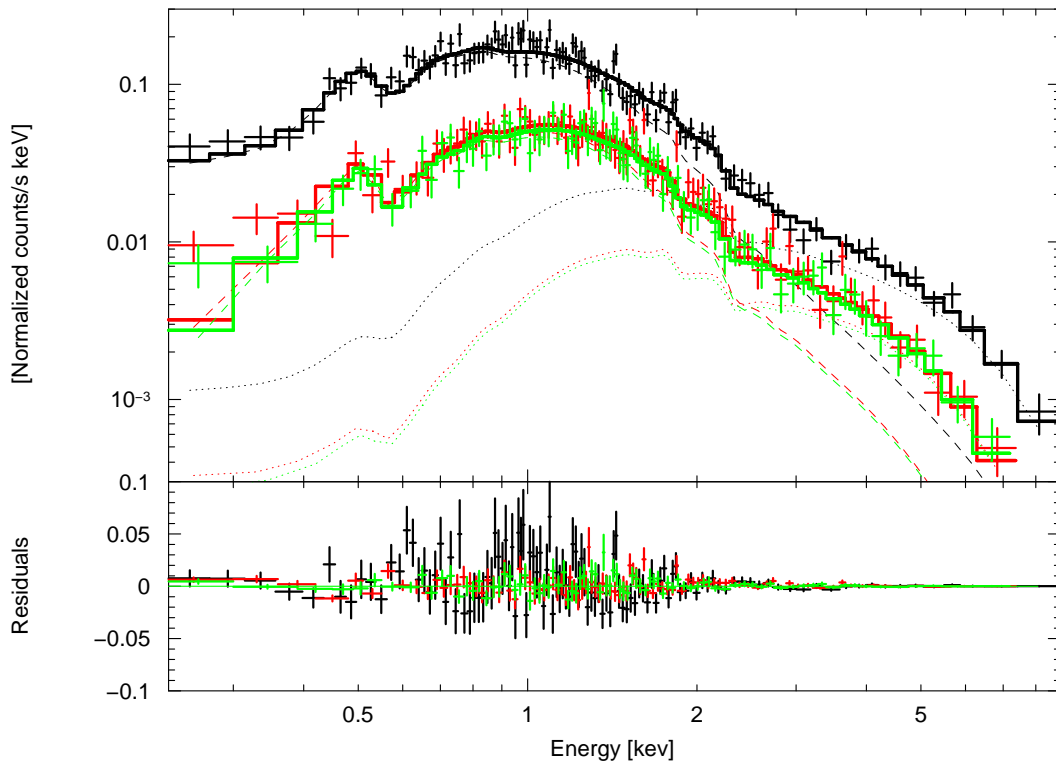
Figure 3.1: X-ray spectrum (top) and residuals (bottom) of NGC 1313 X-2 from the 2000 *XMM-Newton* observation. The EPIC-MOS data are shown in red and green and pn data in black. The solid lines represent the combined best fitting model spectra for the two cameras, while the dashed and dotted lines are the MCD and power-law components respectively.

In conclusion, from our detailed spectral analysis we found that the X-ray spectral fitting alone can not discriminate the nature of the central accreting source. The spectral results should be interpreted in the context of all the available data (as in the case of NGC 1313 X-2, the identification of the optical counterpart and its properties).

XMM-Newton observed again NGC 1313 in 8 different epochs between 2003 and 2004. All the observations are listed in Table 3.1. Following the results of the previous analysis of the 2000 *XMM-Newton* exposure, we concentrate our attention on multiple component spectral models, in particular a MCD+PL to mimic the behavior of Galactic BHCs. In the following, high counting statistics is needed so we analyzed the EPIC pn exposures that typically have twice more counts than a single MOS camera. Also in this case data reduction and extraction has been carried out with the dedicated *XMM-Newton* software. All the observations are affected by solar flares. The good time intervals left after subtraction of the high background periods are reported in Table 3.1. For the analysis we consider only the exposures with a good time interval larger than 1 ks. After performing standard cleaning of the event lists, we extracted source counts from a circle of $40''$ centered on the position of NGC 1313 X-2 (Zampieri et al., 2004). The background counts were extracted from a circle of $50''$ on the same CCD. The absorbing column density inferred from the different datasets is consistent with a constant value. We then performed again the fits fixing N_H to the average value weighted by the exposure time ($N_H = 4.02 \times 10^{21} \text{cm}^{-2}$). For consistency, we

also repeated the analysis of the 2000 EPIC pn spectrum of NGC 1313 X-2 following the procedure described above. Results from the spectral fits are reported in Table 3.8.

In Tables 3.3 and 3.8, we quote also the unabsorbed X-ray flux derived from all the available observations of NGC 1313 X-2. The fluxes and corresponding luminosities were consistently derived from the best fit parameters of the X-ray spectral analysis (a distance of 3.7 Mpc was assumed for the host galaxy; Tully 1988). When necessary, we used Web PIMMS to extrapolate the fluxes to the 0.2–10 keV interval. For the *Einstein* and *ROSAT*-HRI data, fluxes were estimated assuming the spectral parameters of the 2000 *XMM-Newton* observation. An approximate estimate of the errors, based on counting statistics, is 5-10%. The *Chandra* point is not included because of pile-up problems. For the *XMM-Newton* data, the errors have been estimated from the maximum and minimum values of the flux, obtained varying systematically the fit parameters. The unabsorbed 0.2–10 keV flux from both the 2000 *XMM* EPIC-MOS and pn instruments agree within 10% and give an average value of 2.4×10^{-12} erg cm^{-2}s^{-1}. This value is lower by a factor ~ 2 than that estimated by Miller et al. (2003).

Until 2000 NGC 1313 X-2 exhibited variability up to a factor of two on a timescale of months, with a maximum luminosity of $\sim 4 \times 10^{39}$ erg s^{-1} (Z04). The more recent data show a quite intense flare lasting a few days, occurring at the end of 2003.

From the observed maximum luminosity ($L_{max} \sim 1.5 \times 10^{40}$erg s^{-1}) and assuming isotropic emission, the black hole mass obtained setting $L_{max} = L_{Edd}$ (L_{Edd} is Eddington luminosity) is $\simeq 120 M_{\odot}$. Sub-Eddington accretion would imply an even larger mass.

Observatory/Instr.	Obs. Id.	Model	N_H [10^{21} cm^{-2}]	Parameters	$\chi^2_{red}(d.o.f.)$	F_X^a	F^b [0.2-10 keV] [10^{-12} erg cm^{-2} s^{-1}]
$ROSAT$/PSPC	rp600045n00	Power-law	$1.06^{+2.14}_{-0.50}$	$\Gamma = 2.40^{+1.40}_{-0.60}$	0.83 (20)	1.4	2.6
		Black body	$0.17^{+0.20}_{-0.15}$	$kT = 0.27^{+0.05}_{-0.03}$ keV	1.01 (20)	0.34	0.38
$ROSAT$/PSPC	rp600504n00	Power-law	$1.74^{+2.95}_{-1.31}$	$\Gamma = 2.20^{+1.50}_{-0.90}$	1.43 (22)	1.5	1.8
		Black body	$0.09^{+0.23}_{-0.09}$	$kT = 0.35^{+0.05}_{-0.07}$ keV	1.32 (22)	0.37	0.44
$ASCA$/GIS+SIS	60028000	Power-law	$4.24^{+0.41}_{-0.41}$	$\Gamma = 1.99^{+0.03}_{-0.09}$	0.99 (171)	1.3	3.2
		MCD	$1.15^{+0.35}_{-0.34}$	$kT = 1.38^{+0.07}_{-0.07}$ keV	0.89 (171)	2.1	2.6
$ASCA$/GIS+SIS	93010000	Power-law	$4.74^{+0.50}_{-0.50}$	$\Gamma = 2.43^{+0.09}_{-0.07}$	1.28 (139)	0.50	2.2
		MCD	$1.06^{+0.31}_{-0.31}$	$kT = 1.08^{+0.04}_{-0.04}$ keV	1.31 (139)	0.86	1.0

[a]Unabsorbed flux in the 0.1–2.0 keV ($ROSAT$), 2.0–10.0 keV ($ASCA$) and 0.2–10.0 keV (XMM-$Newton$) energy bands
[b]Unabsorbed flux extrapolated in the 0.2-10.0 keV band using the web interface to PIMMS
[c]Thermal Comptonization model with Wien soft photon input
[d]Abundance 0.5 solar

Table 3.3: Parameters of the spectral fit of NGC 1313 X-2 from the $ROSAT$ and $ASCA$ observations.

Model	$N_{H\,tbabs}$ $[10^{21}\ \mathrm{cm}^{-2}]$	Parameters	χ^2_{red}	$\chi^2_{red}(d.o.f.)$	Q
WABS+TBABS+PO	$0.23^{+0.02}_{-0.02}$	$\Gamma = 2.4^{+0.07}_{-0.06}$	1.148	333/290	0.041
WABS+TBABS+MCD	$0.03^{+0.02}_{-0.01}$	$kT_1 = 0.89^{+0.06}_{-0.05}$ keV	2.142	621/290	0
WABS+TBABS+DISKPN	$0.04^{+0.03}_{-0.01}$	$kT_1 = 0.94^{+0.07}_{-0.06}$ keV	2.058	595/289	0
		Rin=6Rg*			
WABS+TBABS+TABS	$0.24^{+0.07}_{-0.11}$	$\alpha = 1.4$(peg)	1.132	326/288	0.06
		$N_{H\,ion} = 3.7^{+0.3}_{-0.3}$			
		$\xi = 2072^{+660}_{-680}$			
WABS+TBABS+TEMI	$0.57^{+0.09}_{-0.08}$	$\alpha = 1.9^{+0.1}_{-0.1}$	1.95	562/288	0
		$N_{H\,ion} = 3.7^{+0.2}_{-0.2}$			
		$\xi = 1599^{+560}_{-640}$			
WABS+TBABS+TRFL	$0.66^{+0.09}_{-0.12}$	$\alpha = 1.9^{+0.1}_{-0.1}$	3.36	966/288	0
		$N_{H\,ion} = 3.7^{+0.2}_{-0.2}$			
		$\xi = 1000^{+4500}_{-300}$			

* This parameter is fixed

[b] $\alpha = \Gamma - 1$

Table 3.4: Parameters of the spectral fit of NGC 1313 X-2 with single component models from the longer *XMM-Newton* observation (Obs.Id. 0106860101). Galactic absorption, described as a WABS component, has $N_H = 3.93 \times 10^{20} \mathrm{cm}^{-2}$.

Model	$N_{H\,tbabs}$ $[10^{21}$ cm$^{-2}]$	Parameters	χ^2_{red}	$\chi^2_{red}(d.o.f.)$	Q
WABS+TBABS+MCD+PO	$0.24^{+0.05}_{-0.04}$	$\Gamma = 2.2^{+0.1}_{-0.2}$ $kT_1 = 0.24^{+0.07}_{-0.05}$ keV	1.052	303/288	0.26
WABS+TBABS+PO+MCD	$0.35^{+0.05}_{-0.07}$	$\Gamma = 3.6^{+0.4}_{-0.5}$ $kT_1 = 2.13^{+5.40}_{-0.4}$ keV	1.088	313/288	0.14
WABS+TBABS+MCD+COMPTT	$0.14^{+0.06}_{-0.03}$	$kT_1 = 0.26^{+0.03}_{-0.05}$ keV $kT_2 = 3.05^{+2.46}_{-0.99}$keV $T_0 = 0.19^{+0.05}_{-0.08}$ keV $\tau = 5.1^{+2.0}_{-1.6}$	1.047	300/286	0.28
	$0.11^{+0.06}_{-0.03}$	$kT_1 = 0.16^{+0.01}_{-0.01}$ keV** $kT_2 = 3.14^{+1.96}_{-0.82}$ keV $T_0 = 0.16^{+0.01}_{-0.01}$ keV** $\tau = 4.6^{+2.4}_{-1.1}$	1.063	305/287	0.22
WABS+TBABS+MCD+THCOMP^a	$0.21^{+0.05}_{-0.05}$	$\Gamma = 2.2^{+0.3}_{-0.4}$ $kT_1 = 0.23^{+0.04}_{-0.05}$ keV $kT_e = 993^{+254}_{-306}$ keV $T_0 = 0.36^{+0.03}_{-0.03}$ keV	1.055	303/286	0.25
	$0.24^{+0.04}_{-0.05}$	$\Gamma = 2.2^{+0.4}_{-0.3}$ $kT_1 = 0.20^{+0.01}_{-0.02}$ keV** $kT_e = 705^{+235}_{-450}$ keV $T_0 = 0.20^{+0.01}_{-0.02}$ keV**	1.057	303/287	0.24

* This parameter is fixed

** These parameters are linked

^{b} $\alpha = \Gamma - 1$

Table 3.5: Parameters of the spectral fit of NGC 1313 X-2 with multiple component models from the longer *XMM-Newton* observation (Obs.Id. 0106860101). Galactic absorption, described as a WABS component, has $N_H = 3.93 \times 10^{20}$cm^{-2}.

Model	$N_{H\,tbabs}$ $[10^{21}\ \mathrm{cm}^{-2}]$	Parameters	χ^2_{red}	$\chi^2_{red}(d.o.f.)$	Q
WABS+TBABS+BB+MCD	$0.07^{+0.02}_{-0.02}$	$kT_1 = 0.27^{+0.02}_{-0.02}$ keV $kT_2 = 1.77^{+0.16}_{-0.13}$ keV	1.070	308/288	0.19
WABS+TBABS+DISKPN+PO	$0.23^{+0.05}_{-0.04}$	$\Gamma = 2.1^{+0.1}_{-0.1}$ $kT_1 = 0.23^{+0.06}_{-0.05}$ keV Rin=6Rg*	1.099	319/290	0.12
	$0.24^{+0.05}_{-0.04}$	$\Gamma = 2.1^{+0.1}_{-0.1}$ $kT_1 = 0.25^{+0.06}_{-0.06}$ keV Rin=20Rg*	1.099	319/290	0.12
	$0.24^{+0.04}_{-0.04}$	$\Gamma = 2.1^{+0.1}_{-0.1}$ $kT_1 = 0.25^{+0.06}_{-0.06}$ keV Rin=100Rg*	1.099	319/290	0.12
	$0.23^{+0.07}_{-0.03}$	$\Gamma = 2.1^{+0.2}_{-0.1}$ $kT_1 = 0.27^{+0.09}_{-0.04}$ keV Rin=47^{+4}_{-4}Rg	1.058	304/287	0.24
	$0.24^{+0.05}_{-0.04}$	$\Gamma = 2.1^{+0.1}_{-0.1}$ $kT_1 = 0.25^{+0.07}_{-0.06}$ keV Rin=37^{+3}_{-3}Rg	1.057	303/287	0.24
	$0.24^{+0.05}_{-0.04}$	$\Gamma = 2.1^{+0.1}_{-0.2}$ $kT_1 = 0.25^{+0.07}_{-0.05}$ keV Rin=234^{+266}_{-234}Rg	1.057	303/287	0.24

* This parameter is fixed

** These parameters are linked

[b] $\alpha = \Gamma - 1$

Table 3.6: Parameters of the spectral fit of NGC 1313 X-2 with multiple component models from the longer *XMM-Newton* observation (Obs.Id. 0106860101). Following from Table 3.5.

Model	$N_{H\,tbabs}$ $[10^{21}\ \mathrm{cm}^{-2}]$	Parameters	χ^2_{red}	$\chi^2_{red}(d.o.f.)$	Q
WABS+TBABS+DISKPN+COMPTT	$0.22^{+0.06}_{-0.12}$	$kT_1 = 0.18^{+0.03}_{-0.03}$ keV** $kT_2 = 3.88^{+75.02}_{-10.88}$ keV $T_0 = 0.18^{+0.03}_{-0.03}$ keV** $\tau = 4.1^{+2.0}_{-1.4}$ Rin=6Rg*	1.061	304/286	0.23
WABS+TBABS+ST95+PO	$0.23^{+0.02}_{-0.02}$	$\Gamma = 2.1^{+0.2}_{-0.3}$ $M_{BH} = 189^{+536}_{-159}\ M_\odot$ $\dot{M}=1\ L_{Edd}/c^{2*}$	1.057	287	0.25
WABS+TBABS(TABS+TEMI)	$0.32^{+0.12}_{-0.2}$	$\alpha = 1.7^{+0.1}_{-0.1}$ $N_{H\,ion} = 3.7^{+0.2}_{-0.2}$ $\xi = 3999^{+978}_{-856}$	1.088	312/287	0.14
WABS+TBABS(TABS+TEMI+TRFL)	$0.32^{+0.09}_{-0.15}$	$\alpha = 1.4$(peg) $N_{H\,ion} = 3.7^{+0.2}_{-0.2}$ $\xi = 1532^{+512}_{-340}$	1.056	302/286	0.25
WABS+TBABS(TABS+TRFL)	$0.26^{+0.11}_{-0.20}$	$\alpha = 1.46^{+0.1}_{-0.1}$ $N_{H\,ion} = 5.0^{+0.4}_{-0.4}$ $\xi = 1931^{+435}_{-205}$	1.047	301/287	0.28

* This parameter is fixed

** These parameters are linked

[b] $\alpha = \Gamma - 1$

Table 3.7: Parameters of the spectral fit of NGC 1313 X-2 with multiple component models from the longer *XMM-Newton* observation (Obs.Id. 0106860101). Following from Table 3.5.

Obs. Id.	Count rate	Flux [0.2-10 keV] $[10^{-12}$ erg cm^{-2} s$^{-1}]$	F_{MCD}/F_{PL}	L $[10^{39}$ erg s$^{-1}]$	kT_{MCD} [keV]	Γ	$\chi^2_{red}(d.o.f.)$
0106860101	0.24	$4.00^{+0.82}_{-0.62}$	0.93	$6.52^{+1.34}_{-1.02}$	$0.16^{+0.02}_{-0.01}$	$2.3^{+0.1}_{-0.1}$	1.24(75)
0150280101	0.67	$5.07^{+0.23}_{-14.0}$	–	$8.30^{+0.04}_{-22.0}$	–	$2.3^{+0.2}_{-0.2}$	1.06(44)
0150280301	0.80	$9.46^{+1.55}_{-1.65}$	0.63	$15.43^{+2.53}_{-2.69}$	$0.13^{+0.01}_{-0.02}$	$1.9^{+0.1}_{-0.1}$	1.11(144)
0150280401	0.89	$9.19^{+3.10}_{-1.74}$	0.94	$14.99^{+5.06}_{-2.84}$	$0.15^{+0.03}_{-0.03}$	$1.8^{+0.1}_{-0.1}$	0.99(140)
0150280601	0.39	$5.63^{+2.97}_{-1.00}$	0.47	$9.18^{+4.84}_{-1.63}$	$0.13^{+0.03}_{-0.02}$	$2.5^{+0.1}_{-0.1}$	0.82(67)
0150281101	0.34	$4.38^{+1.01}_{-1.12}$	0.45	$7.14^{+1.65}_{-1.83}$	$0.17^{+0.02}_{-0.03}$	$2.3^{+0.1}_{-0.1}$	1.01(66)

Table 3.8: Parameters of the spectral fits of all *XMM* EPIC pn data of NGC 1313 X-2 in the 0.2-10.0 keV band. The adopted model is an absorbed MCD+PL with N_H frozen at 4.02×10^{21}cm^{-2}. Fluxes and luminosities (at a distance of 3.7 Mpc) are unabsorbed.

3.3 Identification and study of the optical counterpart of NGC 1313 X-2

Although ULXs have been identified thanks to their X-ray emission, a decisive step forward in understanding their nature has been made possible also by the identification of their optical counterparts. The study of their photometric and spectral properties is of fundamental importance to finally resolve the issue of the existence of IMBHs. Up to now only a few sources have an identified counterpart. Among them NGC 1313 X-2 is one of the best studied.

3.3.1 ESO 3.6m observations

The first optical identification of the actual counterpart of NGC 1313 X-2 was performed thanks to an observation taken with the 3.6 m telescope of the European Southern Observatory (ESO) at La Silla (Chile) by Zampieri et al. (2004). Optical images of the field of NGC 1313 X-2 in the R-band (Bessel filter) were taken on 16 January 2002 (see Table 3.9). We used EFOSC2 with a Loral/Lesser CCD of 2048×2048 pixels yielding a field of view of $\sim 5' \times 5'$ at a resolution of $0.314''$/pixel (re-binned by a factor 2). The night was clear with a seeing of about $1''$. Four images were obtained for a total exposure time of 1320 s (see Figure 3.2). Standard reduction of the data (including bias subtraction and flat-field correction) was performed within the IRAF environment.

A spectrum of one of the field objects (object A; see Figure 3.2) was secured on the same night. We performed low-resolution (13.4 A, grism#4) spectroscopy for a total exposure time of 1200 s. After applying standard corrections and sky subtraction, cosmic rays were removed and the spectrum was corrected for atmospheric extinction. At the time of the optical observations object A had already been imaged at the 1.1 m Las Campanas telescope by Stocke et al. (1995) and was considered a possible counterpart of NGC 1313 X-2. Although the new accurate *Chandra* position rules out an association with this object (see below), the spectrum can be used to gain insight on the properties of the surrounding nebula associated with the X-ray source (see e.g. Pakull & Mirioni 2002 and Section 3.3.1).

Astrometry and photometry of field objects

Our four ESO 3.6m images were astrometrically calibrated using an IRAF task (PLT-SOL) and performing a polynomial interpolation starting from the positions of GSC2 ESO field stars. The internal accuracy of this procedure was estimated comparing the actual positions of a number of GSC2 stars not used for astrometric calibration with the positions contained in the catalog. The accuracy is $0.3''$ (1σ). The four calibrated images were then summed together and the resulting image is shown in Figure 3.2.

In order to check for the relative systematics between the optical and X-ray astrometric calibrations, we used the position of SN 1978K. This supernova is inside the *Chandra* field of view but outside our optical image. Thus, we analyzed also an archival image of SN 1978K (from the Padova-Asiago Supernova Archive) taken on

Instrument	Obs. type	Date	Filter/Grism $band/\lambda_c$	Exp. time [s]	Seeing $['']$
3.6m+EFOSC	Image	2002-01-16	R	600+300×2+120	1.0
3.6m+EFOSC	Spec.	2002-01-16	4085-7520 A	1200	
VLT+FORS1	Image	2003-12-24	B	840×2	1.0
VLT+FORS1	Image	2003-12-25	V	600×2	0.8
VLT+FORS1	Image	2003-12-24	R	500×2	0.8
VLT+FORS1	Spec.	2003-12-22	5900 A	1300×2	...
VLT+FORS1	Spec.	2003-12-24	5900 A	1300×2	...
VLT+FORS1	Spec.	2003-12-30	5900 A	1300×2	...
VLT+FORS1	Spec.	2004-01-15	5900 A	1300×2	...
HST+ACS(I epoch)	Image	2003-11-22	F555w	580×2	...
HST+ACS	Image	2003-11-22	F435w	630×4	...
HST+ACS(II epoch)	Image	2004-02-22	F555w	600×4	...

Table 3.9: Log of the 3.6m+EFOSC and VLT+FORS1 observations of NGC 1313 X-2.

13 September 1999 with the same telescope and a similar instrumental set-up (ESO 3.6m+EFOSC/2.9+R#642, exposure time 180 s). After calibrating the archival image, the position of SN 1978K is α = 03h 17m 38.605s, δ = -66^0 33' 03.13'' (J2000). This is within 0.28'' from the radio position of Ryder et al. (1993), improving significantly upon the previous optical position by the same Authors. The difference between the centroids of the optical and *Chandra* positions of SN 1978K is 0.69'' ($\alpha_{opt} - \alpha_X$ = -0.085s, $\delta_{opt} - \delta_X$ = -0.47''). Although this difference is small and comparable with the statistical errors, we decided to apply this correction to the *Chandra* position of NGC 1313 X-2 to eliminate any systematic error between the optical and X-ray astrometric calibrations. The resulting *Chandra* position of NGC 1313 X-2 is reported in Table 3.2.

The photometry of the objects in our optical image was performed calibrating the frame with the *R*-band magnitudes of 23 stars from the SuperCosmos Sky Survey (Hambly et al., 2001) homogeneously distributed over the field of view. The internal accuracy of this calibration is 0.2 mag. Aperture (1.5'' radius) magnitudes are reported in Table 3.10.

Our *Chandra* position of NGC 1313 X-2 (Table 3.2) is shown in Figure 3.2, together with the *ROSAT* HRI (Schlegel et al., 2000) and *XMM* EPIC-MOS (Miller et al., 2003) error boxes, overlaid on our ESO image. All measurements are consistent within 1σ. The distance of the centroids of objects A, B and D with respect to the *Chandra* position is 3.6'', 4.1'' and 7.3'', respectively. Even taking into account the statistical error on the optical positions (0.3''), the identification with these three objects can be ruled out at a significance level of at least 3σ. On the other hand, object C is inside the Chandra error box and its position coincides within 1σ with that of NGC 1313 X-2, making it a likely counterpart.
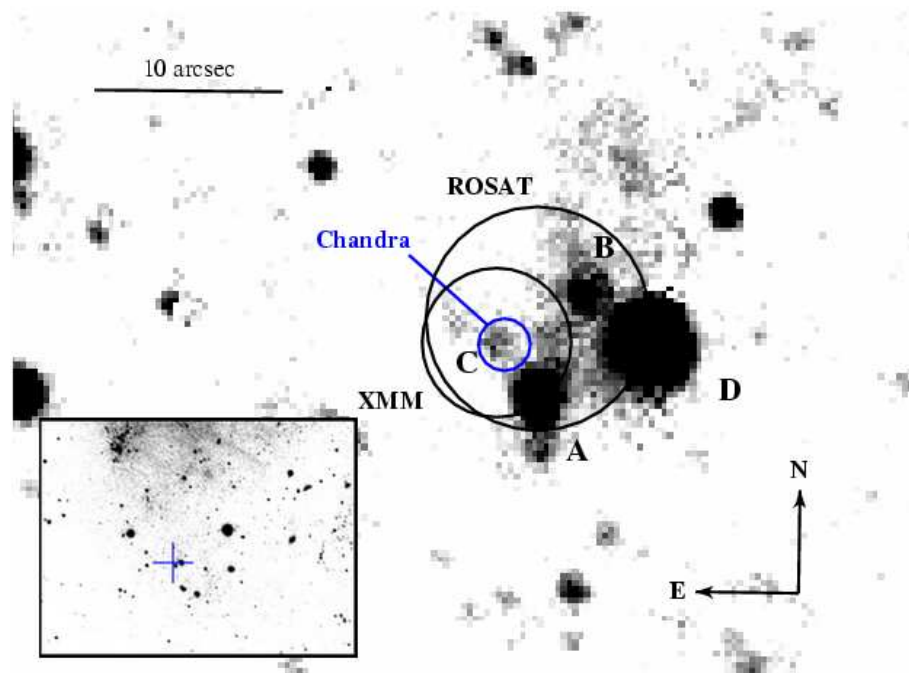
Figure 3.2: First detection of the optical counterpart of NGC 1313 X-2 on an ESO 3.6m *R*-band (Bessel filter) image (Zampieri et al., 2004). The circles show the *ROSAT* HRI, *XMM* EPIC-MOS and *Chandra* ACIS-S positions. The estimated 90% confidence radii are 6″ for HRI, 4″ for EPIC-MOS and 1.4″ for ACIS-S. Labels A, B, C and D mark the four field objects inside or close to the X-ray error boxes. The insert at the bottom-left shows a larger portion of the image with the position of the X-ray source (*cross*).

Observatory	Object[a]	B	V	R	B-V	V-R	Ref.
ESO/3.6m	A	–	–	19.8±0.2	–	–	Zampieri et al. (2004)
ESO/3.6m	B	–	–	20.7±0.2	–	–	Zampieri et al. (2004)
ESO/3.6m	C	–	–	22.9±0.2	–	–	Zampieri et al. (2004)
ESO/3.6m	D	–	–	17.8±0.2	–	–	Zampieri et al. (2004)
VLT	A	23.5±0.15	21.7±0.05	20.6±0.05	1.8±0.15	1.1±0.1	Mucciarelli et al. (2005)
VLT	B	22.4±0.15	22.7±0.05	22.5±0.05	-0.3±0.15	0.2±0.1	Mucciarelli et al. (2005)
VLT	C1	23.5±0.15	23.6±0.15	23.7±0.15	-0.1±0.2	-0.1±0.2	Mucciarelli et al. (2005)
VLT	C2	$\gtrsim$25.2	24.1±0.15	23.6±0.15	$\gtrsim$1.1	0.5±0.2	Mucciarelli et al. (2005)
VLT	D	20.3±0.15	18.9±0.05	18.1±0.05	1.4±0.15	0.8±0.1	Mucciarelli et al. (2005)
HST I epoch	C1	23.72±0.04	23.75±0.04	–	-0.10±0.06	–	Mucciarelli et al. (2007)
HST I epoch	C2	26.02±0.04	24.46±0.04	–	1.5±0.06	–	Mucciarelli et al. (2007)
HST II epoch	C1	–	23.61±0.04	–		–	Mucciarelli et al. (2007)
HST Ii epoch	C2	–	24.57±0.04	–		–	Mucciarelli et al. (2007)

[a] See Figure 3.2.

Table 3.10: Magnitudes of the optical counterpart(s) of NGC 1313 X-2 and of field objects.
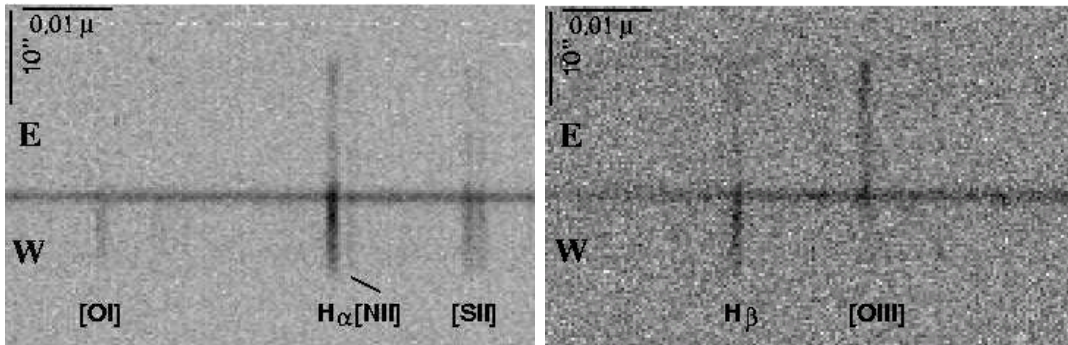
Figure 3.3: Two-dimensional spectrum (ESO 3.6m+EFOSC2+grism#4) of the field around object A. The slit (1.2″) is oriented in the east-west direction. The wavelength intervals are 4500–5300 A (left panel) and 6150–6900 A (right panel).
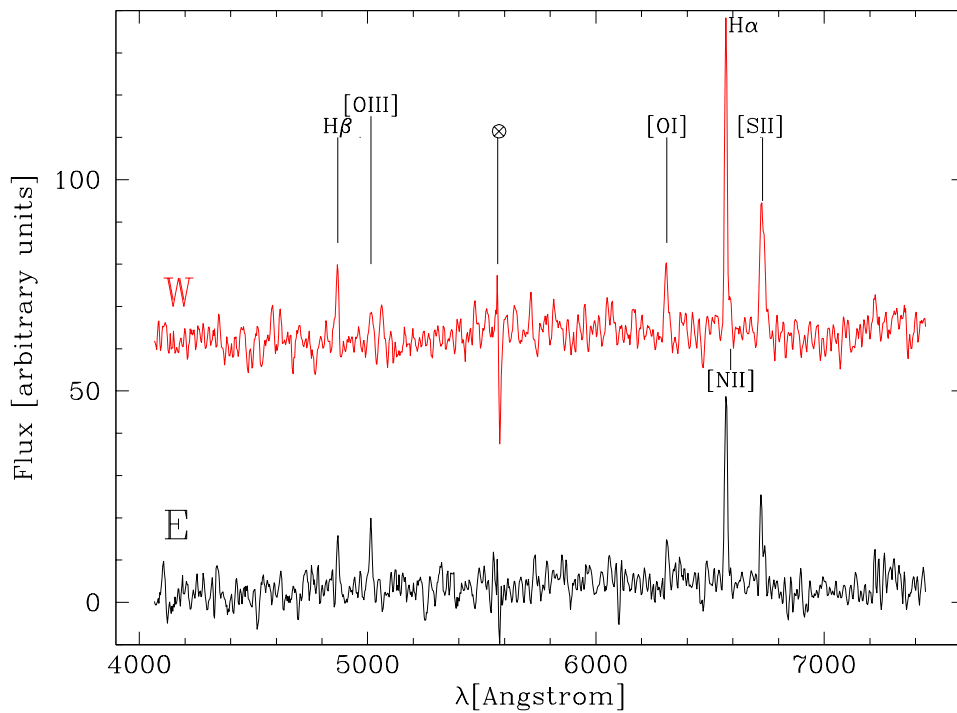
Figure 3.4: One-dimensional spectrum (F_λ) of the nebula around NGC 1313 X-2. The lower (upper) spectrum is extracted in a region east-ward (west-ward) of the position of object A (see text for details). The symbol ⊗ marks a residual contamination from an emission line of the sky.

The nebula around NGC 1313 X-2

A number of ULXs seems to be associated with optical emission nebulae, whose nature is still not entirely understood. Although some nebulae are associated with supernova episodes, it is clear that in many cases the ULX is the engine of the nebular emission (Pakull & Mirioni, 2002; Zampieri et al., 2004). NGC 1313 X-2 is associated with a spectacular and complex nebula that we independently detected in our 3.6m spectrum.

The EFOSC two-dimensional spectrum of the field around object A (Figure 3.3)
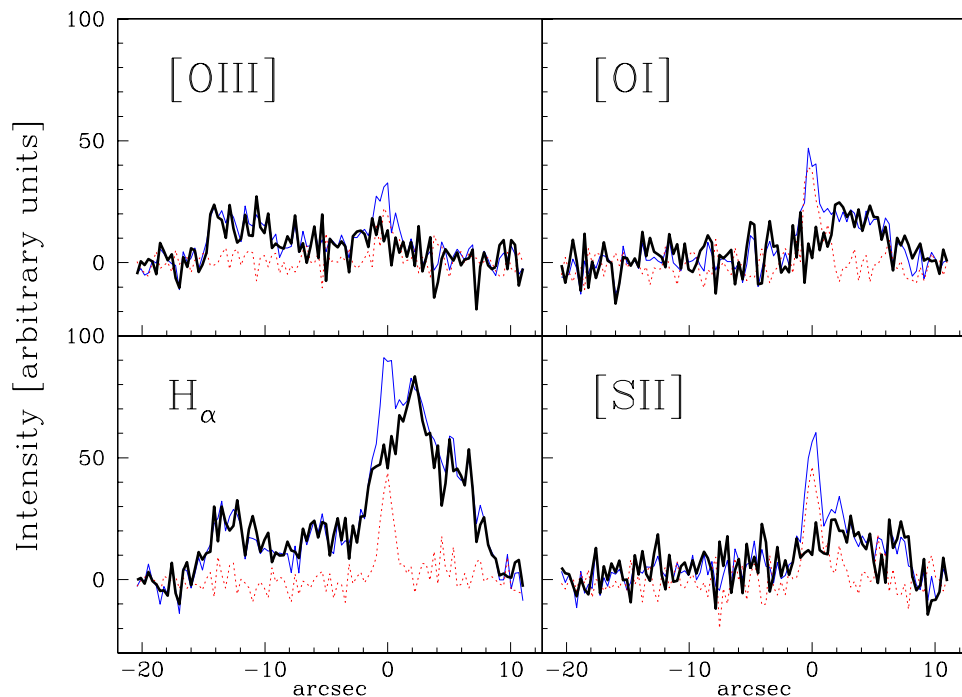
Figure 3.5: Line intensity profile of the nebular emission of H_α, [SII], [OI] and [OIII] around NGC 1313 X-2. The total emission is in *blue*, the stellar emission of object A (at the center of the spatial scale) is in *red* and the difference is in *solid black*.

shows clear emission lines extending for tens of arcsecs from east to west (~ 400 pc). This extended optical emission nebula was first found in deep H_α images by Pakull & Mirioni (2002). A one-dimensional spectrum of the nebula was extracted over an aperture of $0.9''$ (3 pixels) from two regions east-ward and west-ward of the position of object A and adjacent to it (Figure 3.4). Wavelength and relative flux calibration were applied to the data. The one-dimensional spectrum shows strong emission lines of H_α, H_β, [SII] $\lambda\lambda$ 6717–6731 A, [OI] λ 6300 A and [OIII] $\lambda\lambda$ 4959-5007 A. The shift of the centroid of the lines (~ 10 A) is consistent with the recession velocity of the galaxy and indicates that the emission nebula is located in NGC 1313.

It is worth emphasizing the abrupt change in the absolute and relative intensity of the emission lines from east to west, indicating variations in the physical conditions and/or geometry of the emission nebula. In particular, strong emission from [OIII] is present on the east side but almost absent on the west side, while emission from H_α, [SII], [OI] and other elements is present on the west side but weaker or absent on the east side. A careful inspection of the line intensity profiles (see Figure 3.5, in particular the profiles of H_α and [SII]) reveals a fairly symmetric, broadly peaked profile, centered at $\sim 2''$ west of the position of object A, and a weaker, roughly constant intensity component extending in the east direction.

3.3.2 VLT observations

We analyzed archive ESO VLT+FORS1 images (BVR) and spectra of NGC 1313 X-2 taken between December 2003 and January 2004 (Program ID 072.D0614). The observations are listed in Table 3.9. The images were astrometrically calibrated using 29 GSC2 stars. The calibration uncertainty, tested with GSC2 stars not used for the calibration, is $\sim 0.3''$. Finally, for each band the images were combined and cleaned from cosmic rays. Figure 3.6 shows the combined R, V and B images. On the same night a short exposure of the standard PG 0231+051 Landolt field (Landolt, 1992) was also taken in each band. Aperture photometry ($1''$ radius) was performed on the combined images. The instrumental magnitudes were then calibrated with the Landolt standard stars in the Bessel-Cousins system (see Patat, 2003, for extinction coefficients and color terms). The internal accuracy of the photometric calibration is 0.2 mag.

In Figure 3.2 the optical counterpart, object C is close to the limit of detectability and appears as a single object. Thanks to the higher resolution of the VLT image, in the R and V exposures we are able to resolve object C in two distinct point sources, C1 and C2. Both are inside the *Chandra* error box (see Figure 3.6). Object C2 is not detected in the B band frame. Aperture magnitudes, colors and astrometric positions of the two candidate counterparts, C1 and C2, and of objects A, B, and D are reported in Table 3.10. The photometric errors are the 2σ statistical errors on the measurements with the different Landolt standards.

In addition to the images, we also analyzed four VLT+FORS1 spectra (λ_c=5900 A, $\lambda/\Delta\lambda$=440 at λ_c) of objects C1+C2 taken in different nights (Table 3.9). The slit ($1''$) was oriented to include object D. After performing standard reduction, all spectra were sky subtracted, wavelength calibrated through comparison lamp exposures and flux calibrated using standard star spectra obtained in the same night. In these VLT+FORS1 spectra the two sources (C1 and C2) are not spatially resolved. The 2D spectrum taken on 15 January 2004 is shown in Figure 3.7. Nebular emission lines of [OII] λ 3727 A, H$_\gamma$, H$_\beta$, [OIII] $\lambda\lambda$ 4959-5007 A, [OI] λ 6300 and 6364 A, H$_\alpha$, [NII] λ 6583 A and [SII] $\lambda\lambda$ 6717-6731 A are clearly detected. Note that this is the first detection of a [OII] line from this nebula. A one dimensional spectrum was extracted over an aperture of $2.2''$ centered on object C1+C2 from each of the four combined spectra. Two nebular spectra were extracted from different $1''$ apertures, eastward and westward of the source position and adjacent to it. The two spectra were then averaged and the resulting spectrum subtracted from that of object C1+C2. All these spectra, taken on January 15th, are shown in Figure 3.8. The nebula-subtracted source spectrum shows no evident emission or absorption lines. Residuals are present in coincidence with some nebular lines (especially [OIII] and H$_\alpha$), with an upper limit to the equivalent width of $\sim$ 30 A. In particular the residual flux in the [OIII] line is a non negligible fraction of the nebular flux. This appears to be caused by an increased emission of the nebular line around the position of object C1+C2. It is not clear if this is simply induced by a change in the rather irregular spatial profile of the nebular line or by a variation of the physical conditions produced by the presence of the nearby ULX. Finally, marginal evidence of an excess in emission may be seen at

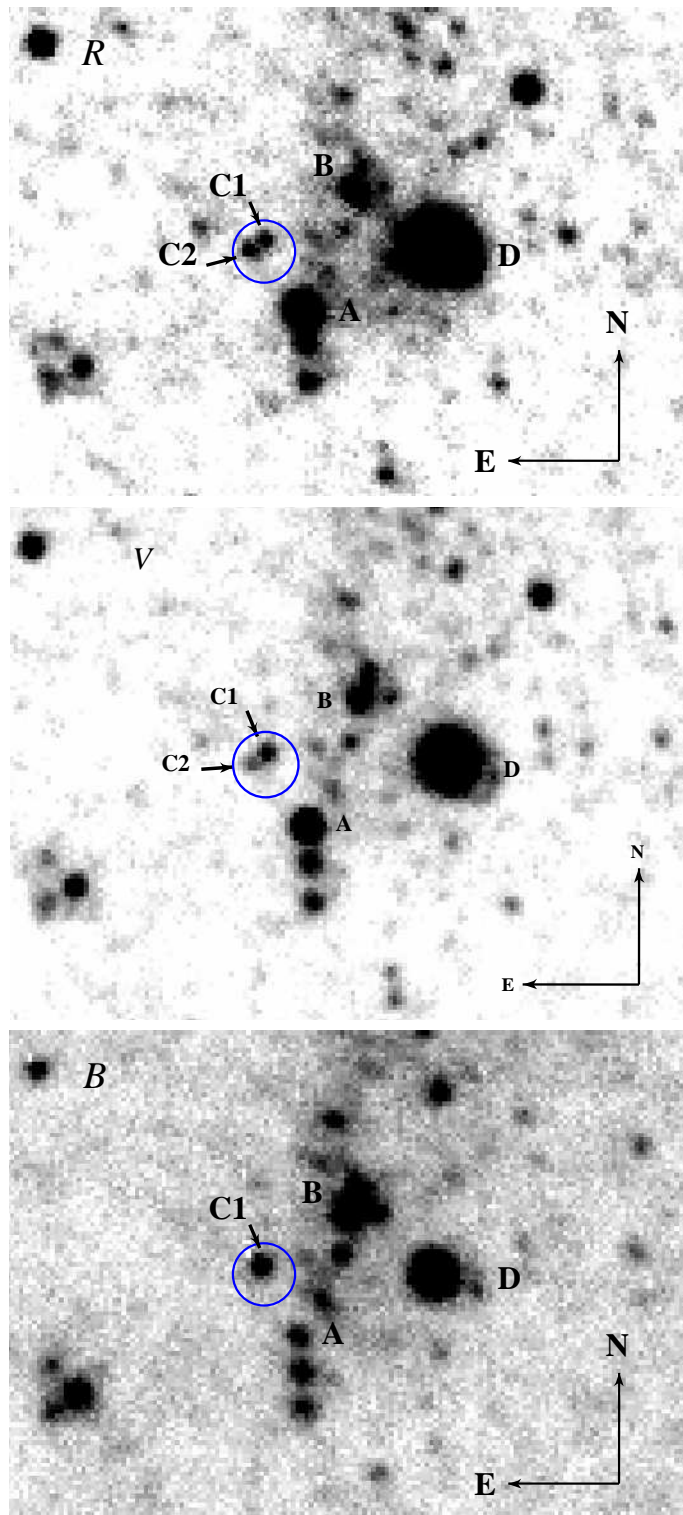Figure 3.6: *R* (*top*), *V* (*center*)and *B* (*bottom*) VLT+FORS1 images of the field around NGC 1313 X-2 (30″×20″). The circle is the 2σ *Chandra* error-box (1.4″). In the *R* frame, the counterpart is clearly resolved in two point sources, C1 and C2.
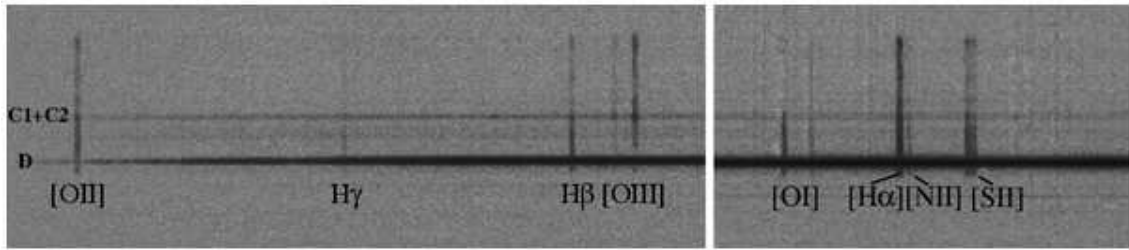
Figure 3.7: Two-dimensional spectrum (VLT+FORS1) of objects C1+C2. The slit (1″) is oriented to include object D. The wavelength intervals are 3600-5200 A (*left*) and 6200-7100 A (*right*).

4686 A, corresponding to HeII emission, but the line is not statistically significant.

3.3.3 *HST* observations

HST images of the field of NGC 1313 X-2 were also obtained with ACS in two epochs (see Figure 3.9). These *HST* and the VLT observations were performed in parallel with the *XMM-Newton* observations reported in Section 3.2. The observation log of the *HST* images considered here are reported in Table 3.9. Aperture photometry was performed on the drizzled calibrated data (reduced by the *HST* pipeline) and transformed to the Cousins system following Sirianni et al. (2005) (see Table 3.11).

The uncertainty on the magnitudes are dominated by the calibration error (~ 0.03 for the *HST* photometry of point sources), including filter transformation. As a further check of the internal consistency of the *HST* photometry, we compared the magnitudes of thirteen field stars obtained in the two epochs. The difference is significant only for one source in the sample (~ 0.3 mag). Excluding this source, the variability of which is probably intrinsic, the magnitude changes are randomly scattered around zero, with a mean absolute deviation of 0.04 mag.

The *HST* images clearly confirms that two distinct possible optical counterparts, C1 and C2 (Section 3.3.2), are present in the *Chandra* error box.

3.4   Results

3.4.1   X-ray to optical flux ratio

The first hypotheses on the nature of NGC 1313 X-2 where based on ROSAT HRI data from Stocke et al. (1995) and an optical identification with object A. From the very high X-ray to optical flux ratio and extremely soft component in the X-ray spectrum they suggested that the ULX could be a very massive XRB hosting a BH in NGC 1313 or a very nearby (approximately 100 pc) isolated, old neutron star slowly accreting interstellar matter onto its magnetic poles. With new X-ray and optical data we where able to exclude the latter possibility. From its irregular variability and the properties of the X-ray and optical spectrum, we could also ruled out that NGC 1313 X-2 is a X-ray emitting SN.
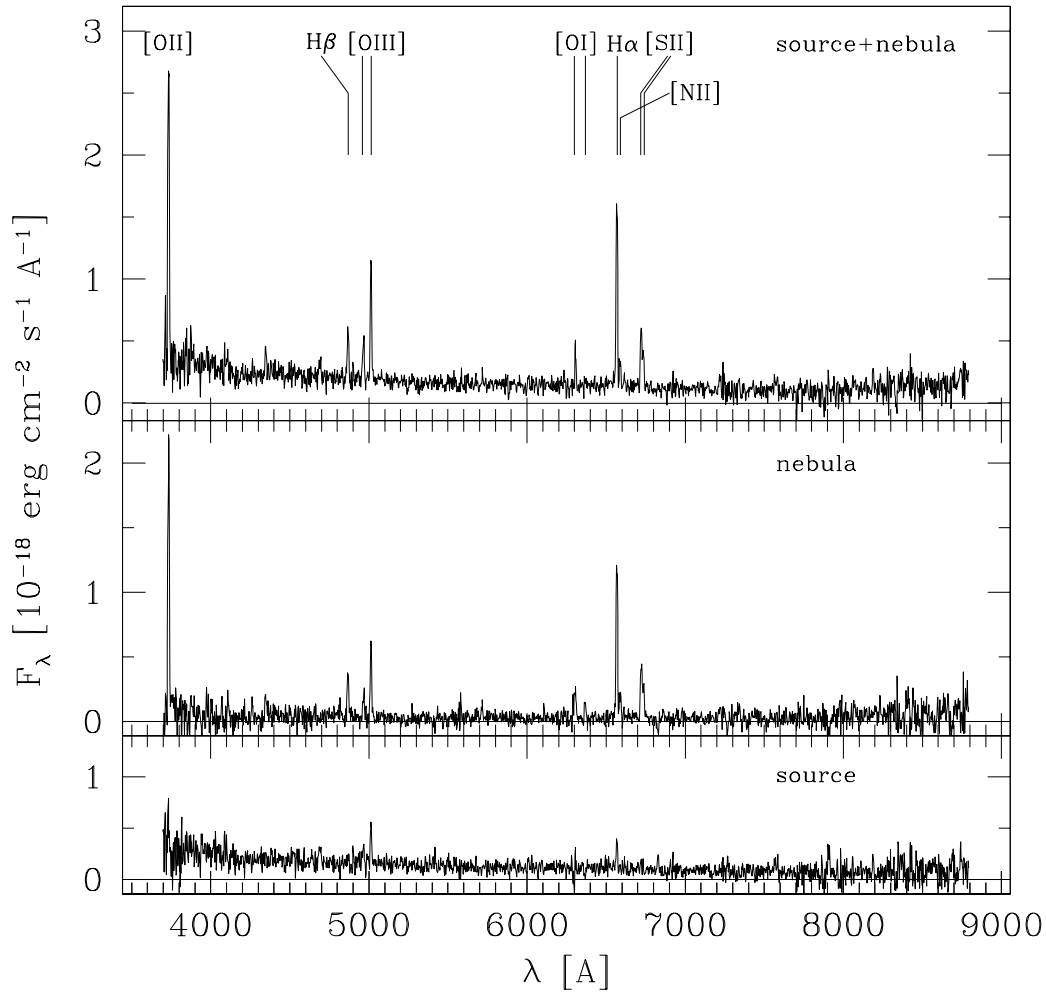
Figure 3.8: From top to bottom: VLT+FORS1 spectrum of 15 January 2004 (3700-8900 A), extracted from an aperture of 2.2″ centered on the unresolved object C1+C2; average spectrum of the nebula, extracted from two 1″ apertures located eastward and westward of the source position and adjacent to it; the nebula-subtracted spectrum of object C1+C2.
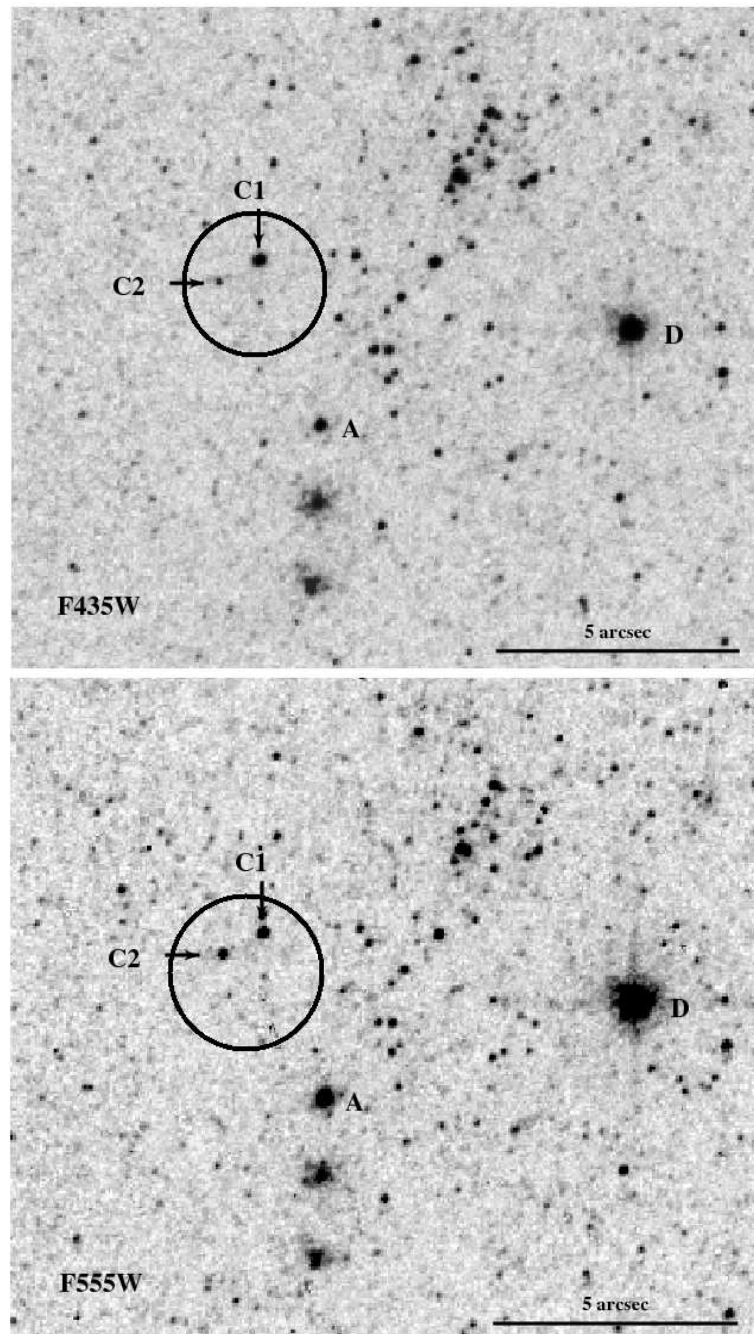
Figure 3.9: *HST*+ACS images of NGC 1313 X-2: F435W (B) band (*top panel*) F555W (V) band (*bottom panel*). The *Chandra* error box, the candidate optical counterparts C1 and C2 and the field sources A and D are shown.

From the R magnitude of objects C1 and C2 (23.7 and 23.6 respectively), and the maximum X-ray flux observed with *XMM-Newton* ($f_X \sim 9 \times 10^{-12}$ erg cm^{-2} s^{-1}), NGC 1313 X-2 turns out to have a X-ray to optical flux ratio $f_X/f_R \gtrsim 8000$. This value is very high, in agreement with the suggestion by Cagnoni et al. (2002) that ULXs can be selected on the basis of their large f_X/f_{opt}. Only Isolated Neutron Stars

(INSs) and heavily obscured AGNs can reach such large values of the X-ray/optical flux ratio.

INSs are extreme in this respect, with blue $B > 26$ optical counterparts and typical X-ray-to-optical flux ratios $\gtrsim 10^5$ (see e.g. Kaplan et al. 2003). Furthermore, known INSs exhibit different spectral properties with no significant variability.

On the other hand, a heavily obscured AGN is expected to have a rather hard X-ray spectrum and to emit significantly in the near-infrared (see e.g. Brusa et al. 2002). Given the X-ray luminosity of NGC 1313 X-2, an infrared magnitude $K \approx 12$ is expected if it is an obscured AGN. The lack of any IR counterpart on a K image of the 2MASS All Sky Image Service down to a limiting magnitude $K \simeq 14$ (10σ) and the softer X-ray spectrum of NGC 1313 X-2 make this possibility unlikely. To produce the same X-ray flux but a f_X/f_R ratio of ~ 100, the R magnitude should be ~ 20. Therefore the additional reddening required to make the objects look like an obscured AGN is $A_R \simeq 3.5$ mag, corresponding to a column density $\sim 9 \times 10^{21}$ cm^{-2} (Bohlin et al., 1978), much larger than that inferred from X-ray spectral fits ($\sim 3^{+0.9}_{-0.4} \times 10^{21}$ cm^{-2}). Most importantly we are led to rule out an identification with an (obscured) AGN because no statistically significant emission line at wavelengths longer than H$_\alpha$ is observed in the optical spectrum nor any other feature that may be identified with a highly redshifted emission line (see Figure 3.8).

3.4.2   An estimate of the BH mass from the X-ray spectrum

If NGC 1313 X-2 is a black hole binary, the X-ray spectral parameters can be used to estimate the BH mass. Although our analysis shows that there is not a preferred model for the spectral emission, following the similarities with XRBs, we could use the temperature of the MCD (hereafter referred to as T_{MCD}) to derive the mass of the compact remnant. This is similar to what done by Miller et al. (2003) using the normalization of the MCD fit and, as discussed below, we reach similar conclusions. The effective temperature of a standard accretion disk depends on radius as:

$$T^4 = \left(\frac{3GM_{BH}\dot{M}}{8\pi\sigma r_{in}^3} \right) \left(\frac{r_{in}}{r} \right)^3 \left[1 - \left(\frac{r_{in}}{r} \right)^{1/2} \right], \qquad (3.1)$$

where $\dot{M}$ is the accretion rate and r_{in} is the innermost disk radius (e.g. Frank et al. 2002). Assuming that T_{MCD} represents the maximum disk temperature, it is:

$$\alpha T_{MCD} = \left(\frac{3GM_{BH}\dot{M}}{8\pi\sigma r_{in}^3} \right)^{1/4}, \qquad (3.2)$$

with $\alpha \simeq 2$ (see Chapter 2, Section 2.1.3). Neglecting relativistic corrections and assuming that the disk terminates at the innermost stable circular orbit of a Schwarzschild BH, it is:

$$\frac{M_{BH}}{M_\odot} = \left(\frac{\dot{M}c^2}{L_{Edd}} \right) f^4 \left(\frac{\alpha T_{MCD}}{1.5 \times 10^7\,\mathrm{K}} \right)^{-4}, \qquad (3.3)$$

where f is a color correction factor ($f \sim 1.6 - 1.7$, Shimura & Takahara 1995; Zampieri et al. 2001).

The *ASCA* GIS+SIS data can be fitted by a single MCD component (see also Makishima et al., 2000). The value of T_{MCD} inferred from this fit (~ 1 keV) implies a BH mass of only a few $M_\odot$, not consistent with the large values of M_{BH} ($\gtrsim 120\,M_\odot$) obtained assuming that the X-ray emission is unbeamed. Makishima et al. (2000) invoke a rapidly spinning BH with beamed emission in NGC 1313 X-2. On the other end the low inner disk temperature obtained from the MCD plus power-law fit to the *XMM* EPIC spectrum ($kT \sim 240$ eV) implies $M_{BH} \approx 60 f^4\,M_\odot$ ($\alpha \simeq 2$) for Eddington limited accretion, comparable to that derived from the flux. This agrees with the conclusion of Miller et al. (2003) that , assuming isotropic emission, NGC 1313 X-2 contains an IMBH, although their estimate of the BH mass is larger. It is worth noting that, although the large BH mass does not require that the emission is beamed, we cannot rule out that a moderate jet activity, producing radio emission (and possibly inflating the emission nebula), is present in NGC 1313 X-2 (see e.g. the case of an ULX in NGC 5408; Kaaret et al. 2003). However, presently available radio images of the field of NGC 1313 X-2 (Sydney University Molonglo Sky Survey at 843 MHz and Australia Telescope Array at ~ 5 GHz; Stocke et al. 1995) are not sufficiently deep to allow detection.

3.4.3   X-ray spectra and variability

As discussed at length in Section 3.2.2, the 2000 *XMM-Newton* observation of NGC 1313 X-2 has the longer exposure time and then the best counting statistics. We then performed a joint fit of the MOS+pn data, exploring a number of different spectral models (Section 3.2.2 and Tables 3.5, 3.6 and 3.7). A composite absorbed MCD plus PL component model gives an acceptable fit, at the same level with other models of that type ("soft thermal + hard tail").

In fact, there is also some evidence of a closer similarity, inasmuch some ULXs appear to show state transitions (Makishima et al., 2004; Winter et al., 2005). We used the *XMM-Newton* observations presented in Section 3.2.2 to analyze the X-ray spectral variability of NGC 1313 X-2. The more significant result is that the slope of the PL component seems to correlate with the flux, i.e. at higher fluxes the spectrum hardens (see Table 3.2.2). This behavior can be noticed also comparing the two *ASCA* observations and is opposite to that usually shown by Galactic XRBs. A similar correlation was also observed in a few ULXs in the Antennae galaxy by Fabbiano et al. (2003b). Concerning the MCD component, it is statistically significant in the Oct 2000 and in the 2003 pointings with higher counting statistics, while it is not needed in the shorter *XMM-Newton* observations. Although this might reflect an intrinsic variability of the thermal component, no definite conclusion can be reached at present because of the low statistics. Spectral variability was recently inspected by Feng & Kaaret (2007b), using the six *XMM-Newton* observations of the present analysis plus other 6 newer exposures. They found that the cool disk component failed to follow the expected relation $L \propto T^4$. On the contrary, a fit with the p-free model is also adequate and the spectral evolution of the parameters is consistent with

the expected relation and appears to be a high-luminosity extension of the $L - kT$ relation of Galactic BHCs. Finally, we note that the flux of the MCD component is comparable to that of the PL component (see Table 3.8).

3.4.4   X-ray light curve

Before 2000, variability of up to a factor 2 on a timescale of months is clearly present in the X-ray light curve of NGC 1313 X-2 and is reminiscent of the behavior observed in Galactic X-ray binaries. Around December 23, 2003 (see the insert in Figure 3.10), the source experienced a short, but quite intense flare, reaching a maximum unabsorbed flux of $\sim 9.5 \times 10^{-12}$erg cm^{-2} s^{-1} (Table 3.3). At the distance of NGC 1313 this corresponds to an intrinsic luminosity of $\sim 10^{40}$erg s^{-1}. Clearly this value depends on the adopted spectral model and hence should be taken with care. We also measured the fluxes of another ULX in the field (NGC 1313 X-3), known to be an interacting supernova (SN 1978K), in order to check if the significant increase in the flux was real or artificially produced by residual systematic effects between the different observations. The flux of the supernova ($\sim 8.2 \times 10^{-13}$erg cm^{-2} s^{-1}) is consistent with a constant, within the uncertainties (the variation is $\lesssim 20\%$). Hence we conclude that the luminosity increase of NGC 1313 X-2 is significant and fully qualifies it as a fairly bright ULX.
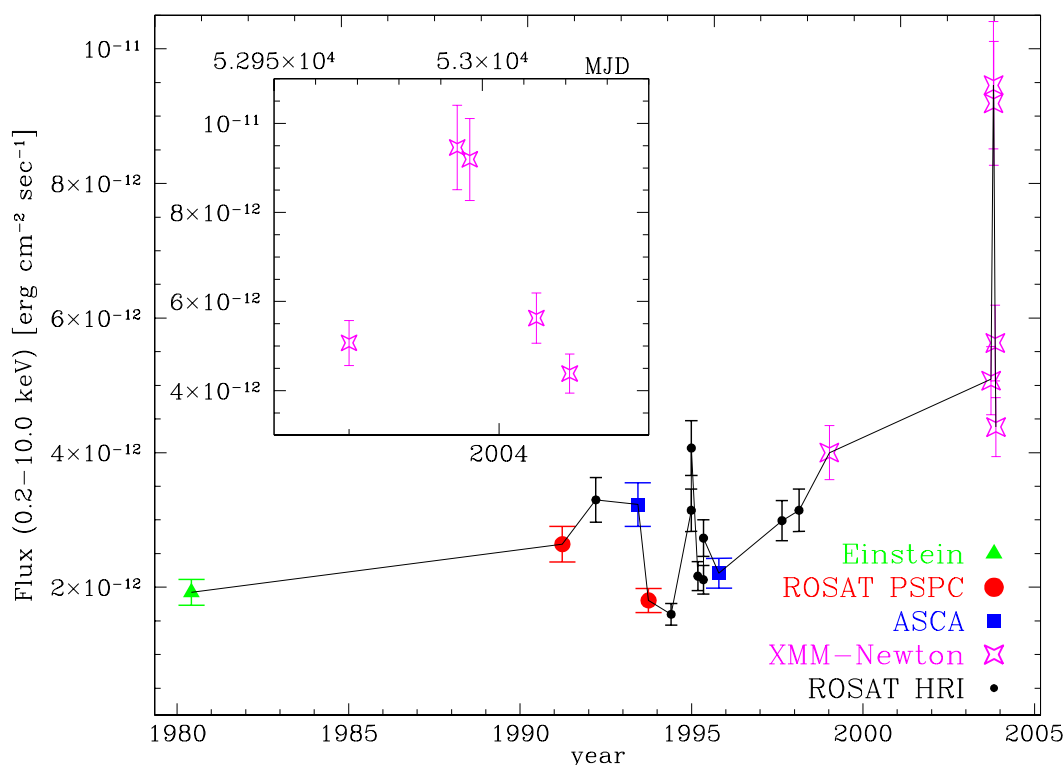

Figure 3.10: Long term X-ray light curve of NGC 1313 X-2. Fluxes are unabsorbed and refer to the [0.2-10.0] keV energy interval (see Table 3.8). The insert refers to the more recent *XMM-Newton* data.

3.4.5 Two possible optical counterparts for a ULX

As discussed in Section 3.3.1, the actual optical counterpart of NGC 1313 X-2 was identified for the first time on our ESO 3.6m image (Zampieri et al., 2004). The object appears like a single unresolved source, named object C. The superb quality of the available VLT and *HST* images reveals that object C is resolved in two distinct objects, C1 and C2, both inside the *Chandra* error box of NGC 1313 X-2 in the R and V bands (Section 3.3.2 and 3.3.3; Mucciarelli et al., 2005, 2007). From the astrometric positions reported in Table 3.2, we infer a separation of $0.75''$ and a position angle (C2 with respect to C1) of $\sim 131°$. All the VLT and *HST* magnitudes and colors of the two objects are reported in Table 3.11.

Within the photometric errors, the VLT colors of object C1 appear to be consistent with those of a A3-O9 I or a A2-B0 V star, while those of C2 with a G8-G7 I star (see e.g. Cox 2000; Braddley 1982). Unfortunately, the optical spectral continuum does not provide useful information for assessing the spectral type because the light from both objects contributes to it. Observationally, the slope of the continuum can be characterized by a power law, $\lambda^{-1.8}$. The absence or extreme weakness of the HeII λ 4686 A emission line in the optical spectrum suggests that X-ray irradiation is not dominant. Taking Galactic absorption into account and assuming $A_V \simeq 0.3$ (Cardelli et al. 1989 extinction law with $R_V = A_V/E_{B-V} = 3.1$ has been used throughout), the de-reddened colors of object C1 are $(V-R)_0 = -0.2 \pm 0.2$ and $(B-V)_0 = -0.2 \pm 0.2$, consistent with those of a B8-O I or A0-O5 V star. For object C2 it is $(V-R)_0 = 0.4 \pm 0.2$ and $(B-V)_0 \gtrsim 1.0$, consistent with a G4 I star. Liu et al. (2005) performed a 6.4 m Magellan/Baade observation of the field around NGC 1313 X-2 and found a $I = 23.3$ mag object in coincidence with the position of C1+C2 (that appear unresolved in their I frame). Assuming that the flux in the I band originates mainly from the redder object C2, we then obtain $(R-I) = 0.3 \pm 0.2$, consistent with our tentative spectral classification.

At the distance of NGC 1313 ($d = 3.7$ Mpc; Tully 1988) the VLT magnitudes in the V band of C1 and C2 translate into the absolute magnitudes $M_V \sim -4.6$ and ~ -4.1, respectively. Comparing these values with the absolute magnitudes of main sequence and supergiant stars (e.g. Cox 2000; Braddley 1982), we found that both colors and magnitudes are consistent only with a B0-09 main sequence star for C1, while they are consistent with a G4 supergiant of type Ib for C2. Therefore, we conclude that both C1 and C2 are stars in NGC 1313, with C1 an early type main sequence star of $\sim 20\ M_\odot$ and C2 a supergiant of $\sim 10\ M_\odot$. The bolometric luminosities of the two objects are $\sim 3 \times 10^{38}$ erg s^{-1} and $\sim 2 \times 10^{37}$ erg s^{-1}, respectively.

A photometric analysis of a large sample of field stars (> 30) was performed on the three BVR VLT images. A color-color plot of these objects is shown in Figure 3.11. Almost all of them have stellar colors, apart from two on the lower right part of the diagram that are bluer than ordinary stars. Given their apparent magnitude, objects earlier than spectral type F (including C1) are stars in NGC 1313, while the others may be Galactic foreground stars or belong to NGC 1313. However, object C2 cannot be a Galactic foreground star because its absolute visual magnitude would be $M_V \sim 9$, too large to be consistent with its colors.

	Filter/Color	C1	C2
HST I epoch	B	23.72±0.04	26.02±0.04
VLT	B	23.50±0.15	$\gtrsim 25.2$
HST I epoch	V	23.75±0.04	24.46±0.04
VLT	V	23.60±0.15	24.10±0.15
HST II epoch	V	23.61±0.04	24.57±0.04
HST I epoch	B-V	-0.1±0.06	1.5±0.06
VLT	B-V	-0.1±0.2	$\gtrsim 1.1$

Table 3.11: *HST* and VLT magnitudes and colors of the two candidate optical counterparts of NGC 1313 X-2.

The *HST* images clearly confirm that two distinct objects are present inside the X-ray error box of NGC 1313 X-2 (see Figure 3.9). If we take Galactic absorption into account, the de-reddened colors inferred from the 1st *HST* epoch are $(B-V)_0 \sim -0.1$ and ~ 1.5 for C1 and C2, respectively (see Table 3.11). The color for object C1 is consistent with that previously derived from VLT data. The detection of object C2 in the B band *HST* frame permit us to overcome the VLT upper limit in the B magnitude. The measured value of the B magnitude of object C2 and the derived (B-V) color are close to that of a K3-K4 supergiant. For both objects, there is evidence of variability in the V band between the two *HST* epochs (~ 0.1 mag; see also Ramsey et al. 2006).

Given the density of objects in the field of view ($\sim 50-100$ arcmin^{-2}), a significant fraction of which are supergiants in NGC 1313, the probability that C1 or C2 fall by chance inside the 2σ *Chandra* error box is not negligible (~ 0.1). However, the chance occurrence of two objects, separated by only 0.7″, inside the X-ray error box is $\sim 5 \times 10^{-3}$, sufficiently small to be considered rather unlikely. Actually, if both C1 and C2 are stars in NGC 1313, a physical association may not be implausible (the distance corresponding to the apparent separation on the sky is ~ 10 pc).

Irrespectively of which of the two objects is the actual counterpart, NGC 1313 X-2 appears to be a high mass X-ray binary with a very massive donor star.

3.4.6   The nebula and the environment of NGC 1313 X-2

We now turn to discuss how our optical observations can be used to constrain the environment of NGC 1313 X-2. Figures 3.3 and 3.7 reveal that NGC 1313 X-2 is likely to be associated with an optical emission nebula, recognizable also in a H$_\alpha$ image of Pakull & Mirioni (2002) (see also Figure 3.12). From the velocity (80 km s^{-1}) and flux of H$_\beta$, Pakull & Mirioni (2002) derive an impressive mechanical energy of $3 - 10 \times 10^{52}$ erg for the expanding ionized gas, and suggest that the nebula is inflated by a relativistic jet from NGC 1313 X-2. Our measured ratio of [SII]/H$_\alpha$ (~ 0.5) is consistent with that expected from a shock-ionized supernova remnant, a stellar wind-shocked nebula or diffuse ionized gas (Matonick & Fesen, 1997). However, the inferred diameter and energy of the nebula are too large to be consistent with a single supernova event, unless it was produced by a hypernova similar to SN 1998bw (see e.g. Iwamoto et al. 1998). In fact, it could be the result of several explosion
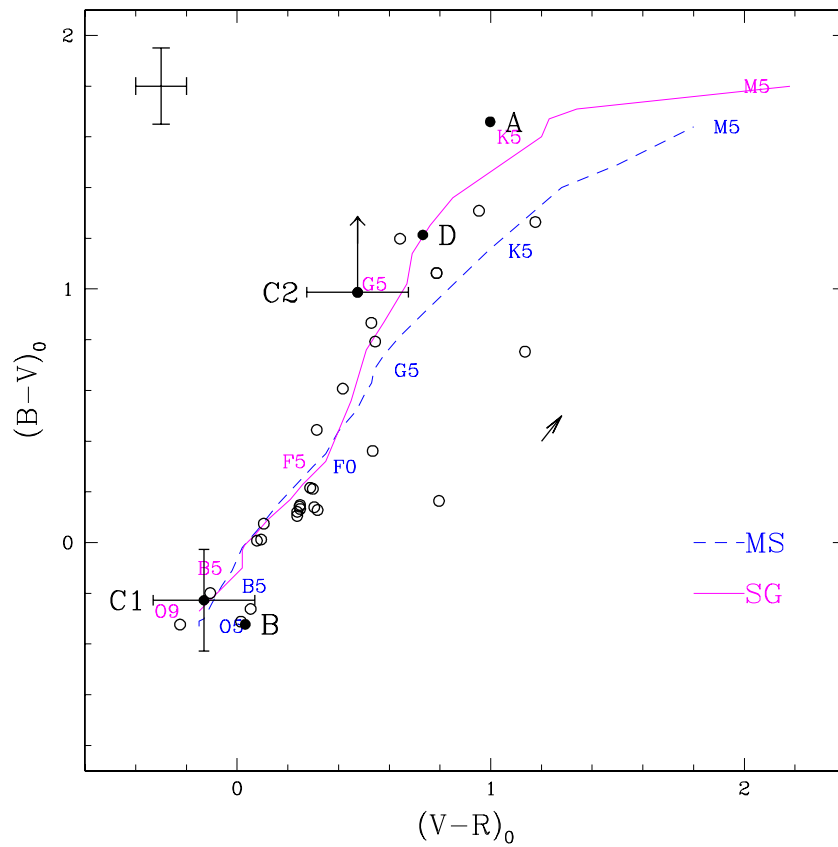
Figure 3.11: $(B - V)_0$ vs. $(V - R)_0$ diagram for a sample of field objects around NGC 1313 X-2, including A, B, C1, C2 and D. Error bars are shown at the upper left corner. Measurements were corrected for Galactic extinction ($A_V = 0.3$, $E_{B-V} = 0.1$, corresponding to a column density $N_H = 6 \times 10^{20}$ cm^{-2}). The arrow indicates the reddening vector corresponding to $E_{B-V} = 0.1$. The solid and dashed lines represent the colors of supergiant (SG) and main sequence (MS) stars
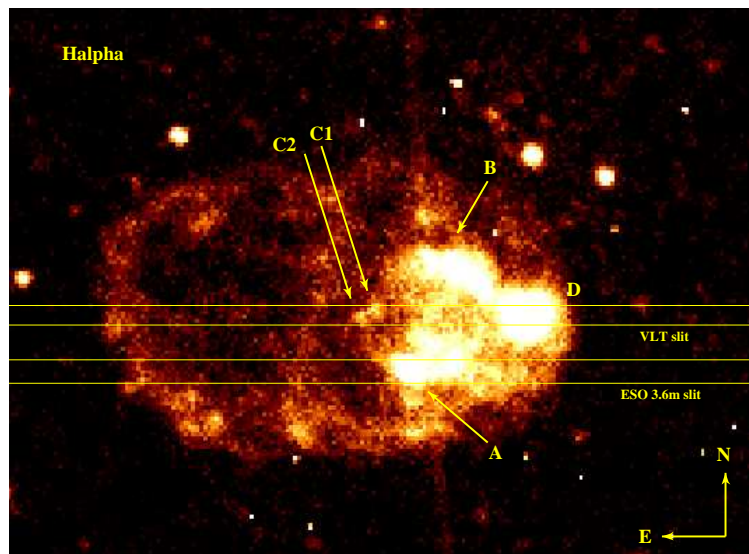
Figure 3.12: VLT H_α image of the nebula surrounding NGC 1313 X-2. The candidate optical counterparts C1 and C2 and the field sources A, B, and D are shown. The rectangular regions represent the ESO 3.6m ($1.2''$) and VLT ($1''$) slits of the optical spectra reported in Figures 3.3 and 3.7.

events (multiple supernova remnant) or be originated by the intense wind of hot stars, possibly the parent stellar association of NGC 1313 X-2. As discussed in Section 3.3.1, the nebula appears to have some internal structure: a comparatively brighter, fairly symmetric component west of the position of NGC 1313 X-2 and a weaker, slightly elongated one extending in the east direction. The brighter part of the nebula has [SII]/H_α=0.58, the weaker one has [SII]/H_α=0.44 and intense [OIII] emission (see Figure 3.5). Different possibilities may explain the irregular appearance of the nebula. As suggested by Pakull & Mirioni (2002), the varying line intensity may be caused by reprocessed emission from the X-ray ionized interstellar medium where the physical conditions (in particular the density) vary on a scale ~ 100 pc. However, the nebular emission may also arise from two physically distinct components: a weaker wind-shocked nebula produced by a possible parent stellar association of NGC 1313 X-2 and a brighter multiple supernova remnant. This hypothesis seems to be confirmed also by the marginal detection of (possibly extended) UV emission in an image of the *XMM-Newton* Optical Monitor (see Figure 3.13), in coincidence with the brighter component. Clearly, the weaker component may still be a jet-inflated nebula, as suggested by Pakull & Mirioni (2002). Finally, we note that, although NGC 1313 X-2 is somewhat hotter and much more luminous, the [OIII] signature in the eastern portion of the nebula is reminiscent of predictions for the radiation-limited nebulae around supersoft sources (Di Stefano et al. 1995; Chiang & Rappaport 1996).

3.4.7   Mass supply for the ULX binary system

From the observed luminosity, the estimated accretion rate of the system (assuming 10% efficiency) is $\dot{M} \sim 10^{-7}\, M_\odot\, \mathrm{yr}^{-1}$, forcing the mass reservoir to be a companion
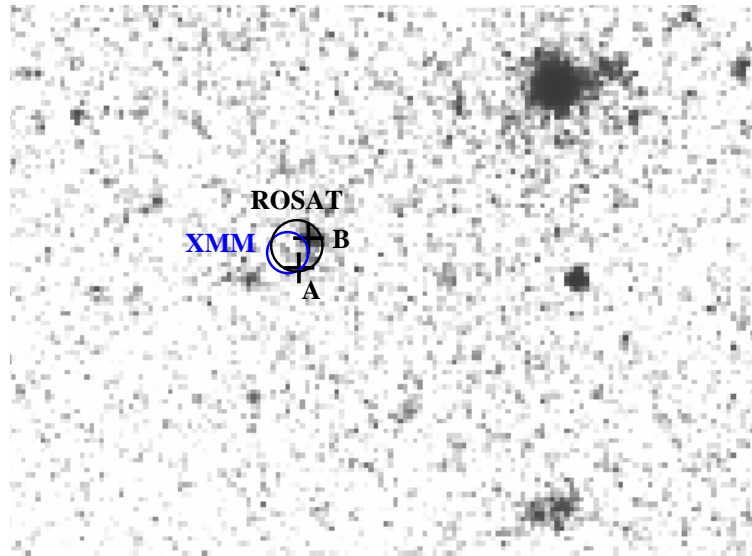
Figure 3.13: UV-band (UVW1 filter, 1800–3200 A) exposure of the field of NGC 1313 X-2, obtained with the *XMM-Newton* Optical Monitor. The circles represent the *XMM-Newton* and *ROSAT* positions (90% confidence level). Object A and B are also shown. A region of possible diffuse emission is visible NW of the error boxes in positional coincidence of the brighter part of the nebula.

star. The mass accretion rate required to produce the observed luminosity may in principle be provided by Roche-lobe overflow from a massive companion or by a wind from a supergiant. In the first case, evolutionary swelling of the companion keeps pace with the increase in Roche lobe size and the system remains self-sustained: accretion is likely to proceed through a disk. In the second case, assuming 10% accretion efficiency and that the BH can capture $\sim 1\%$ of the mass outflow, the wind must be very powerful ($\dot{M} \sim 10^{-5} \, M_\odot \, \mathrm{yr}^{-1}$). A lower efficiency would require too high a gas supply, so a disk is needed even in a wind-fed system. In this case, however, the disk is probably much smaller than in a Roche-lobe overflow system and the optical emission dominated by the supergiant. On the other hand, in a Roche-lobe overflow system, an extended, possibly re-irradiated accretion disk should contribute significantly in the UV and B bands.

3.4.8 X-ray and optical variability

One of the 2003 *XMM-Newton* pointings of NGC 1313 X-2 is within 2-3 days from the 1st *HST* epoch (Nov 25, 2003), while another is close to the VLT observation (Dec 23, 2003). It is therefore of interest to compare the V and B magnitudes of objects C1 and C2 in these two epochs. The variation of the unabsorbed X-ray flux between the same epochs is $\sim$80% (see Table 3.8). At the same time, however, the V and B band magnitudes of C1 do not show significant evidence of variability. The relative photometric error between the *HST* and VLT data as measured on a sample of field stars is in fact $\simeq 0.3$ mag (see Figure 3.14). A similar conclusion is reached also for object C2. The magnitude change between the *HST* and VLT epochs is always
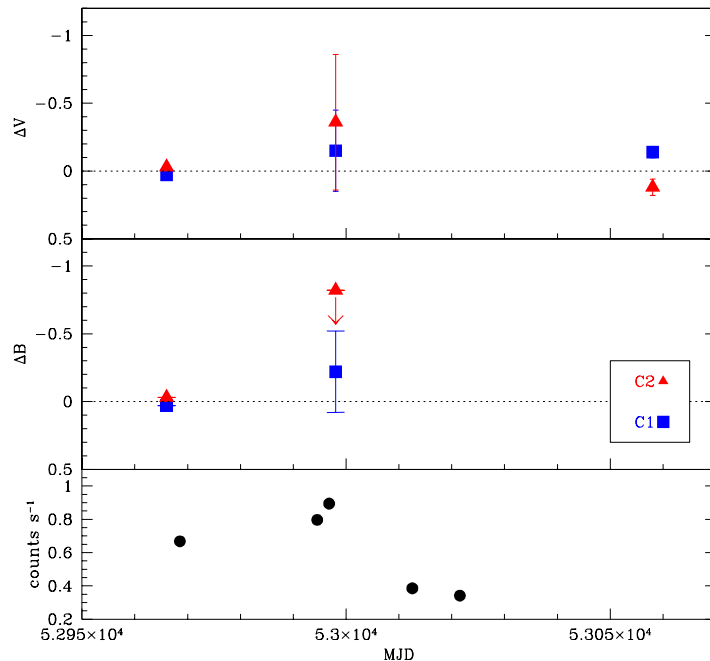
Figure 3.14: *Top and middle panels*: $\Delta V = V - V(HST\,Iepoch)$ and $\Delta B = B - B(HST\,Iepoch)$ for objects C1 and C2 for the available epochs. The error bars correspond to 0.3 and 0.5 mag for V and B respectively (see text for details). *Lower panel*: *XMM-Newton* count rates of NGC 1313 X-2 in the [0.2-10.0] keV range.

smaller than the relative photometric error ($\simeq 0.5$ mag for objects fainter than V=24; see again Figure 3.14).

An optical-through-X-ray spectral model for a binary system

In order to study the optical emission properties of objects C1 and C2 and compare them with the *HST*+VLT photometry, we implemented a model to compute the optical spectrum of a binary system with an IMBH taking irradiation effects into account. Our calculation relies on the same assumptions discussed in Copperwheat et al. (2005), who recently presented a thorough investigation of the infrared-through-optical emission properties of X-ray binaries with IMBHs. More specifically, we assume that accretion onto the IMBH is fueled by a giant companion filling its Roche lobe and that the X-ray emission is isotropic; the consequences of introducing some degree of beaming are discussed later on. A standard Shakura-Sunyaev disk (e.g. Frank et al. 2002) is assumed and both the X-ray irradiation of the companion (including the effects of disk shadowing) and the self-irradiation of the disk are accounted for. However, in order to keep our treatment simple, the companion star is taken to be spherical, neglecting the effects produced by the Roche lobe geometry and also those related to the (possible) deformation induced by radiation pressure (see again Copperwheat et al. 2005). Also, we use a simplified description of radiative transfer and

do not include limb and gravity darkening.

The model depends on the masses of the two components, the binary period (which, in turn, fixes the orbital separation), the accretion rate and the (non-irradiated) temperature of the donor, in addition to the inclination angle and the orbital phase. The accretion efficiency and the albedo of the donor surface layers were chosen to be 0.17 and 0.9 respectively. Following Copperwheat et al. (2005), we took the hardness ratio $\xi = F_X(< 1.5\,\mathrm{keV})/F_X(> 1.5\,\mathrm{keV}) = 0.1$. The absorption parameters in the same two spectral bands were selected as $k_s = 2.5$ and $k_h = 0.01$. The V and B magnitudes of the (irradiated) disk plus donor have been computed for several values of the parameters of the binary. Each sequence of models, at fixed inclination angle i, accretion rate $\dot{M}$ and donor mass M, corresponds to a track in the color-magnitude diagram (CMD; B-V vs. V here) along which the BH mass varies. The mass and luminosity class of the donor fix its (non-irradiated) surface temperature T_{eff}. Different tracks have been obtained varying the orbital period P_{orb} which, in turn, determines the Roche lobe radius. The maximum allowed period is that for which the Roche lobe radius is equal to the donor radius. The computed tracks are compared with the optical (de-reddened) magnitudes and colors of objects C1 and C2 for both the VLT and *HST* observations.

A systematic exploration of the parameter space

As an initial guess for the donor parameters in our model we use the values inferred on the basis of VLT photometry (M05): an O9-B0 V star of $\sim 20 M_\odot$, $T_{eff} \sim 30000$ K for C1, and a G-K I star of $\sim 10 M_\odot$, $T_{eff} \sim 4500$ K for C2. Results for object C1 are shown in Figure 3.15 for two different values of $\dot{M}$, chosen in such a way to match the *XMM-Newton* flux measured in the two observations of 2003 November 25 and December 23. The tracks on the CMD diagram are in agreement with the observed V band magnitude and (B-V) color of object C1 for $P_{orb} \simeq 1.7$ d, $M \simeq 15 M_\odot$ and $T_{eff} \simeq 25000$ K (corresponding to an early B main sequence star). Taking into account for current uncertainties on both color and magnitude, the companion mass and temperature may vary in the ranges $10 \lesssim M/M_\odot \lesssim 18$ and $20000\,\mathrm{K} \lesssim T_{eff} \lesssim 30000\,\mathrm{K}$, respectively. The orbital period is in the interval ~ 1.5–2 d. Independently of the inclination angle, the VLT and *HST* observations are consistent with the same value of the IMBH mass. Results shown in Figure 3.15 refer to orbital phase zero (superior conjunction). The variation in the V (B) band between the 1st *HST* epoch and the VLT one is $\simeq 0.23$ ($\simeq 0.25$), consistent (within the errors) with what observed. Thus, although in these systems X-ray irradiation is very intense, the induced optical variability is not very large owing to the high intrinsic emission of the massive B donor. The calculation for phases 0.25 and 0.5 gives results similar to those obtained for phase 0, typically within 0.15 mag. Thus, this is the expected amplitude of the modulation possibly induced by the orbital motion. It is interesting to note that this result is consistent with the degree of variability observed in the V band between the two *HST* observations (~ 0.1 mag; see Figure 3.14).

A direct comparison of the three cases illustrated in Figure 3.15 shows that relatively large values of the inclination angle ($i \gtrsim 50° - 60°$) are required in order to

obtain the correct optical flux for a BH mass $M_{BH} \sim 120 M_\odot$. At lower inclination angles (top and middle panels of Figure 3.15), the black hole masses needed to reproduce the optical magnitudes and color of object C1 are too small for the X-ray flux to be below the Eddington limit (if the emission is isotropic). Therefore, unless the Eddington limit can be circumvented, the binary system is expected to have a significant inclination angle. On the other hand, if the ULX emission is somehow beamed, the BH mass could be smaller: for a beaming factor $\sim 1/6$, M_{BH} can be as small as $20 M_\odot$ without exceeding the Eddington limit. In this case, we expect no X-ray irradiation of both the disk and the companion, being the emission collimated away from the orbital plane. To test this possibility we computed a new sequence of models, following the same procedure outlined above, but switching off the disk/donor irradiation. It turns out that it is possible to reproduce the correct magnitude and color, although the donor is now less massive and cooler. However, this implies that the star is too small to fill its Roche lobe and thus accretion can not proceed through Roche lobe overflow. Wind accretion may still be possible, although it seems unlikely that it can produce the required value of $\dot{M}$.

The situation for object C2 is somehow reversed. We explored the parameter space by varying the donor mass and orbital period, but did not find any combination of values which could reproduce the data in the framework of isotropic emission. In particular, X-ray irradiation causes the (B-V) color always to exceed the observed one. On the other hand, a massive and very extended K-type supergiant ($M_* \sim 16 M_\odot$, $T_{eff} \sim 4000$ K, $P_{orb} \sim 800$ days) would have properties consistent with those of object C2 if the black hole mass is $\sim 20 M_\odot$. This of course requires a (moderate) beaming. We checked that a beaming factor of $\sim 1/6$ is enough and that the companion fills its Roche lobe. The optical magnitudes are correctly reproduced because the (non-irradiated) disk contribution becomes negligible in comparison with the star intrinsic luminosity. However, in this case practically no variation in the optical is expected in response to an increase of the accretion rate, and the predicted magnitudes of C2 are constant. This is in contrast with the evidence of variability observed in the V band between the two *HST* observations (~ 0.1 mag; see Figure 3.14), although some variations may be induced also by the orbital ellipsoidal modulation of the donor (which we did not take into account).

Properties of the NGC 1313 X-2 binary system

If C1 is the counterpart, as it seems more likely, our model indicates that NGC 1313 X-2 is an IMBH X-ray binary with a relatively massive main sequence donor which fills its Roche lobe. Taking a black hole mass of $\sim 120 M_\odot$, as required to account for the observed X-ray flux in terms of isotropic emission, the donor mass is in the interval $10 - 18 M_\odot$ (taking photometric uncertainties into account). This is larger than the maximum main sequence mass of the parent stellar association, $\sim 8 - 9 M_\odot$, estimated using multicolor photometry and isochrone fitting by Pakull et al. (2006) and Ramsey et al. (2006). However, considering that the lower bound for the donor mass is $10 M_\odot$, the difference is small. We note also that, if C1 is the counterpart and C2 belongs to the same stellar association, the estimated masses of the two stars
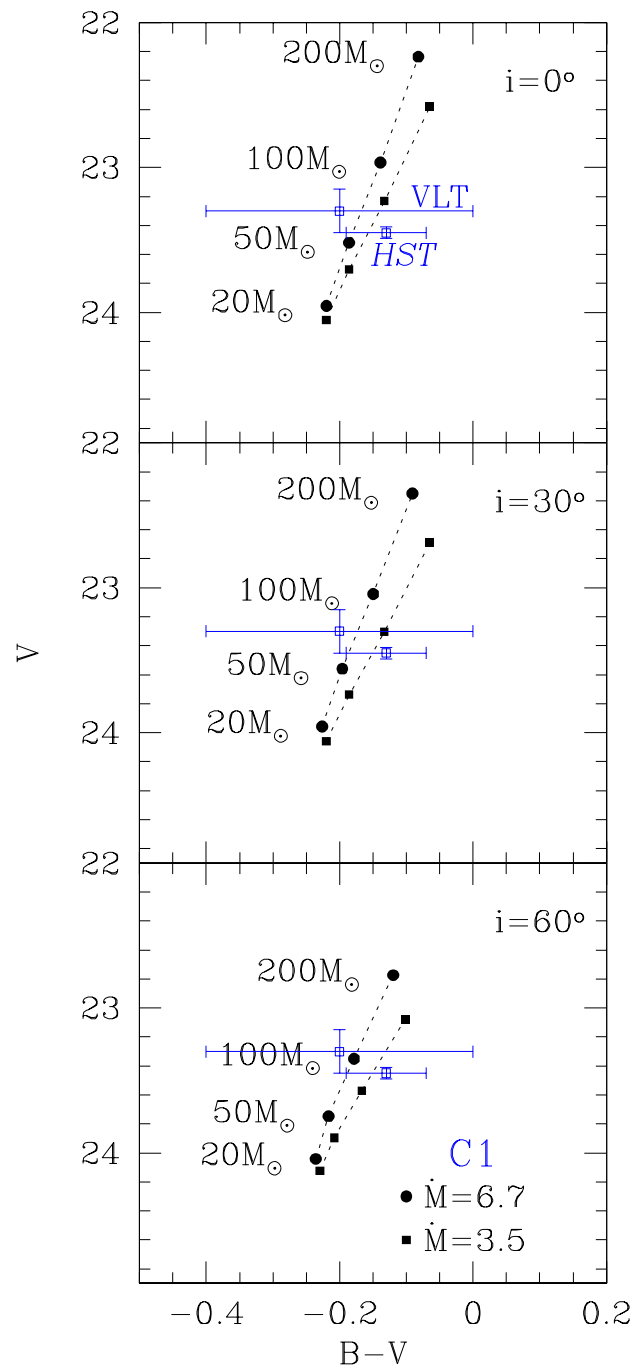
Figure 3.15: Color-magnitude diagram for the (irradiated) disk plus donor model for $P_{orb} \simeq 1.7$ d, $M \simeq 15 M_\odot$ and $T_{eff} \simeq 25000$ K (object C1). Each panel refers to a different inclination angle i. The two tracks correspond to $\dot{M} = 3.5$ and $6.7\, \dot{M}_{Edd}$. The black hole mass increases along the track, as shown by the labels. The V magnitude and B-V color as obtained from VLT and *HST* observations are also shown (*open squares*).

correctly place them on (or close to) and out of the main sequence, respectively. If the counterpart is C2 then the source is a binary formed by a late type, massive supergiant and a stellar mass black hole with beamed X-ray emission. However, this scenario has some shortcomings. First, it predicts little if no optical variability, and this is in apparent contrast with the variations seen in the two HST observations. Second, the duration of the supergiant phase for a $\sim 15 M_\odot$ star is very short (a few$\times 10^5$ yr), making the possibility of catching the binary is such an evolutionary stage not very likely (Patruno et al., 2006).

Recently Liu et al. (2007) confirmed C1 as the variable optical counterpart of NGC 1313 X-2. Thanks to the $F330W$ magnitude, they identified the star as a $Z = 0.2 Z_\odot$ of 8.5 $M_\odot$ of an age of 5×10^6 yr. They also note that this blue star lies on the edge of a young cluster ($< 10^7$ yr), superimposed to the dominant old stellar population.

A crucial question is how a binary system containing an intermediate mass BH may have formed (see e.g. van der Marel 2004). The BH progenitor must have been rather massive. This is consistent with the fact that NGC 1313 is likely to have lower than solar metallicity ($Z \sim 0.5$; Zaritsky et al. 1994) and hence mass loss was less intense. Such a massive BH may have formed through direct collapse without producing a supernova. In this way, if the system was born as a binary, it may have survived after the collapse of the primary. Although less likely, it is also possible that the companion might have been captured from a nearby stellar association. In this case, it is not possible to exclude that the BH may have formed from an early episode of star formation (population III). The position of the ULX nearby an unbounded young cluster let Liu et al. (2007) suggest the formation of the system through the merging of protostar in protocluster (Soria, 2007), enhanced also by the low metallicity environment of NGC 1313.

For object C1, an orbital modulation of amplitude $\Delta V \sim 0.15$ is expected because of orbital inclination and X-ray irradiation effects. This modulation is superimposed to a comparable variation caused by changes in the irradiating X-ray flux (~ 0.2 mag). In this respect, it is interesting to note that similar variations in the observed B band VLT+Subaru photometry of object C1 have been recently reported also by Pakull et al. (2006), consistent with our findings. In principle, with a sufficient and suitably spaced number of observations, the orbital modulation can be singled out and measured with large area ground telescopes or HST. The detection of this modulation would lead to the unambiguous determination of the orbital period of the binary. This, in turn, would allow us to constrain the mass ratio of NGC 1313 X-2 and, eventually, the mass of the black hole.

It is clear that if X-ray observations give essential information on the nature of NGC 1313 X-2, the optical study of the counterpart and its environment is extremely important for the interpretation of this (and other) ULX. The only unambiguous way to derive the mass of the BH is to obtain a dynamical measurement of the mass function of the ULX system through a detailed spectral study of the optical counterpart C1.

M82 X-1: THE FIRST QPO IN AN ULX

Another approach to study the nature of ULXs is through time variability. The analysis of the aperiodic variability in the X-ray flux of X-ray binaries is a powerful tool to study the properties of the inner regions of the accretion disk around compact objects (for a review see van der Klis 2006). In particular, QPOs provide well-defined frequencies, which can be linked to specific time scales in the disk. Since they identify the highest frequencies observed in the systems, they are the best candidates for association with, e.g., the keplerian frequency at the innermost stable orbit, or relativistic precession frequencies. Whatever their physical nature, these features are expected to be produced also in ULXs. However, if ULXs contain IMBHs of 100-1000 $M_{\odot}$, the frequencies involved are much smaller.

4.1   One of the brightest ULXs

M82 X-1 is a very bright ULX reaching a luminosity of 10^{41} erg s^{-1}. The source is hosted in the starburst prototype M82 and it is located nearby the nucleus.

M82 X-1 is also the first ULX where a QPO has been discovered. Strohmayer & Mushotzky (2003) first identified a 53 mHz QPO in a 2001 *XMM-Newton* observation. Fiorito & Titarchuk (2004) reported the identification of another QPO at 106 mHz in the power spectrum of M82 X-1 from *RossiXTE* data, arguing that it may be a harmonic of the QPO at 53 mHz. Dewangan et al. (2005) detected another QPO in a longer *XMM-Newton* exposure. Correlating the PDS properties with the spectral index, they argued that the central object has a mass of 25 - 520 $M\odot$. The X-ray observations show that the field of M82 X-1 is very crowded, with 9 sources within 30 ″ (Matsumoto et al., 2001). This, in addition to the diffuse galactic emission, represents a serious problem for instrument with a large PSF, like *XMM-Newton* and *RossiXTE*. Feng & Kaaret (2007a) used *Chandra* observations to definitely identify M 82 X-1 as the source originating of the QPO.

A periodical modulation at 62 days was discovered in *RossiXTE* data by Kaaret et al. (2006b), that was identified with the orbital period of the binary system. Binary
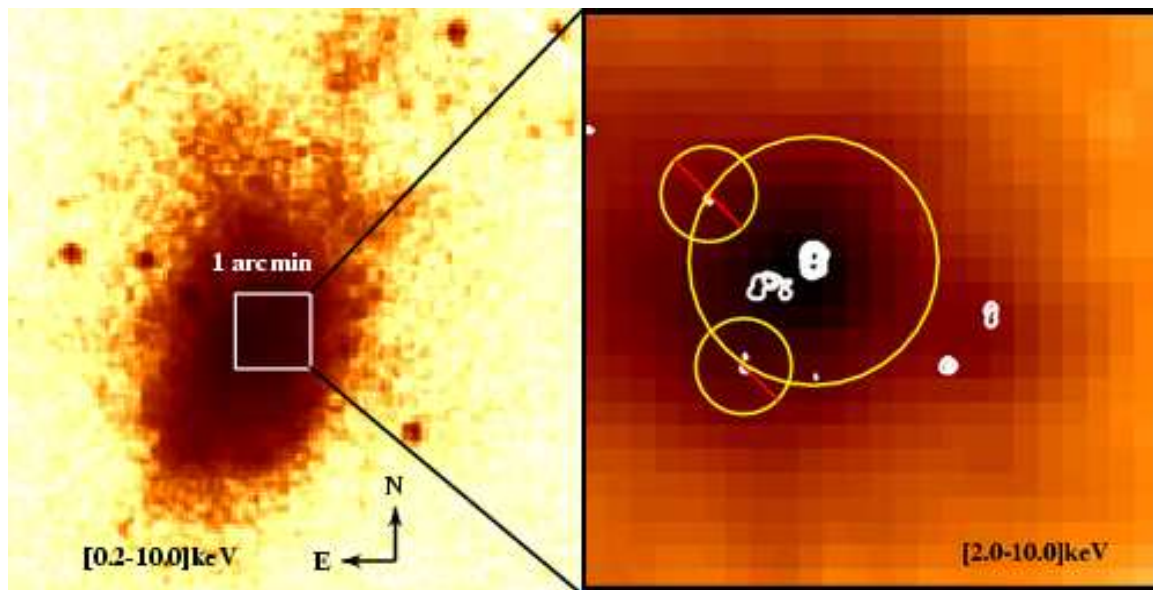
Figure 4.1: *XMM* EPIC MOS1 exposure of M82, taken on April 21, 2004. *Left*: full image of the galaxy in the [0.2-10.0] keV band. *Right*: $1' \times 1'$ region centered on M82 X-1 in the energy range [2.0-10.0] keV. Contour plots show the position of all the sources resolved in the *Chandra* observation of January 2000 (Matsumoto et al., 2001). The big circle $(13'')$ shows the region used for source count extraction, while the two smaller $(5'')$ circular regions are used to subtract the contribution of sources 2 and 3 of Matsumoto et al. (2001).

evolution simulations adopting this periodicity support the hypothesis that this source is powered by an IMBH (Patruno et al., 2006).

4.2   Spectral Analysis of *XMM-Newton* data

M82 was observed several times in the X-ray band not only to study its point sources, but also to analyze the thermal emission of the diffuse dust in the starburst. This is a source of contamination for our purposes, that we tried to avoid with a very careful analysis.

4.2.1   The diffuse emission component

In order to obtain an empirical description of the diffuse emission of M82 in the region of the ULX M82 X-1, we analyzed the spectrum of this component using a public archival *Chandra* observation (Obs.ID 5644; PI: T. Strohmayer), taken on August 17, 2005. The diffuse emission is expected not to be variable, so we can apply the results of this spectral fit also to other non-simultaneous observations.

We extracted the spectrum from a circular region of radius $13''$, centered on the ULX. A previous *Chandra* observation showed several sources in or nearby the position of M82 X-1 (Matsumoto et al., 2001). To remove the contribution of point sources we subtracted the emission of some of them by excluding circular regions of $5''$ radius centered on the *Chandra* positions (see Figure 4.1, including the ULX). A similar

Component	N_H	kT	Energy	Width	Red.$\chi^2(d.o.f.)$
	$[10^{22} \text{ cm}^{-2}]$	[keV]	[keV]	[keV]	
WABS*MEK +	$0.51^{+0.09}_{-0.07}$	$0.58^{+0.03}_{-0.04}$	–	–	–
WABS*MEK +	$1.38^{+0.11}_{-0.10}$	$0.91^{+0.06}_{-0.05}$	–	–	–
WABS*MEK +	$0.72^{+0.17}_{-0.22}$	$51.02^{+29.61}_{-22.54}$	–	–	–
GAUSS +	–	–	$1.33^{+0.01}_{-0.01}$	0.01*	–
GAUSS +	–	–	$1.83^{+0.02}_{-0.02}$	0.10*	–
GAUSS +	–	–	$2.36^{+0.01}_{-0.01}$	0.01*	–
GAUSS +	–	–	$6.64^{+0.07}_{-0.08}$	0.01*	1.26(293)

*: the parameter is frozen to the reported value

Table 4.1: Parameters from the spectral fit of the diffuse emission around the position of M82 X-1 (0.8-10. keV band). Results are presented for a 2005 *Chandra* ACIS-S observation (Obs. ID 5644). The data were extracted from a region of $13''$ radius with circular patches to mask point sources.

region was used for the source in the *XMM-Newton* dataset, see Sections 4.2.2 and 4.2.3. The background was extracted from a circular region of $15''$ radius, in the outskirt of the galaxy where the diffuse X-ray emission is absent. Following Stevens et al. (2003), we tried to fit the spectrum of the diffuse emission as a combination of MEKAL components each with its own absorption. Such a model is not acceptable in our case (reduced χ^2=1.96). Even varying the metal abundance, we do not obtain a satisfactory fit (reduced χ^2=1.97). As our aim is not to provide a physical consistent model of the diffuse emission but to describe it in a statistically acceptable way, in order to subtract it from the emission of the ULX, we decide to add GAUSSIAN components in correspondence of the most evident residuals.

The best fit parameters are reported in Table 4.1, while the best fitting model (hereafter DIFFUSE EMISSION) is plotted in Figure 4.2. Our best fit shows some line-shaped residuals. This does not affect our results because we are mainly interested in fitting the continuum of the diffuse emission in order to quantify the significance of a possible soft component in the spectrum of the ULX. We note that the spectrum of the diffuse emission shows a feature at 6.64 keV, that can be ascribed to fluorescent Kα Fe emission. Its detection in the *Chandra* spectrum confirms the previous suggestion of Mucciarelli et al. (2006) that this Fe feature is associated to the diffuse emission.

4.2.2 *XMM-Newton* observation of April 2004

XMM-Newton observed the galaxy M82 on April 21, 2004 (Observation ID 0206080101) for a total exposure time of 105 ks. The three *XMM* EPIC cameras (pn, MOS1 and MOS2) operated in Full Frame mode with the medium filter. Photon lists, data screening, region selection and events extraction were performed with the software XMM-SAS. Events lists were directly extracted from the observation data files using the tasks EPPROC and EMPROC for the EPIC pn and MOS data, respectively. The last part of the exposure was affected by high background radiation. Standard high flares filtering (total off-source count rate above 10 keV less than 1 count s^{-1} for pn and 0.35 count s^{-1} for MOS) leaves 76 and 72 ks of good time intervals for the pn and MOS cameras, respectively. Slightly different good time intervals were used for
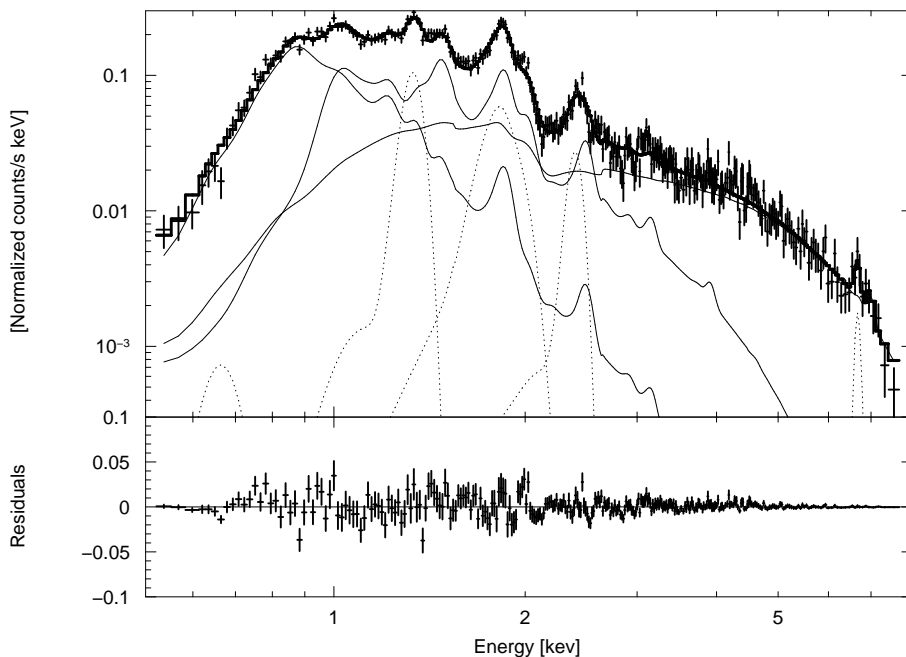
Figure 4.2: *Chandra* ACIS-S spectrum (Obs. ID 5644) of the diffuse emission around the position of M82 X-1 with the best fitting model (*heavy solid line*; see Table 4.1) and components: MEKAL (*thin solid lines*) + GAUSSIAN (*thin dotted lines*). The bottom panel shows the residuals of the fit. The data were extracted from a region of 13″ radius centered on M82 X-1 with circular patches to mask point sources.

the spectral and timing analysis, as specified below.

Source counts of M82 X-1 were extracted from a circular region of radius 13″, centered on the ULX coordinates RA= 09h 55m 50.2s, DEC=+69° 40″ 47′. To avoid as much as possible contamination from nearby point sources we subtracted the contribution of some of them by excluding circular regions of 5″ radius centered on the *Chandra* positions (see Figure 4.1). The nearest sources could not be eliminated in this way. Another strong source of background contamination, especially at low energies, is the host galaxy itself. Strohmayer & Mushotzky (2003) did not attempt to subtract it and limited their analysis to energies $\geq$ 2 keV. Here we try to perform spectral fits of the *XMM-Newton* data in the [0.8-10] keV range considering also the host galaxy diffuse emission.

The background was extracted from a circular area of 40″ in a region free from the contamination of the host galaxy. The background subtracted count rate of M82 X-1 is ∼1.36 count s^{-1} for pn and ∼0.46 count s^{-1} for each MOS.

Spectra were grouped to require at least 150 and 80 counts per bin for pn and MOS, respectively and analyzed with XSPEC. Standard interstellar absorption (WABS model) was taken into account and an overall normalization constant was used to minimize residual detector calibration uncertainties. Results of the spectral fits with various models are reported in Table 4.2. In order to adequately model the residual contribution from the host galaxy at soft energies (< 2 keV), we adopted the DIFFUSE EMISSION model described in the previous subsection (see Table 4.1), freezing all
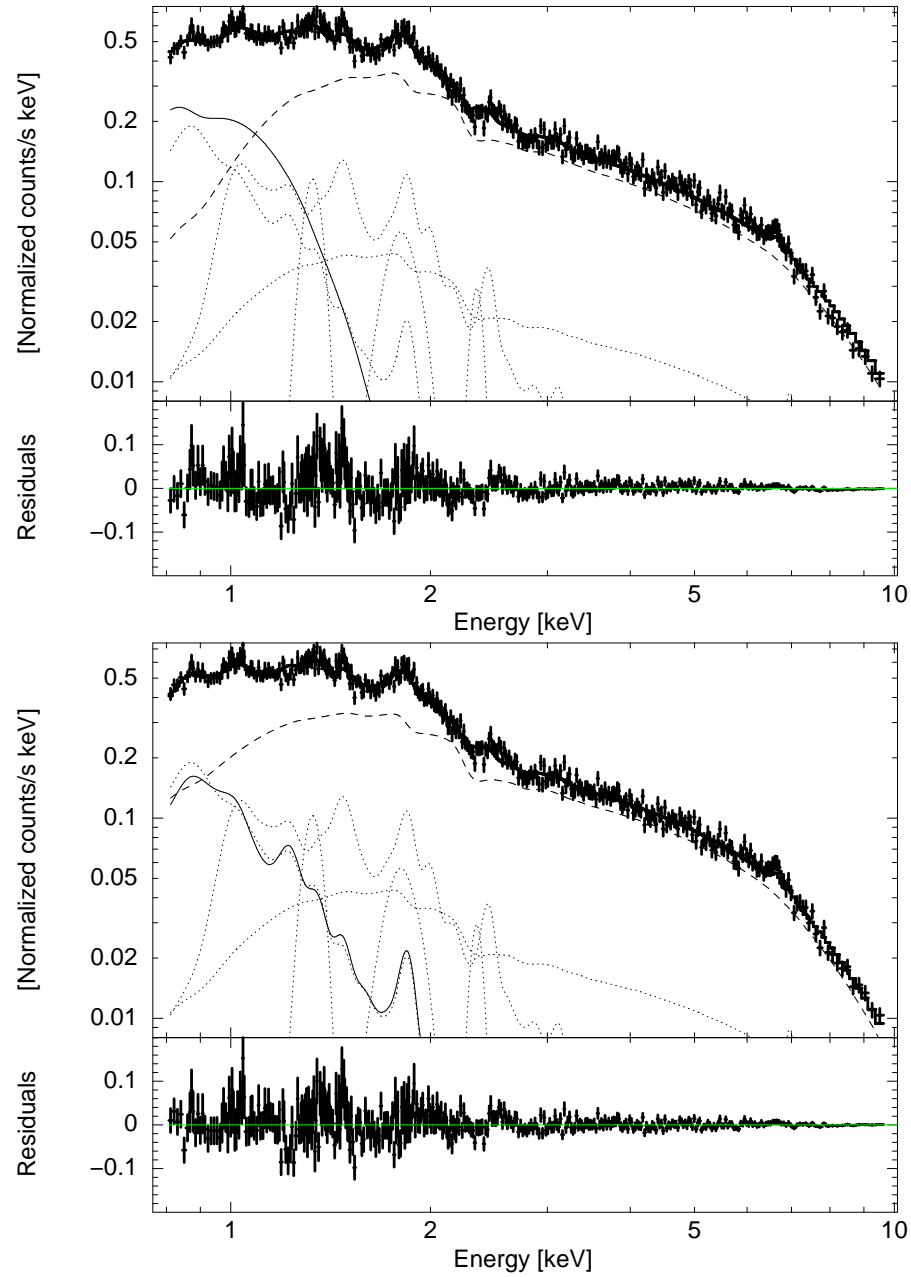
Figure 4.3: 2004 *XMM* EPIC pn spectrum of M82 X-1 (Obs. ID 0206080101) with two of the models reported in Table 4.2 (*heavy solid lines*) and residuals. *Top*: diffuse emission (*thin dotted lines*), power law (*thin dashed line*) and MCD (*thin solid line*). *Bottom*: diffuse emission (*thin dotted lines*), cutoff power law (*thin dashed line*) and MEKAL (*thin solid line*).

the parameters to the values reported in Table 4.1. We also included in the DIFFUSE EMISSION model an arbitrary CONSTANT component, that accounts for normalization.

The fits never reach a satisfactory χ^2. We tried to let the normalization of the DIFFUSE EMISSION model to vary within the *Chandra* and *XMM-Newton* cross-calibration uncertainties (10%, Snowden (2002)) but this is not sufficient to improve significantly the fits. This is probably caused by residuals in fitting the model of the diffuse emission and/or by some feature emitted by dense material in which the ULXs is possibly embedded. However, some firm conclusions can be derived on the basis of the spectral analysis presented here.

The spectrum is rather composite, so that fits with single component models (e.g. an absorbed power law, see Kaaret et al. 2006b) do not give acceptable results (reduced $\chi^2 > 2$). Adding a thermal soft component improves the χ^2 but the residuals are still significant. Therefore, an additional soft component seems to be required by the data but, given the uncertainties, we cannot undoubtedly associate it to emission from an accretion disk. Replacing the simple power law with a cutoff power law component helps to lower the reduced χ^2. This is a consequence of the fact that above 3 keV the slope of the M82 X-1 spectrum shows some curvature, similarly to other ULXs (Stobbart et al., 2006).

The best fits of the joint pn and MOS spectra of M82 X-1 are obtained adding to the DIFFUSE EMISSION model a cutoff power-law component in the hard tail plus a multicolor disk (MCD) or a MEKAL component at low temperature (0.13 and 0.53 keV respectively; see Table 4.2). Plots of the EPIC pn spectrum with two spectral models (power law plus MCD and cutoff power law plus MEKAL) are shown in Figure 4.3.

To check the accuracy of the power-law photon index, we tried to fit only the high energy part of the spectrum of M82 X-1 in the energy interval [3.3-10.0] keV (cfr. Fiorito & Titarchuk 2004). This should clearly minimize the contamination from the galactic diffuse soft emission. In this energy range the fits were performed with a power-law. Obviously, without fixing the value of the column density that is determined from the soft part of the X-ray spectrum, unacceptable fits or unreasonably high or low values of some parameters are obtained. Thus, we kept N_H fixed at the values derived from the power-law fits in Table 4.2. The resulting photon index is in the range $\Gamma = 1.53 - 1.71$, in agreement within 3σ with that derived from the full spectral fit, $\Gamma = 1.54^{+0.03}_{-0.02}$ (see Table 4.2).

4.2.3   *XMM-Newton* observation of May 2001

The *XMM-Newton* observation taken on May 6, 2001 (Observation ID 0112290201), analyzed by Strohmayer & Mushotzky (2003), lasted 31 ks. We re-analyzed it following the procedure outlined in the previous subsection. Standard flares filtering leaves 22 and 29 ks of good time intervals for the pn and MOS cameras, respectively. Source counts were extracted from a 13″ region centered on the same source position. The net count rate is $\sim$1.96 count s^{-1} for pn and $\sim$0.68 count s^{-1} for each MOS. Spectra were grouped to require at least 100 and 50 counts per bin for pn and MOS, respectively, and analyzed with XSPEC. The parameters of the fits are reported in

Model	N_H $[10^{22}\ \mathrm{cm}^{-2}]$	kT [keV]	Γ	Energy cutoff [keV]	Red. $\chi^2(d.o.f.)$
Obs.ID 0206080101 (2004 Observation)					
DIFF.EM + WABS*PL	$0.45^{+0.02}_{-0.02}$	–	$1.32^{+0.09}_{-0.10}$	–	1.99(846)
DIFF.EM + WABS*CUTOFFPL	$0.32^{+0.01}_{-0.01}$	–	$0.64^{+0.05}_{-0.06}$	$4.89^{+0.70}_{-0.58}$	1.85(845)
DIFF.EM + WABS*(PL+MCD)	$0.90^{+0.04}_{-0.03}$	$0.11^{+0.01}_{-0.01}$	$1.54^{+0.03}_{-0.03}$	–	1.65(844)
DIFF.EM + WABS*(CUTOFFPL+MCD)	$0.33^{+0.05}_{-0.06}$	$0.11^{+0.01}_{-0.01}$	$0.64^{+0.06}_{-0.07}$	$5.76^{+0.98}_{-1.25}$	1.55(843)
DIFF.EM + WABS*(PL+MEK)	$0.94^{+0.02}_{-0.03}$	$0.52^{+0.03}_{-0.03}$	$1.46^{+0.03}_{-0.03}$	–	1.68(844)
DIFF.EM + WABS*(CUTOFFPL+MEK)	$0.47^{+0.02}_{-0.01}$	$0.61^{+0.04}_{-0.03}$	$0.73^{+0.05}_{-0.06}$	$6.11^{+0.86}_{-0.62}$	1.51(843)
Obs.ID 0112290201 (2001 Observation)					
DIFF.EM + WABS*PL	0.31	–	0.75	–	2.49*(889)
DIFF.EM + WABS*CUTOFFPL	$0.11^{+0.01}_{-0.02}$	–	$-0.27^{+0.06}_{-0.06}$	$4.05^{+0.98}_{-0.68}$	1.72(888)
DIFF.EM + WABS*(PL+MCD)	$1.13^{+0.06}_{-0.04}$	$0.10^{+0.01}_{-0.01}$	$1.04^{+0.03}_{-0.02}$	–	1.77(887)
DIFF.EM + WABS*(CUTOFFPL+MCD)	$0.58^{+0.06}_{-0.08}$	$0.20^{+0.04}_{-0.02}$	$-0.30^{+0.13}_{-0.22}$	$3.68^{+0.37}_{-0.48}$	1.45(886)
DIFF.EM + WABS*(PL+MEK)	$1.28^{+0.03}_{-0.03}$	$0.15^{+0.01}_{-0.01}$	$1.08^{+0.02}_{-0.02}$	–	1.77(887)
DIFF.EM + WABS*(CUTOFFPL+MEK)	$0.28^{+0.04}_{-0.03}$	$0.62^{+0.02}_{-0.02}$	$-0.37^{+0.09}_{-0.06}$	$3.64^{+0.32}_{-0.18}$	1.37(886)

*: reduced $\chi^2 > 2$, it is not possible to calculate the errors

Table 4.2: Parameters from the spectral fits of M82 X-1 in the [0.8-10.0] keV band. Results are presented for the 2004 (Obs. ID 0206080101) and 2001 *XMM-Newton* observations (Obs. ID 0112290201). For both observations data were extracted from a region of 13″ radius centered on M82 X-1 with circular patches to mask nearby point sources. The contribution of the DIFFUSE EMISSION (DIFF.EM component) is taken into account importing the *Chandra* fit of Table 4.2.

Table 4.2 and two of the fits (power law plus MCD and cutoff power law plus MEKAL) are plotted in Figure 4.4. As in the 2004 observation, a soft component is needed to improve the fit. The temperature of the soft components is consistent, within 3σ, with that of the April 2004 observation, but the power-law photon index is slightly different.

Also in this case, we checked the accuracy of the PL photon index fitting the spectra in the restricted energy interval [3.3-10.0] keV. As for the 2004 observation, without freezing N_H unacceptable fits or unreasonably high/low values of some parameters are obtained. Fixing the column density at the mean value of the two power-law models reported in Table 4.2, the resulting photon index is in the range $\Gamma = 1.15 - 1.37$, marginally consistent with that of the full spectral fit, $\Gamma = 1.04^{+0.03}_{-0.02}$.

4.3   X-ray light curve

Table 4.3 shows the long time scale flux variability of M82 X-1 from *XMM-Newton* and *Chandra* data. Measurements from *RXTE* are not reported because it does not have imaging capabilities and contamination from the host galaxy and nearby point sources may significantly affect the count rate. For the *XMM-Newton* observations the fluxes are those of the MCD plus power-law fit models of Table 4.2, averaged over the three EPIC instruments and after being subtracted the contribution of the host galaxy (Table 4.1, $F_{DIFF.EM.} = 2.6 \times 10^{-10}$ erg cm^{-2} s^{-1}). For the *Chandra* HRC–I observations, the fluxes are calculated using the web interface to PIMMS. We adopt a simplified MEKAL and MCD+PL model, approximating the MEKAL/MCD component with a Bremsstrahlung/Blackbody at the same temperature. The *Chandra* fluxes are probably underestimated because the shape of the MCD and blackbody spectra start to differ significantly below 0.5 keV. The *Chandra* ACIS data are from Agrawal & Misra (2006) and Kaaret et al. (2006b) and the fluxes are extrapolated to the [0.2-10.0] keV energy interval with webPIMMS, adopting the spectral parameters of the Authors.

The highest recorded flux emitted by M82 X-1 ($F \sim 10^{-10}$ erg cm^{-2} s^{-1}) corresponds to a luminosity $L \sim 2\times10^{41}$ erg s^{-1} (assuming a distance of $D = 3.9$ Mpc, Sakai & Madore 1999). Making the usual assumption that, at maximum, the source emits at the Eddington limit, we can derive a rough estimate of the BH mass, $M_{BH} \sim 1500 M_{\odot}$. It is worth noticing that the high luminosity of this source is not easily explained also invoking alternative anisotropic models. A Super-Eddington luminosity up to a factor $\sim$10 can be reached in various models (see Section 2.1.4). Assuming that M82 X-1 at maximum is emitting 10 times above the Eddington limit, we obtain a lower limit for the mass of the accretor in M82 X-1 of 150 $M_{\odot}$.
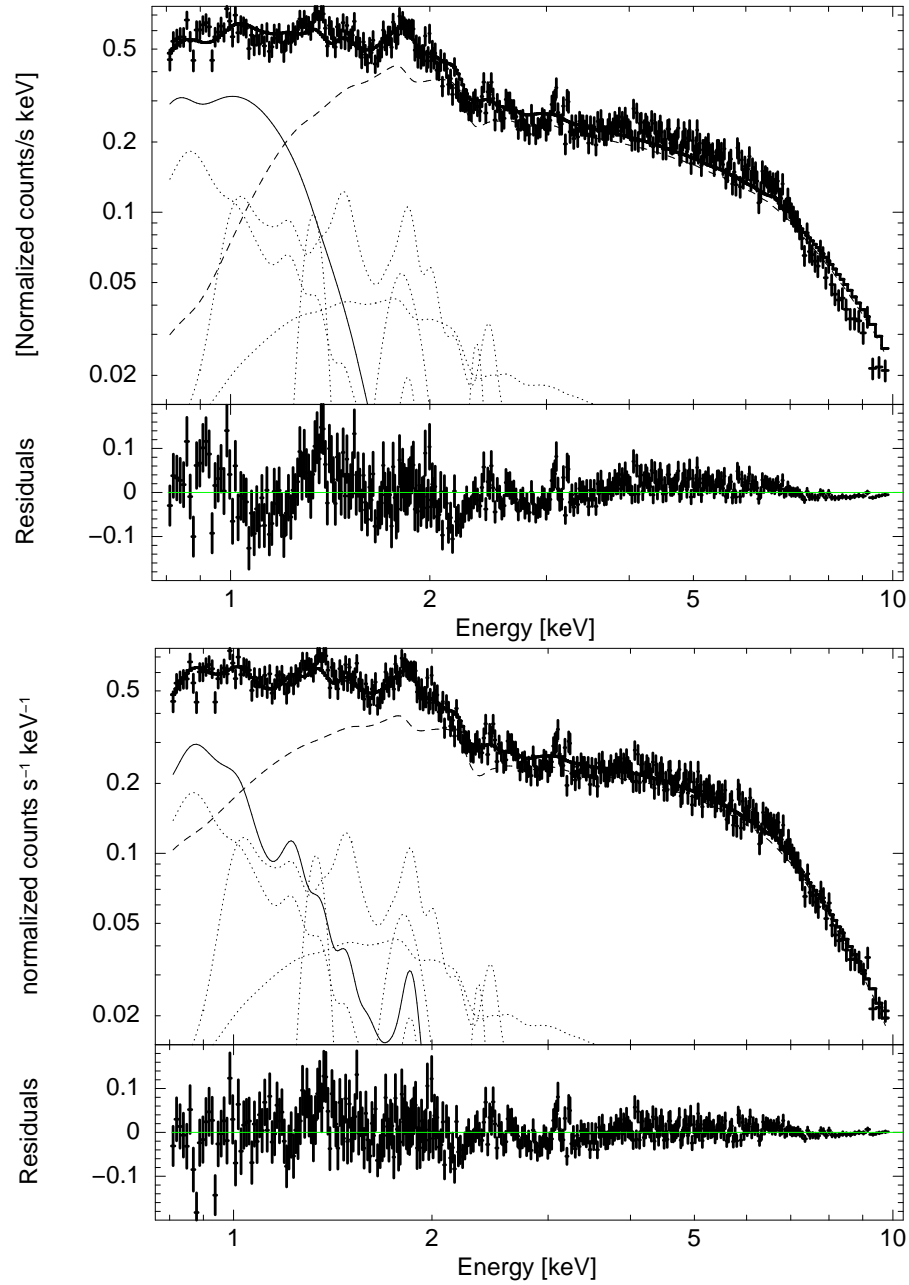
Figure 4.4: 2001 *XMM* EPIC pn spectrum of M82 X-1 (Obs. ID 0112290201) with two of the models reported in Table 4.2 (*heavy solid lines*) and residuals. *Top*: diffuse emission (*thin dotted lines*), power law (*thin dashed line*) and MCD (*thin solid line*). *Bottom*: diffuse emission (*thin dotted lines*), cutoff power law (*thin dashed line*) and MEKAL (*thin solid line*).

Observatory	Date	Count Rate [count s^{-1}]	Absorbed Flux [erg cm^{-2} s^{-1}]	Unabsorbed flux [erg cm^{-2} s^{-1}]
Chandra ACIS-I[a]	1999-09-20	0.12	2.5×10^{-12}	3.8×10^{-12}
Chandra HRC-I	1999-10-28	0.07[b]	$7.8 \times 10^{-12}/5.1 \times 10^{-12}$ [c]	$3.9 \times 10^{-11}/1.4 \times 10^{-11}$ [c]
Chandra HRC-I	2000-01-20	0.52[b]	$5.8 \times 10^{-11}/3.8 \times 10^{-11}$ [c]	$2.9 \times 10^{-10}/1.1 \times 10^{-10}$ [c]
XMM EPIC	2001-05-06	1.96/0.68[d]	2.35×10^{-11} [e]	3.53×10^{-10} [e]
Chandra ACIS-S[a]	2002-06-18	0.13	2.8×10^{-12}	3.6×10^{-12}
XMM EPIC	2004-04-21	1.36/0.46[d]	1.16×10^{-11} [e]	9.60×10^{-11} [e]
Chandra ACIS-S[f]	2005-02-04	1.17	1.8×10^{-11}	3.1×10^{-11}

[a] From Agrawal & Misra (2006), adopting their spectral parameters

[b] From Matsumoto et al. (2001)

[c] See text for details about the adopted spectral model

[d] pn/MOS count rates including the diffuse emission of the galaxy

[e] Average of the pn and MOS fluxes as calculated by XSPEC.
 The diffuse emission of the galaxy was previously subtracted

[f] From Kaaret et al. (2006b), adopting their spectral parameters

Table 4.3: The [0.2-10] keV fluxes of M82 X-1 from the *Chandra* and *XMM-Newton* observations.

4.4 Timing analysis

4.4.1 *XMM-Newton* data

For the timing analysis of the 2004 data we avoided the interval with high background radiation and limited the extraction to the longest (nearly) uninterrupted segment of data (66 ks) free from solar flares with count rate higher than 30 count s^{-1}. To minimize galactic contamination, source counts were extracted from a circular region of 8″ radius and at energies > 2 keV. We produced a light curve from pn+MOS data with a time binning of 0.5 s. A few gaps of typical duration of ∼100 s were present in the light curve and were filled with a Poissonian realization around the mean value of counts before and after the gap. We produced a power spectrum (normalized after Leahy et al. 1983) from the resulting light curve and rebinned it by a factor of 256 reaching a frequency resolution of 3.9 mHz (see Figure 4.5). A rather strong QPO peak is evident in the figure. We fitted the power spectrum with a model consisting of a constant (for the Poissonian level) plus two Lorentzian components (see Belloni et al. 2002): one zero-centered for the broad band-limited noise and one for the QPO peak. The characteristic frequency for the band-limited noise component (Belloni et al., 2002) is 39.4±8.6 mHz and its integrated fractional rms is ∼22% (after subtracting the contribution of the host galaxy). The parameters of the QPO can be seen in Table 4.4. The quality value Q, defined as the ratio of the centroid frequency over the FWHM of the QPO, is 4.3±0.5. We repeated the analysis in two separate energy bands, 2-4 keV and 4-10 keV. The fractional rms of the QPO (the measure of the pulsed fraction emitted in the signal, in this case the QPO, in percentage respect the total source flux) in these bands resulted to be 13.8% and 23.9% respectively. The significance of the QPO reported in Table is defined as in van der Klis (1998):

$$n_\sigma = 0.5 \frac{S^2}{S+B} r_s^2 \sqrt{\frac{T}{\Delta\nu}} \tag{4.1}$$

where S and B are the source and background count rate, respectively, r_s is the fractional rms, $\Delta\nu$ the width of the feature and T the integration time.

In order to investigate the possible variability of the QPO during the observation, we produced a spectrogram, by aligning power spectra obtained from consecutive stretches of data 2048 seconds long. The spectrogram is shown in Figure 4.6. A trend towards lower QPO frequencies is apparent, correlated with the source count rate (top panel). In order to quantify the decrease in centroid frequency, we divided the 66 ks interval in two segments of 33 ks each and repeated the power spectral analysis described above. The two resulting power spectra are shown in Figure 4.7. A fit with the same model used for the total power spectrum confirms that the centroid frequency of the QPO decreased by 10.8±4.0% (see Table 4.4).

In Galactic BHCs the frequency of some QPOs is correlated with certain spectral parameters, in particular with the power law spectral index (see e.g. the QPO frequency-Γ relation in GRS 1915+105; Vignarca et al. 2003). We then analyzed the spectra of M82 X-1 in the two 33 ks intervals after filtering for solar flares, adopting

Figure 4.5: Total power spectrum from the 2004 *XMM-Newton* observation (limited to the range 0.001-1 Hz) of M82 X-1. The line represents the best fit model (see Paragraph 4.4.1).

Parameter	Total observation	First half	Second half
ν_0 (mHz)	113±2	120±3	107±4
$FWHM(mHz)$	26±3	21±4	19±3
Frac % rms	18.3±1.0	17.5±1.1	17.3±1.1
Signif. (n_σ)	8.9	8.3	8.2

Table 4.4: Parameters of the *XMM-Newton* QPO detected in the 2004 observation of M82 X-1. Errors are at 1σ level.
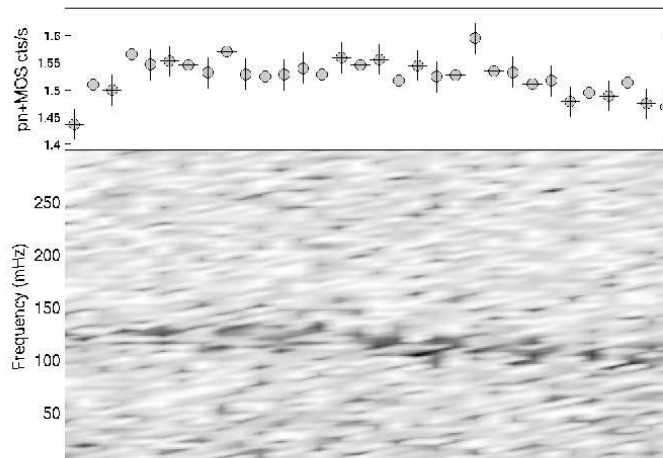
Figure 4.6: Spectrogram of the QPO of M82 X-1 obtained from 2048 s stretches of the 2004 *XMM-Newton* observation. Darker gray corresponds to higher power. A trend towards lower QPO frequencies is apparent, correlated with the source count rate (*top panel*).
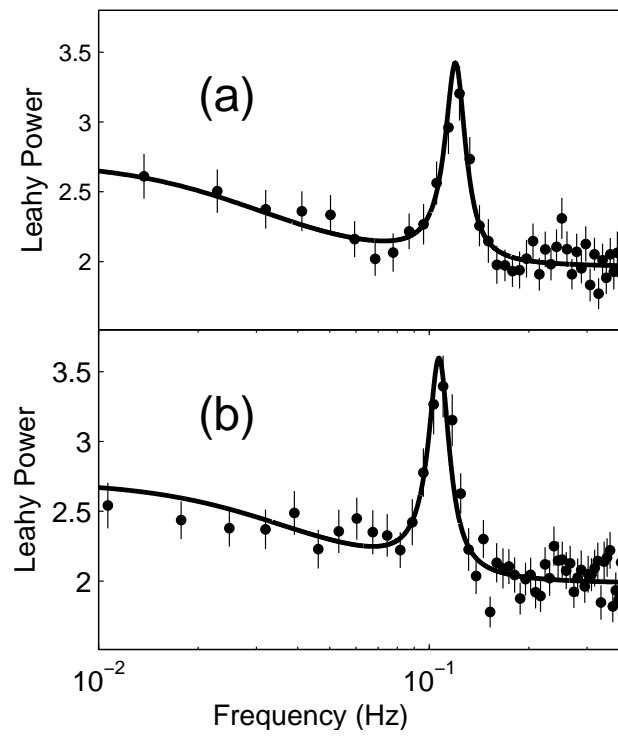
Figure 4.7: (a) Power spectrum from the first half of the *XMM-Newton* 2004 data. (b) Power spectrum from the second half. The lines show the best fit models described in the text. The centroid frequency of the QPO decreased by 10.8±4.0%.
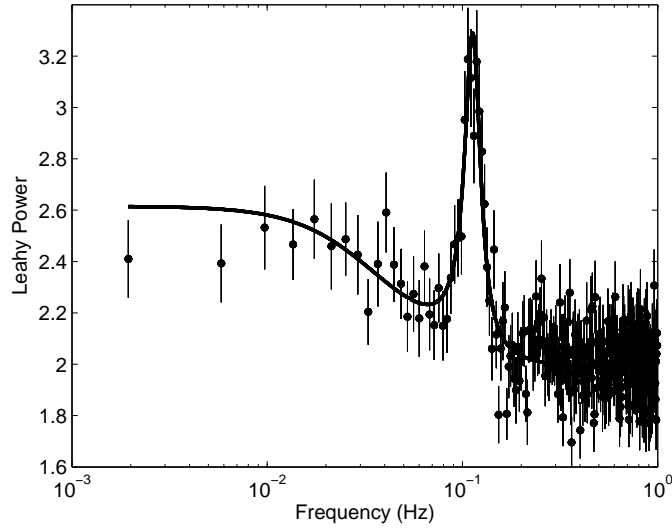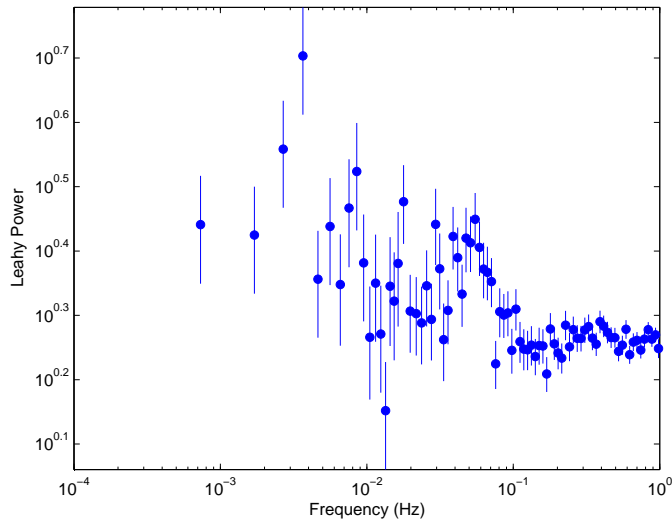
Figure 4.8: Total power spectrum from the 2001 *XMM-Newton* observation (limited to the range 0.001-1 Hz) of M82 X-1.

the spectral model in the previous section. The spectral analysis does not show any evidence of variability in the PL spectral index in the two intervals.

We also re-analyzed the *XMM-Newton* observation 0112290201 of Strohmayer & Mushotzky (2003). The analysis of the power density spectrum confirms the presence of the QPO found by Strohmayer & Mushotzky (2003) (see Figure 4.8).

4.4.2 *RXTE* data

In order to investigate the variability of the QPO frequency on longer time scales, we extracted from the *RXTE* public archive all 30 public observations of M82, spanning over the year 1997. For each observation, we accumulated PCA light curves in the channel range 0-35, corresponding to 2-13 keV, with a 0.5 s bin size and produced power spectra in the same way as for the *XMM-Newton* data. We detected a significant QPO in seven observations, including the three reported by Strohmayer & Mushotzky (2003) and Fiorito & Titarchuk (2004). These detections are summarized in Table 4.5 and a timing history of their centroid frequencies is shown in Figure 4.9, where also the *XMM-Newton* detections are indicated. Although the frequencies are variable, they are roughly consistent with three groups in harmonic 1:2:3 ratio, as recently suggested by Fiorito & Titarchuk (2004). In order to calculate the significance of such an harmonic relation we did a numerical simulation and found the nine QPO frequencies (the seven from RXTE data plus the two from *XMM-Newton*) to be consistent at 2.8 σ with being harmonics of a fundamental frequency of 54.9 Hz. However, this is not sufficient to completely rule out that such a distribution occurs by chance. More detections are clearly needed in order to address this issue.

ObsID	Date	Exp. (s)	QPO ν (mHz)	n_σ
20303-02-01-00	1997 Feb 02	3709	166±6	6.8
20303-02-02-00	1997 Feb 24	3616	54±5	5.3
20303-02-03-00	1997 May 16	3312	50±5	6.0
20303-04-04-00	1997 Jun 07	3872	114±5	5.8
20303-04-05-00	1997 Jun 10	2848	87±22	4.4
20303-08-07-00	1997 Jul 16	3127	67±5	6.5
20303-02-04-00	1997 Jul 21	2896	110±2	4.3

Table 4.5: Parameters of the *RXTE* QPO of M82 X-1. Errors are at 1σ level.
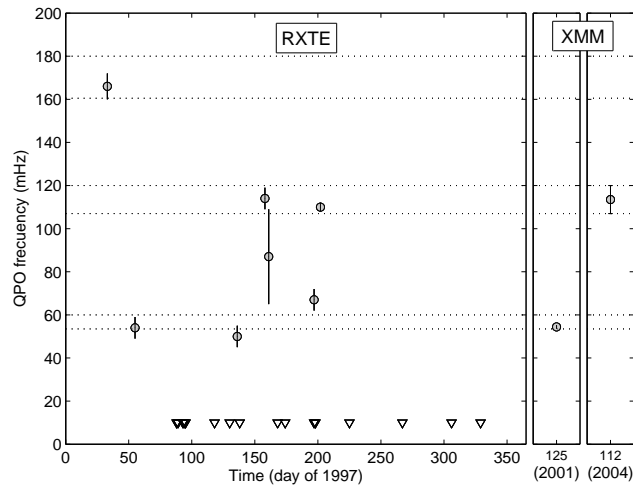

Figure 4.9: Time history of the centroid frequencies detected from M82 X-1 in the *XMM-Newton* and *RXTE* data. The triangles indicate the times of *RXTE* observations when no significant QPO was detected. The pairs of dotted lines indicate the range of frequencies detected by *XMM-Newton* in 2004 and the corresponding intervals at half and 1.5 times the frequency.

4.5   Results

4.5.1   Energy spectra

M82 X-1 is one of the best studied ULXs. It suffers from huge contamination in the soft X-rays from the diffuse emission of the host galaxy, the starburst prototype M82 (Origlia et al., 2004; Ranalli et al., 2008). We derive the spectral shape of the diffuse emission from a *Chandra* observation, assuming this component not to be variable, and apply it to observations taken at different epochs. We modeled this emission with a 3-MEKAL model with different absorbing columns plus GAUSSIAN components. Despite the care in subtracting the contribution of this emission, line shaped residual contamination is present in the spectra. A gaussian component is clearly needed at 6.64 keV. This feature is due to fluorescent Kα Fe emission. Its presence in the spectrum of the galactic emission confirms the previous suggestion of Mucciarelli et al. (2006) that this feature is associated to the diffuse emission in M82 and does not come from the ULX. Moreover, residuals are not evident in the X-ray spectrum of the ULX at this energy.

   The emission of the ULX M82 X-1 is affected also by a second source of contamination: the nearby point sources. The HRI instrument on board *Chandra* allowed Matsumoto et al. (2001) to resolve the central part of the galaxy, revealing the presence of a number of point sources in addition to M82 X-1 (the *Chandra* source CXOM 82 J095550.2+694047, labeled source 7 by Matsumoto et al. 2001, see Figure 4.10). A total of 9 sources are present in a field of $1' \times 1'$ centered on the galaxy. Most of these sources are rather close to M82 X-1, below the resolving power of the *XMM* EPIC cameras. For this reason, as mentioned in §4.2, we subtracted from the spectral extraction region circular patches ($5''$) in coincidence with the position of the *Chandra* sources. Although we are aware that for *XMM-Newton* this is not as effective as for *Chandra* (because a region of $5''$ corresponds to a *XMM-Newton* encircled energy fraction of about 30-50%), this appears to be a reasonable compromise between minimizing the contamination from these sources and preserving the counting statistics of M82 X-1. This procedure could not be adopted to eliminate the contribution from the three nearest sources to M82 X-1 (sources 4, 5 and 6 in Matsumoto et al. 2001). In a recent work, Feng & Kaaret (2007a) analyzed this problem in detail. In particular, they found that the most important contribution to the emission of M82 X-1 comes from source 5 (also named X42.3+59), that is also a highly variable source (see Figure 4.11). In the *Chandra* observation of October 1999 the count rate of this source was only 30% of that of M82 X-1. Later, in the *Chandra* observation of January 2000, the former decreased by an order of magnitude while the latter increased by a factor ~ 7. Therefore, while sources 4 and 6 are roughly constant and weak with respect to M82 X-1, significant contamination from source 5 can not be ruled out. Feng & Kaaret (2007a) show that, during the first *XMM-Newton* observation (2001), source 5 is brighter than M82 X-1. Considering the size of the PSF of *XMM-Newton*, the source is too close to the ULX in order its emission to be masked as for other nearby sources. Consequently the 2001 spectrum of M82 X-1 is likely to be highly contaminated by this source. In the 2004 observation source 5 contribute only 15% to the
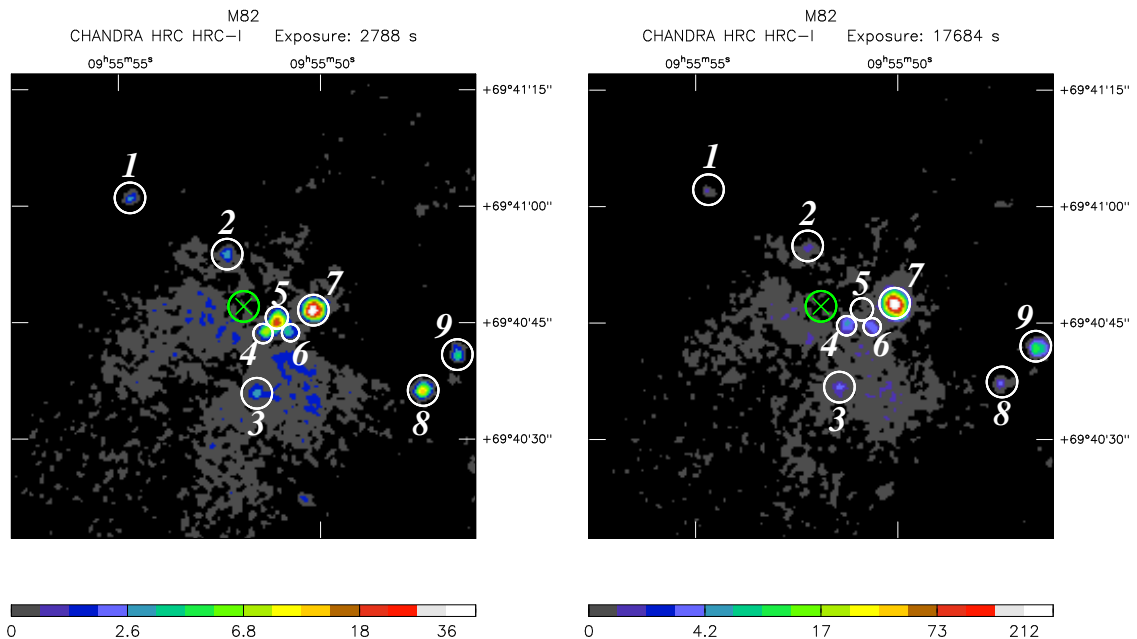
Figure 4.10: *Chandra*-HRC central $1' \times 1'$ ($1' = 1.1$ kpc) region of M82: (a) 1999 October 28, (b) 2000 January 20. The green cross shows the radio kinematic center, and the green circle is its position error circle with a radius of $2''$. The X-ray sources are designated with white circles and numbers. The images are from Matsumoto et al. (2001).

observed emission.

Spectral fits of the *XMM-Newton* observations of M82 X-1 include a soft component with low temperature (kT_{MCD}=0.10-0.20 keV, kT_{MEKAL}=0.15-0.62 keV). Adding this component results in a statistical improvement of the fit. The $\Delta\chi^2$ contours of kT vs. normalization of the MCD soft component shows that the temperature is in general well constrained within 3σ while the normalization varies in a broader range. However, even in the worst case the lower bound is well above zero.

Given the accurate modeling of the Galactic diffuse emission from *Chandra* data and the fact that the 2004 *XMM-Newton* observation is not significantly contaminated by nearby point sources, we believe that the detection of the soft component in the 2004 observation is significant. Under the assumption that the softest emission is entirely due to an accretion disk, the temperature of the MCD fits (T_{MCD}) can be used to estimate the BH mass (see Section 3.4.2). Assuming that T_{MCD} represents an estimate of the maximum temperature of a standard accretion disk, we derived a range of values for the mass of the BH from the values of this spectral parameter ($kT_{MCD} = [0.10\text{-}0.20]$ keV). If the accretion is Eddington limited, the BH mass turns out to be in the range $M_{BH} \approx [200-2000]f^4 \, M_{\odot}$, in agreement with the value inferred from the X-ray flux.

4.5.2 Timing

M82 X-1 is the first ULX where a QPO has been discovered. There are a total of 9 detections, two of which in the *XMM-Newton* data and seven in the *RXTE* data, with
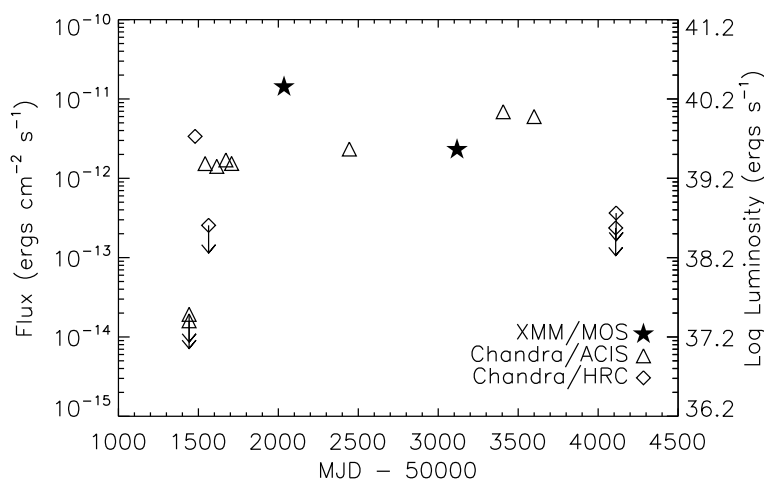
Figure 4.11: A seven year light curve of the ULX X42.3+59 from *XMM-Newton* and *Chandra* data (from Feng & Kaaret 2007a). The left axis indicates the [2-10]keV flux and the right axis is the corresponding luminosity at a distance of 3.63 Mpc.

frequencies in the range ∼50-170 mHz.

One of the main concerns about this detection is the possible contamination from nearby point like sources. To this purpose Feng & Kaaret (2007a) reanalyzed the two *XMM-Newton* observations of M82, using the *XMM-Newton* brightness profiles and the known *Chandra* source positions. They clearly show that the QPOs detected with *XMM-Newton* originate from M82 X-1 and not from the other bright ULX, the nearby field source 5 (X42.3+59; Matsumoto et al. 2001).

An important issue is of course the possible identification of this QPO with one of the QPO types observed in the X-ray light curves of stellar-mass BHCs. As mentioned in Section 2.1.5 these QPOs can be broadly divided into three different categories. The "very low frequencies QPOs" shows very low frequencies (<0.02 Hz) and are probably associated to oscillations and instabilities in the accretion disk. "Low-Frequency (LF) QPOs" have typical frequencies between 0.1 and 10 Hz and are classified in 3 sub classes. The "hecto-Hertz QPOs" at higher frequency (100-300 Hz) are observed to appear in pairs.

In the following we will summarize the main properties of the QPO in M82 X-1, and discuss its similarities and differences with the QPOs observed in BHCs.

i) The lowest and highest observed frequencies are 50±5 mHz and 166±6 respectively (see Figure 4.9).

ii) The frequency distribution over this range is suggestive of a harmonic 1:2:3 ratio between them. Nevertheless the significance at 2.8 σ with being harmonics of a fundamental frequency of 54.9 Hz is not sufficient to completely rule out that such a distributions occurs by chance.

iii) In the 2004 *XMM-Newton* observation the frequency is observed to vary by a factor of ∼10% between the first and the second half of the observation.

iv) The QPO peak has a quality value higher than 4 (up to ∼6 in one case).

v) The 2004 QPO shows a high fractional rms (up to ∼18%).

vi) The underlying band limited noise in the 2004 QPOs is strong (fractional rms ∼22%) and has a characteristic frequency comparable to the QPO frequency.

vii) The integrated fractional rms of the QPO in the [2-4] keV interval is higher than in the [4-10] keV.

We now compare the properties outlined above with those of the various types of QPOs observed in BHCs.

An association of the QPO in M82 X-1 with the *very low frequency QPOs* ($\nu \lesssim 0.02$ Hz) observed in GRS 1915+105 is unlikely as their frequency is *lower* than those observed in M82 X-1. This, assuming an inverse scaling with the black-hole mass, would imply a very low (∼solar) mass black hole in M82 X-1, which is not in agreement with the spectral evidences.

The observed short-time scale variability seems to exclude an association with the *high-frequency "hecto-Hertz" QPOs* observed in BHCs, since the latter have been detected at rather stable frequencies. However, it is worth noticing that, assuming a 10^3 scaling factor between the two phenomena, the ∼ 10 mHz variation of the centroid frequency on a time scale of ∼ 30 ks observed in M82 X-1 would correspond to a ∼ 10 Hz variation on a time scale of ∼ 30 s in a 10 solar mass BHC. Such a short time scale variability is impossible to detect in BHCs with the present instrumentation. On the other hand, the presence of a strong underlying band limited noise, with a characteristic frequency comparable to the QPO frequency, is clearly at variance with the high-frequency "hecto-Hertz"QPOs observed in BHCs. Furthermore, the rms amplitude of the QPO itself in M82 X-1 is roughly an order of magnitude bigger than that of the "hecto-Hertz" QPOs in BHCs, thus making the association very unlikely. For the sake of completeness we stress that the detection of the QPO at ∼ 166 mHz reported in this paper lowers the upper limit for the mass of the black hole in M82 X-1 (assuming that this frequency is associated with the Keplerian frequency at the innermost circular orbit around a Schwarzschild black hole, $\nu_k \propto (GM_{BH}/r_k^3)^{1/2}$) to ∼ $1.2 \times 10^4 M_\odot$.

Three main types of *low-frequency QPOs* are observed in BHCs (see Casella et al. 2005). In two of them, the type-A and the type-B QPOs, the peak appears always at frequencies near 8 and 6 Hz respectively. Moreover, they are both characterized by a weak (a few %) underlying red noise component. These properties make an association with the variable, strong QPO observed in M82 X-1 unlikely. In the case of type-A QPOs, its low coherence and amplitude make the association even less likely. The properties of the QPO in M82 X-1 are on the contrary reminiscent of those of the third type of BHCs low-frequency QPO, the type C, whose characteristic frequencies vary in the range 0.1-15 Hz. The similarities in fractional rms, variability, quality value, and underlying noise strongly suggest an association between the two features. Furthermore, in the 2004 *XMM-Newton* observation there is evidence for a positive correlation of the QPO frequency with the count-rate, and a similar correlation is often observed in type-C QPOs. However, during the 2001 *XMM-Newton* observation (when the QPO was detected at a lower frequency) the count rate was higher than

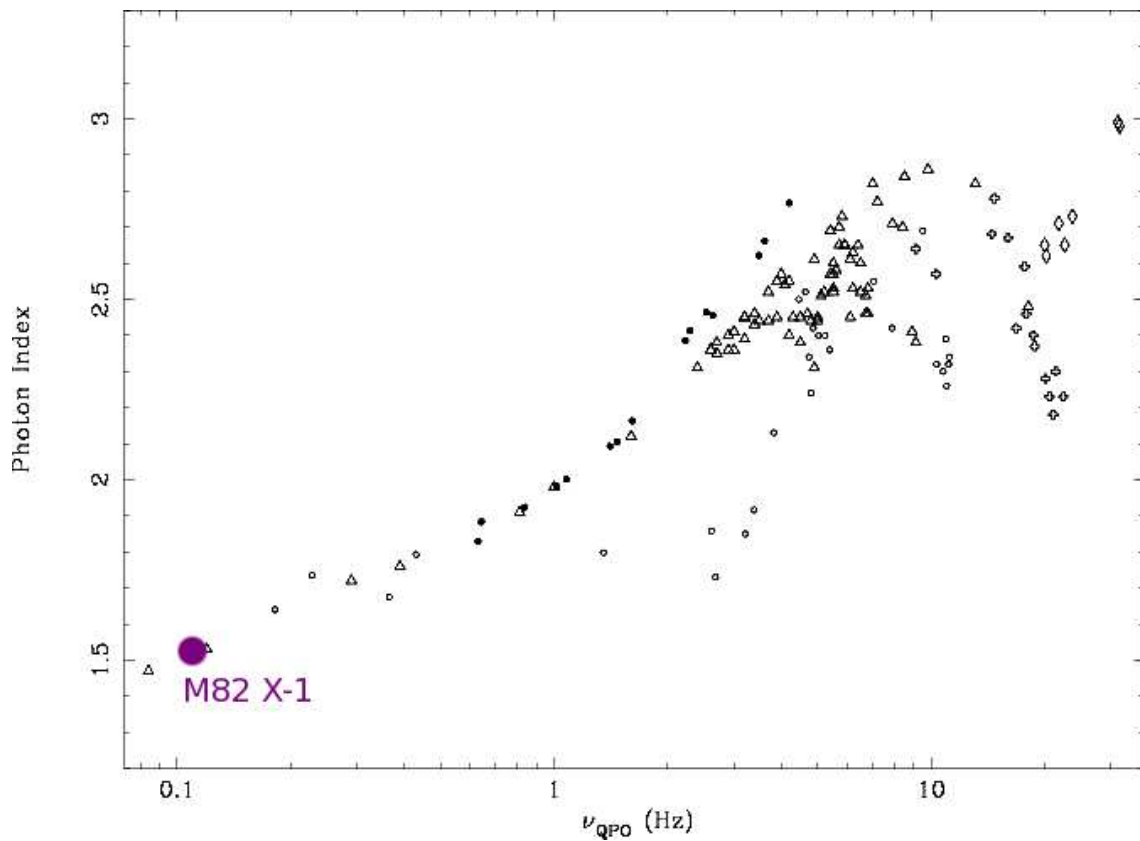Figure 4.12: Plot of power law photon index versus QPO centroid frequency from Vignarca et al. (2003), their Figure 10, and the M82 X-1 point. Full circles are data from GRS 1915+105 (plateau state); empty crosses from GRO J1655-40; empty circles from 4U 1630-47; diamonds from XTE J1748-288; empty triangles from XTE J1550-564. The purple point represent the 2004 *XMM-Newton* observation of M82 X-1.

during the 2004 observation. Since the count-rate vs. frequency correlation in BHCs is "outburst dependent" (which means that during different outburst a source can show similar frequencies at different count-rates) no conclusion can be derived from the observed phenomenology in M82 X-1. No information on the count-rate variability could be obtained from the *RXTE* observations, given the lack of imaging capabilities of the satellite.

Assuming that the QPO detected in M82 X-1 is a type-C QPO, and scaling the frequency inversely to the BH mass, the observed frequency range (from 50 to 166 mHz) would yield M_{BH} anywhere in the range 10-1000 $M_\odot$. However, type-C QPOs are observed in BHCs throughout the whole Hard-Intermediate State (HIS, see Homan & Belloni 2005), and their frequency is known to decrease with the hardness of the energy spectrum. At the lowest observed frequencies, the spectrum is hard and there is often no evidence for the presence of a soft thermal component. As the contribution from a disk appears and increases, the QPO frequency also increases. The *XMM-Newton* spectra of both observations in which a QPO has been detected in M82 X-1 show possible evidence for a disk contribution (see Section 4.2.2). To the extent that the two phenomena can be compared, the presence of a soft component would exclude that the type-C QPO in M82 X-1 is in the lowest frequency range. This in turn increases the lower limit for the BH mass.

It is also interesting to test a correlation between the QPO frequency and the spectral parameters. Vignarca et al. (2003) reported a correlation between the power-law index and the QPO frequency. Using the PL+MCD model, the 2004 *XMM-Newton* observation, where little contamination from source 5 is expected, has a photon index $\Gamma \sim 1.5$ and a QPO frequency $\nu_{QPO} = 113$mHz, falling on the relation valid for well studied Galactic XRBs (see Figure 4.12). An interesting consideration arises on the position of the turn-off in the ν_{QPO} vs Γ relation. This turn-off is shown by several BHCs and is not yet fully understood. It is tempting to relate it to the mass of the central BH. The highest observed QPO frequency in M82 X-1 is ~ 170 mHz. Assuming that this corresponds to the turnoff frequency and that it is inversely proportional to the BH mass (see Vignarca et al., 2003), a scaling with the values for GRS 1915+105 gives an upper limit of ~ 300 $M_\odot$ for the BH mass in M82 X-1. Clearly, if the turn-off frequency is higher or it is unrelated to the BH mass, this limit does not apply. We note also that, falling our single value on the relation, it is not possible to exclude a mass for the BH in M82 X-1 of the order of the mass of Galactic BHCs.

4.6 Conclusions

Our analysis of *XMM-Newton* and *RXTE* observations of the ultraluminous X-ray source M82 X-1 gives useful constraints to the mass of the BH hosted in this ULXs but indicates also that more observations are needed to understand the properties of the QPO observed in this source.

As for as the properties of the QPO are concerned, the similarities in fractional rms, variability, quality value, and underlying noise strongly suggest an association between the QPO in M82 X-1 and the low-frequency, type-C QPOs observed in BHCs.

The combined spectral and timing analysis allows us for the first time to put constrains to the mass of the central black hole in this source, yielding to a value between a few tens to a thousand solar masses.

A number of arguments has been proposed to reduce the uncertainty on the determination of the mass of the compact object in M82 X-1. They have been discussed in this Chapter and are briefly summarized in Table 4.6. It is tempting to conclude that a likely value for the mass of M82 X-1 may be few hundreds $M_\odot$.

Hopefully, new *Chandra* observations will allow us to further investigate the spectral and timing properties of this source, eliminating the uncertainties caused by the contamination of both the diffuse emission of the galaxy and the presence of nearby point-like sources. The work performed on M82 X-1 may reveal a useful template for the study of other ULXs from the point of view of their timing behavior.

Method	BH Mass	Notes
Luminosity	$\sim 1500\ M_\odot$	assuming isotropic emission and $L \sim L_{Edd}$
Super Eddington accretion	$> 150\ M_\odot$	assuming $L \sim 10 L_{Edd}$
T_{MCD}	200-2000 $f^4\ M_\odot$	soft excess due to accretion disk
Type C QPO, cfr Galactic BHC	10-1000 $M_\odot$	assuming ν scaling inversely with mass
Spectral hardness $\propto 1/\nu_{QPO}$	few 10-1000 $M_\odot$	assuming a BHCs-like HIS +
		presence of the soft component
Vignarca relation Γ vs ν_{QPO}	$< 300\ M_\odot$	assuming QPO at turn-off +
		assuming ν scaling inversely with mass
Higher observed ν_{QPO}	$< 1.2 \times 10^4\ M_\odot$	assuming Keplerian frequency
Higher observed $\nu_{QPO}{}^*$	$< 1.87 \times 10^4\ M_\odot$	assuming Keplerian frequency

*: from Strohmayer & Mushotzky (2003)

Table 4.6: Summary of BH mass estimates for the compact object in the ULX M82 X-1.

CHAPTER 5

CONCLUSIONS

First revealed by the *Einstein* observatory, UltraLuminous X-ray sources (ULXs) have been defined as point-like, irregularly variable, off-nuclear X-ray sources in external galaxies with luminosities significantly in excess of the Eddington limit for a BH of 10 $M_\odot$. The number of such sources discovered with the present instrumentation in nearby galaxies, both ellipticals and spirals, accounts to more than 150 objects. It is now clear that the spectral and timing properties of most of these sources are consistent with those of binary systems accreting on to a compact object. The debate is now centered on the mass of the central remnant hosted in these sources. Assuming Eddington-limited accretion, masses in the range 100-1000 $M_\odot$ would be inferred for the compact object from the observed flux. The existence and the mechanism of formation of Intermediate Mass Black Holes (IMBHs) represent major challenges in modern Astrophysics and have important implications in other areas, such as the study of dynamical interactions in high density systems. However, this BH mass estimates, as derived from considerations involving the Eddington limit, are questionable because these sources need not to be spherically symmetric, nor stationary. It has been proposed that many of the ULX properties can be explained assuming that they do not emit isotropically or are dominated by emission from a relativistic jet. In this case, they may harbor stellar mass BHs and may be similar to Galactic microquasars.

5.1 Investigating ULXs

X-ray spectra of ULXs have been obtained with the *Einstein*, *ROSAT* and *ASCA* observatories. Recently, a number of long *XMM-Newton* and *Chandra* observations have become available, providing high counting statistics spectra of several bright ULXs. In these cases, the best fit is often obtained with a two-component model of the type "soft thermal component + hard tail". If the soft component is identified with emission from an accretion disk, the observed temperature turns out to be $\sim$ 150-300 eV, much lower than in Black Hole Candidates (BHCs). These low temperatures (together with the large normalization) have been taken as further evidence for the

presence of an IMBH in some ULXs. In the last few years, the identification of the soft component with emission from an accretion disk has been questioned and alternative methods to estimate the mass of the central remnant were proposed.

Optical observations of ULXs play a central role in the understanding their nature, because they allow the direct study of optical counterparts of ULXs and their environment. Unfortunately they are still rather scarce. Although some ULXs have counterparts in the Digitized Sky Survey or *HST* images, only a limited number have been optically identified and studied in detail. The majority of these ULXs are hosted in young stellar environment and their optical counterparts have spectral types consistent with early O-B stars. Instead two ULXs seem to be associated with globular clusters in elliptical galaxies. Several ULXs are also associated with extended optical emission nebulae of a few hundred parsecs in diameter that provide important clues on the geometry and energetics of the X-ray source.

A complementary approach to study the nature of ULXs is through time variability. The analysis of the aperiodic variability in the X-ray flux of X-ray binaries is a powerful tool to investigate the properties of the inner regions of the accretion disk around compact objects. In particular, Quasi-Periodic Oscillations (QPOs) provide well-defined frequencies, which can be linked to specific time scales in the disk. Their detection in ULXs allows for a firm identification of such system as compact objects. Furthermore the comparison of their properties with those of the QPOs present in Galactic BHCs provides important constraints to the mass of the BH.

5.2   Results from this Thesis

Despite the significant progress of the past years, our knowledge of ULXs is still far from being satisfactory and we are still at a stage when observations of single sources can provide invaluable information about the entire class. In this context I performed a detailed study (X-ray spectral and timing observations, optical photometry and spectroscopy of the proposed counterparts) of two of the best studied ULXs: NGC 1313 X-2 and M 82 X-1.

5.2.1   NGC 1313 X-2

At present NGC 1313 X-2 is one of the best studied ULXs. Its X-ray spectrum was extensively analyzed. Here we performed a detailed analysis of the longest *XMM-Newton* observation with the best counting statistics, exploring a number of different spectral models. A composite absorbed MCD plus power law model produces an acceptable fit. Similarly good fits can be obtained with other models of the type "soft thermal component + hard tail". On the other hand the temperature obtained from the MCD fit implies $M_{BH} \approx 60 f^4 \, M_\odot$ for Eddington limited accretion, comparable to that derived from the flux.

Crucial information have been obtained also from the analysis of optical observations. We first identified the optical counterpart of NGC 1313 X-2 on an ESO 3.6m image. *HST* and VLT images of the field of NGC 1313 X-2 allowed us to resolve the

counterpart in two distinct objects, named C1 and C2, with R magnitudes 23.7 and 23.6, both inside the *Chandra* error box and separated by $0.75''$. The two candidate counterparts show properties consistent with stars in NGC 1313: the first turns out to be a B0-O9 main sequence star of $\sim 20 M_\odot$, while the second is a G supergiant of $\sim 10 M_\odot$. Irrespectively of which of the two objects the actual counterpart is, this implies that NGC 1313 X-2 is a high mass X-ray binary with a massive donor.

We also exploited quasi-simultaneous observations with *XMM-Newton*, *HST* and VLT in order to study the possible correlation of the X-ray light curve with the optical emission of the two proposed ULX counterparts. At the end of December 2003 the source experienced a short, but quite intense flare, reaching a maximum luminosity of 10^{40} erg s^{-1}, fully qualifying NGC 1313 X-2 as a bright ULX. At the same time, the optical flux of both counterparts did not show pronounced variations.

We then implemented a model to compute the optical spectrum of a binary system with an IMBH taking irradiation effects into account. If C1 is the counterpart (as it seems more likely), our model indicates that NGC 1313 X-2 is an IMBH X-ray binary with a relatively massive main sequence donor which fills its Roche lobe. Taking a black hole mass of $\sim 120 M_\odot$, as required in order to account for the observed X-ray flux in terms of isotropic emission, the donor mass is in the range $10 - 18 M_\odot$. If the counterpart is C2 then the source is a binary formed by a late type, massive supergiant and a stellar mass black hole with beamed X-ray emission.

A crucial question is how a binary system containing an intermediate mass BH may have formed. The BH progenitor must have been rather massive. This is consistent with the fact that the host galaxy NGC 1313 is likely to have lower than solar metallicity. Such a massive BH may have formed through direct collapse. In this way, if the system was born as a binary, it may have survived after the collapse of the primary.

5.2.2 M 82 X-1

M 82 X-1 is one of the most luminous ULXs and is the first source in which a QPO was detected. Our analysis of *XMM-Newton* and *RXTE* observations gives useful constraints to the mass of the BH hosted in this ULX.

We carefully subtracted the contribution of the galaxy contamination (obtained from the analysis of *Chandra* data) from the emission of the ULX and masked some of the nearby point-like sources. We found that a very soft thermal component is present in the *XMM-Newton* spectrum of M 82 X-1. Modeling it with a standard accretion disk would imply a black hole mass in the range $M_{BH} \approx [200 - 2000] f^4 M_\odot$.

The highest recorded luminosity emitted by M 82 X-1 is $L \sim 2 \times 10^{41}$ erg s^{-1} (assuming a distance of $D = 3.9$ Mpc). Making the assumption that, at maximum, the source emits at the Eddington limit, we can derive a rough estimate of the BH mass, $M_{BH} \sim 1500 M_\odot$. It is worth noticing that the high luminosity of this source is not easily explained invoking alternative anisotropic models.

The power density spectrum of the *XMM-Newton* observation shows a variable QPO at a frequency of 113 mHz with properties similar to those of the QPO discovered by Strohmayer & Mushotzky (2003). The QPO was also found in 7 archival *RXTE* observations. The frequency distribution of the centroids of the QPO detected

in the different observations is suggestive of a harmonic 1:2:3 ratio, although only one peak is visible in each observation. As far as the properties of the QPO are concerned, the similarities in fractional rms, variability, quality value, and underlying noise strongly suggest an association between the QPO in M 82 X-1 and the low-frequency, type-C QPOs observed in BHCs. Scaling the frequency inversely to the BH mass, the observed QPO frequency range (from 50 to 166 mHz) would yield M_{BH} anywhere in the interval 10 to 1000 $M_\odot$. Some arguments have been proposed to reduce the uncertainty on the determination of the mass of the compact object in M 82 X-1, using in particular the correlation between the spectral and timing properties observed in BHCs. It is tempting to conclude that a likely value for the mass of M 82 X-1 may be few hundreds solar masses.

5.3 Future perspectives

Recently, analyses of the X-ray and optical variability of ULXs, theoretical modeling of super-Eddington accretion flows, and statistical studies of the properties of ULXs and their environment have produced significant advances in this field. Despite this significant progress, our knowledge of ULXs is still far from being satisfactory.

The available X-ray and multiwavelength observations suggest that ULXs are a composite population, a significant fraction of which shows the properties of galactic accreting binaries. Discriminating between a binary system hosting a solar mass BH and one with an IMBH is an extremely challenging task. Marginal evidences supporting both these conclusions have been found but up to now there is still no a definitive proof of the existence (or not) of IMBHs.

In my opinion the properties of the majority of ULXs may be explained with the presence of a black hole of mass greater than $20M_\odot$ up to several tens $M_\odot$. Super-Eddington emission or beaming models account for some of the observational properties of ULXs, but the simplest scenario is still represented by the presence of such "small" intermediate mass black holes. Moreover it is very difficult to explain the brightest ULXs, such as M 82 X-1, as powered emission from a stellar mass black hole.

We are still at a stage when detailed studies of individual sources can provide invaluable information for understanding the properties of the whole class. A crucial development in this field will certainly come from the detailed spectroscopy observation of the few identified ULX optical counterparts, as the one of NGC 1313 X-2. These objects are massive, early type stars embedded in star-forming regions or regions of recent star formation. Monitoring their optical variability in association with the X-ray flux variations will allow us to discriminate between possible multiple associations. The identification of emission and/or absorption lines in the optical spectra of these stars held the promise to provide *dynamical measurement of the mass function of ULX binary systems* and, eventually, of the black hole mass. This represents the only unambiguous method to lead to the definitive answer to the existence of IMBHs in ULXs.

LIST OF ACRONYMS

ACIS	AXAF Charged Coupled Imaging Spectrometer
ACS	Advanced Camera for Surveys
ADAF	Advection Dominated Accretion Flow
AGN	Active Galactic Nucleus
ASCA	Advanced Satellite for Cosmology and Astrophysics
ATCA	Australia Telescope National Facility
AXAF	Advanced X-ray Astrophysics Facility
BB	Black Body
BH	Black Hole
BHC	Black Hole Candidate
CCD	Charged Coupled Device
CTE	Charge Transfer Efficiency
GBH	Galactic Black Hole
GC	Globular Cluster
HMXB	High Mass X-ray Binary
HRC	High Resolution Camera
HRI	High Resolution Imager
HSS	High Soft State
HST	Hubble Space Telescope
IMBH	Intermediate Mass Black Hole
IPC	Imaging Proportional Counter
IS	Intermediate State
LHS	Low Hard State
LLAGN	Low Luminosity AGN
LMXB	Low mass X-ray Binary
MC	Magellanic Cloud
MCD	Multi Color Disk
MOS	Metal Oxide Semi–conductor
MS	Main Sequence
NS	Neutron Star

OM	Optical Monitor
PDS	Power Density Spectrum
PL	Power Law
PSF	Point-Spread Function
QPO	Quasi-Periodic Oscillation
ROSAT	ROentgen SATellite
RXTE	Rossi X-ray Timing Explorer
SN	SuperNova
SNR	SuperNova Remnant
SSC	Super Star Cluster
ULX	Ultra-Luminous X-ray source
ULXN	ULX Nebula
UV	Ultra Violet
XIN	X-ray Ionized Nebula
XLF	X-ray Luminosity Function
XMM	X–Ray Multi–Mirror Mission
XMM SAS	XMM Standard Analysis System
XRB	X-ray Binary
WD	White Dwarf
VHS	Very-High State
VLT	Very Large Telescope
YSC	Young Stellar Cluster

REFERENCES

Abolmasov, P., Fabrika, S., Sholukhova, O., & Afanasiev, V., 2007, *Astrophysical Bulletin*, **62**, 36

Abramowicz, M. A., Czerny, B., Lasota, J. P., & Szuszkiewicz, E., 1988, *ApJ*, **332**, 646

Agrawal, V. K. & Misra, R., 2006, *ApJ*, **638**, L83

Angelini, L., Loewenstein, M., & Mushotzky, R. F., 2001, *ApJ*, **557**, L35

Bahcall, J. N. & Ostriker, J. P., 1975, *Nature*, **256**, 23

Bailyn, C. D., Jain, R. K., Coppi, P., & Orosz, J. A., 1998, *ApJ*, **499**, 367

Begelman, M. C., 2002, *ApJ*, **568**, L97

Begelman, M. C., Blandford, R. D., & Rees, M. J., 1984, *Reviews of Modern Physics*, **56**, 255

Begelman, M. C., King, A. R., & Pringle, J. E., 2006, *MNRAS*, **370**, 399

Belloni, T., Klein-Wolt, M., Méndez, M., van der Klis, M., & van Paradijs, J., 2000, *A&A*, **355**, 271

Belloni, T., Mendez, M., King, A. R., van der Klis, M., & van Paradijs, J., 1997, *ApJ*, **488**, L109

Belloni, T., Psaltis, D., & van der Klis, M., 2002, *ApJ*, **572**, 392

Bohlin, R. C., Savage, B. D., & Drake, J. F., 1978, *ApJ*, **224**, 132

Braddley, S., 1982, *Planet. Space Sci.*, **30**, 1077

Bregman, J. N., Houck, J. C., Chevalier, R. A., & Roberts, M. S., 2003, *ApJ*, **596**, 323

Brusa, M., Comastri, A., Daddi, E., Cimatti, A., Mignoli, M., & Pozzetti, L., 2002, *ApJ*, **581**, L89

Cagnoni, I., Elvis, M., Kim, D. W., Nicastro, F., & Celotti, A., 2002, *ApJ*, **579**, 148

Canizares, C. R., Kriss, G. A., & Feigelson, E. D., 1982, *ApJ*, **253**, L17

Cardelli, J. A., Clayton, G. C., & Mathis, J. S., 1989, *ApJ*, **345**, 245

Casella, P., Belloni, T., & Stella, L., 2005, *ApJ*, **629**, 403

Chevalier, R. A. & Fransson, C., 1994, *ApJ*, **420**, 268

Chevalier, R. A. & Fransson, C., 2003, in K. Weiler (ed.), *LNP Vol. 598: Supernovae and Gamma-Ray Bursters*, pp 171–194

Chiang, E. & Rappaport, S., 1996, *ApJ*, **469**, 255

Clark, D. M., Christopher, M. H., Eikenberry, S. S., Brandl, B. R., Wilson, J. C., Carson, J. C., Henderson, C. P., Hayward, T. L., Barry, D. J., Ptak, A. F., & Colbert, E. J. M., 2005, *ApJ*, **631**, L109

Clark, G., Doxsey, R., Li, F., Jernigan, J. G., & van Paradijs, J., 1978, *ApJ*, **221**, L37

Colbert, E. J. M. & Mushotzky, R. F., 1999, *American Astronomical Society Meeting*, **31**, 873

Colbert, E. J. M., Petre, R., Schlegel, E. M., & Ryder, S. D., 1995, *ApJ*, **446**, 177

Colbert, E. J. M. & Ptak, A. F., 2002, *ApJS*, **143**, 25

Copperwheat, C., Cropper, M., Soria, R., & Wu, K., 2005, *MNRAS*, **362**, 79

Cox, A. N., 2000, *Allen's astrophysical quantities*, Allen's astrophysical quantities, 4th ed. Publisher: New York: AIP Press; Springer, 2000. Editedy by Arthur N. Cox. ISBN: 0387987460

Cropper, M., Soria, R., Mushotzky, R. F., Wu, K., Markwardt, C. B., & Pakull, M., 2004, *MNRAS*, **349**, 39

Davis, D. S. & Mushotzky, R. F., 2004, *ApJ*, **604**, 653

Dewangan, G. C., Griffiths, R. E., & Rao, A. R., 2005, astro-ph/0511112

Dewangan, G. C., Griffiths, R. E., & Rao, A. R., 2006, *ApJ*, **641**, L125

Di Stefano, R. & Kong, A. K. H., 2003, *ApJ*, **592**, 884

Di Stefano, R., Paerels, F., & Rappaport, S., 1995, *ApJ*, **450**, 705

Done, C. & Kubota, A., 2006, *MNRAS*, **371**, 1216

Ebisawa, K., Kubota, A., Mizuno, T., & Zycki, P., 2001, in A. Gimenez, V. Reglero, and C. Winkler (eds.), *ESA SP-459: Exploring the Gamma-Ray Universe*, pp 415–418

Ebisawa, K., Życki, P., Kubota, A., Mizuno, T., & Watarai, K.-y., 2003, *ApJ*, **597**, 780

Fabbiano, G., 1989, *ARA&A*, **27**, 87

Fabbiano, G., 1995, *Normal galaxies and their X-ray binary populations*, pp 390–416, X-ray Binaries. Edited by W. H. G. Lewin, J. van Paradijs & E. P. J. van den Heuvel. Cambridge University Press, 1995 p. 390 - 416

Fabbiano, G., 2006, *ARA&A*, **44**, 323

Fabbiano, G., Kim, D.-W., Fragos, T., Kalogera, V., King, A. R., Angelini, L., Davies, R. L., Gallagher, J. S., Pellegrini, S., Trinchieri, G., Zepf, S. E., & Zezas, A., 2006, *ApJ*, **650**, 879

Fabbiano, G., Kim, D.-W., & Trinchieri, G., 1992, *ApJS*, **80**, 531

Fabbiano, G., King, A. R., Zezas, A., Ponman, T. J., Rots, A., & Schweizer, F., 2003a, *ApJ*, **591**, 843

Fabbiano, G. & Trinchieri, G., 1987, *ApJ*, **315**, 46

Fabbiano, G., Zezas, A., King, A. R., Ponman, T. J., Rots, A., & Schweizer, F., 2003b, *ApJ*, **584**, L5

Fabian, A. C. & Terlevich, R., 1996, *MNRAS*, **280**, L5

Fabrika, S., Karpov, S., Abolmasov, P., & Sholukhova, O., 2006, in E. J. A. Meurs and G. Fabbiano (eds.), *IAU Symposium*, pp 278–281

Fender, R. P., 2001, *MNRAS*, **322**, 31

Feng, H. & Kaaret, P., 2005, *ApJ*, **633**, 1052

Feng, H. & Kaaret, P., 2007a, *ApJ*, **668**, 941

Feng, H. & Kaaret, P., 2007b, *ApJ*, **660**, L113

Figer, D. F., Najarro, F., Morris, M., McLean, I. S., Geballe, T. R., Ghez, A. M., & Langer, N., 1998, *ApJ*, **506**, 384

Fiorito, R. & Titarchuk, L., 2004, *ApJ*, **614**, L113

Foschini, L., Di Cocco, G., Ho, L. C., Bassani, L., Cappi, M., Dadina, M., Gianotti, F., Malaguti, G., Panessa, F., Piconcelli, E., Stephen, J. B., & Trifoglio, M., 2002a, *A&A*, **392**, 817

Foschini, L., Ho, L. C., Masetti, N., Cappi, M., Dadina, M., Bassani, L., Malaguti, G., Palazzi, E., Di Cocco, G., Martini, P., Ravindranath, S., Stephen, J. B., Trifoglio, M., & Gianotti, F., 2002b, *A&A*, **396**, 787

Foschini, L., Rodriguez, J., Fuchs, Y., Ho, L. C., Dadina, M., Di Cocco, G., Courvoisier, T. J.-L., & Malaguti, G., 2004, *A&A*, **416**, 529

Frank, J., King, A., & Raine, D. J., 2002, *Accretion Power in Astrophysics: Third Edition*, Accretion Power in Astrophysics, by Juhan Frank and Andrew King and Derek Raine, pp. 398. ISBN 0521620538. Cambridge, UK: Cambridge University Press, February 2002.

Fryer, C. L., 1999, *ApJ*, **522**, 413

Georganopoulos, M., Aharonian, F. A., & Kirk, J. G., 2002, *A&A*, **388**, L25

Giacconi, R., Branduardi, G., Briel, U., Epstein, A., Fabricant, D., Feigelson, E., Forman, W., Gorenstein, P., Grindlay, J., Gursky, H., Harnden, F. R., Henry, J. P., Jones, C., Kellogg, E., Koch, D., Murray, S., Schreier, E., Seward, F., Tananbaum, H., Topka, K., Van Speybroeck, L., Holt, S. S., Becker, R. H., Boldt, E. A., Serlemitsos, P. J., Clark, G., Canizares, C., Markert, T., Novick, R., Helfand, D., & Long, K., 1979, *ApJ*, **230**, 540

Giacconi, R., Murray, S., Gursky, H., Kellogg, E., Schreier, E., & Tananbaum, H., 1972, *ApJ*, **178**, 281

Gilfanov, M., 2004, *MNRAS*, **349**, 146

Gilfanov, M., Grimm, H.-J., & Sunyaev, R., 2004, *Nuclear Physics B Proceedings Supplements*, **132**, 369

Goad, M. R., Roberts, T. P., Knigge, C., & Lira, P., 2002, *MNRAS*, **335**, L67

Goad, M. R., Roberts, T. P., Reeves, J. N., & Uttley, P., 2006, *MNRAS*, **365**, 191

Gonçalves, A. C. & Soria, R., 2006, *MNRAS*, **371**, 673

Greiner, J., Cuby, J. G., & McCaughrean, M. J., 2001, *Nature*, **414**, 522

Grimm, H.-J., Gilfanov, M., & Sunyaev, R., 2002, *A&A*, **391**, 923

Grimm, H.-J., Gilfanov, M., & Sunyaev, R., 2003, *MNRAS*, **339**, 793

Grimm, H.-J., McDowell, J., Zezas, A., Kim, D.-W., & Fabbiano, G., 2005, *ApJS*, **161**, 271

Hambly, N. C., Irwin, M. J., & MacGillivray, H. T., 2001, *MNRAS*, **326**, 1295

Heger, A., Fryer, C. L., Woosley, S. E., Langer, N., & Hartmann, D. H., 2003, *ApJ*, **591**, 288

Helfand, D. J. & Moran, E. C., 2001, *ApJ*, **554**, 27

Homan, J. & Belloni, T., 2005, *Ap&SS*, **300**, 107

Homan, J., Wijnands, R., van der Klis, M., Belloni, T., van Paradijs, J., Klein-Wolt, M., Fender, R., & Méndez, M., 2001, *ApJS*, **132**, 377

Humphrey, P. J., Fabbiano, G., Elvis, M., Church, M. J., & Bałucińska-Church, M., 2003, *MNRAS*, **344**, 134

Irwin, J. A., Athey, A. E., & Bregman, J. N., 2003, *ApJ*, **587**, 356

Irwin, J. A., Bregman, J. N., & Athey, A. E., 2004, *ApJ*, **601**, L143

Iwamoto, K., Mazzali, P. A., Nomoto, K., Umeda, H., Nakamura, T., Patat, F., Danziger, I. J., Young, T. R., Suzuki, T., Shigeyama, T., Augusteijn, T., Doublier, V., Gonzalez, J.-F., Boehnhardt, H., Brewer, J., Hainaut, O. R., Lidman, C., Leibundgut, B., Cappellaro, E., Turatto, M., Galama, T. J., Vreeswijk, P. M., Kouveliotou, C., van Paradijs, J., Pian, E., Palazzi, E., & Frontera, F., 1998, *Nature*, **395**, 672

Jedamzik, K., 1997, *Phys. Rev. D*, **55**, 5871

Jeltema, T. E., Canizares, C. R., Buote, D. A., & Garmire, G. P., 2003, *ApJ*, **585**, 756

Kaaret, P., 2002, *ApJ*, **578**, 114

Kaaret, P., Alonso-Herrero, A., Gallagher, J. S., Fabbiano, G., Zezas, A., & Rieke, M. J., 2004, *MNRAS*, **348**, L28

Kaaret, P., Corbel, S., Prestwich, A. H., & Zezas, A., 2003, *Science*, **299**, 365

Kaaret, P., Simet, M. G., & Lang, C. C., 2006a, *ApJ*, **646**, 174

Kaaret, P., Simet, M. G., & Lang, C. C., 2006b, *Science*, **311**, 491

Kaplan, D. L., Kulkarni, S. R., & van Kerkwijk, M. H., 2003, *ApJ*, **588**, L33

Kawaguchi, T., 2003, *ApJ*, **593**, 69

Kim, D.-W. & Fabbiano, G., 2004, *ApJ*, **611**, 846

King, A. R., 2002, *MNRAS*, **335**, L13

King, A. R., Davies, M. B., Ward, M. J., Fabbiano, G., & Elvis, M., 2001, *ApJ*, **552**, L109

King, A. R. & Pounds, K. A., 2003, *MNRAS*, **345**, 657

Kong, A. K. H. & Di Stefano, R., 2005, *ApJ*, **632**, L107

Kong, A. K. H., Garcia, M. R., Primini, F. A., Murray, S. S., Di Stefano, R., & McClintock, J. E., 2002, *ApJ*, **577**, 738

Körding, E., Colbert, E., & Falcke, H., 2005, *A&A*, **436**, 427

Körding, E., Falcke, H., & Markoff, S., 2002, *A&A*, **382**, L13

Krolik, J. H., 2004, *ApJ*, **615**, 383

Kubota, A. & Done, C., 2004, *MNRAS*, **353**, 980

Kubota, A., Done, C., & Makishima, K., 2002, *MNRAS*, **337**, L11

Kubota, A., Makishima, K., & Ebisawa, K., 2001a, *ApJ*, **560**, L147

Kubota, A., Mizuno, T., Makishima, K., Fukazawa, Y., Kotoku, J., Ohnishi, T., & Tashiro, M., 2001b, *ApJ*, **547**, L119

Kubota, A., Tanaka, Y., Makishima, K., Ueda, Y., Dotani, T., Inoue, H., & Yamaoka, K., 1998, *PASJ*, **50**, 667

La Parola, V., Peres, G., Fabbiano, G., Kim, D. W., & Bocchino, F., 2001, *ApJ*, **556**, 47

Lachowicz, P., Czerny, B., & Abramowicz, M. A., 2006, submitted MNRAS, astro-ph/0607594

Landolt, A. U., 1992, *AJ*, **104**, 340

Leahy, D. A., Darbro, W., Elsner, R. F., Weisskopf, M. C., Kahn, S., Sutherland, P. G., & Grindlay, J. E., 1983, *ApJ*, **266**, 160

Lightman, A. P. & Shapiro, S. L., 1977, *ApJ*, **211**, 244

Lira, P., Lawrence, A., & Johnson, R. A., 2000, *MNRAS*, **319**, 17

Liu, J.-F. & Bregman, J. N., 2005, *ApJS*, **157**, 59

Liu, J.-F., Bregman, J. N., Irwin, J., & Seitzer, P., 2002, *ApJ*, **581**, L93

Liu, J.-F., Bregman, J. N., Miller, J., & Kaaret, P., 2007, *ApJ*, **661**, 165

Liu, J.-F., Bregman, J. N., & Seitzer, P., 2004, *ApJ*, **602**, 249

Liu, J.-F., Bregman, J. N., Seitzer, P., & Irwin, J., 2005, astro-ph/0501310

Liu, Q. Z. & Mirabel, I. F., 2005, *A&A*, **429**, 1125

Long, K. S. & van Speybroeck, L. P., 1983, in W. H. G. Lewin and E. P. J. van den Heuvel (eds.), *Accretion-Driven Stellar X-ray Sources*, pp 117–146

Madau, P. & Rees, M. J., 2001, *ApJ*, **551**, L27

Makishima, K., Ebisuzaki, S., Kubota, A., Miyawaki, R., Mizuno, T., Namiki, M., Sugiho, M., Tanaka, T., & Tsunoda, N., 2004, in *Bulletin of the American Astronomical Society*, p. 750

Makishima, K., Kubota, A., Mizuno, T., Ohnishi, T., Tashiro, M., Aruga, Y., Asai, K., Dotani, T., Mitsuda, K., Ueda, Y., Uno, S., Yamaoka, K., Ebisawa, K., Kohmura, Y., & Okada, K., 2000, *ApJ*, **535**, 632

Markoff, S., Falcke, H., & Fender, R., 2001, *A&A*, **372**, L25

Masetti, N., Foschini, L., Ho, L. C., Dadina, M., Di Cocco, G., Malaguti, G., & Palazzi, E., 2003, *A&A*, **406**, L27

Matonick, D. M. & Fesen, R. A., 1997, *ApJS*, **112**, 49

Matsumoto, H., Tsuru, T. G., Koyama, K., Awaki, H., Canizares, C. R., Kawai, N., Matsushita, S., & Kawabe, R., 2001, *ApJ*, **547**, L25

Matsushita, S., Kawabe, R., Matsumoto, H., Tsuru, T. G., Kohno, K., Morita, K.-I., Okumura, S. K., & Vila-Vilaró, B., 2000, *ApJ*, **545**, L107

McClintock, J. E. & Remillard, R. A., 2006, *Black hole binaries*, pp 157–213, Compact stellar X-ray sources. Edited by Walter Lewin & Michiel van der Klis. Cambridge Astrophysics Series, No. 39. Cambridge, UK: Cambridge University Press, ISBN 978-0-521-82659-4, ISBN 0-521-82659-4, DOI: 10.2277/0521826594, 2006, p. 157 - 213

Miller, J. M., Fabbiano, G., Miller, M. C., & Fabian, A. C., 2003, *ApJ*, **585**, L37

Miller, J. M., Fabian, A. C., & Miller, M. C., 2004, *ApJ*, **614**, L117

Miller, M. C. & Colbert, E. J. M., 2004, *International Journal of Modern Physics D*, **13**, 1

Miller, N. A., Neff, S. G., & Mushotzky, R. F., 2005, in *X-Ray and Radio Connections (eds. L.O. Sjouwerman and K.K Dyer) Published electronically by NRAO, http://www.aoc.nrao.edu/events/xraydio Held 3-6 February 2004 in Santa Fe, New Mexico, USA, (E5.05) 4 pages*

Miller, S., Schlegel, E. M., Petre, R., & Colbert, E., 1998, *AJ*, **116**, 1657

Mineshige, S., Hirano, A., Kitamoto, S., Yamada, T. T., & Fukue, J., 1994, *ApJ*, **426**, 308

Mineshige, S. & Watarai, K.-Y., 2005, *Chinese Journal of Astronomy and Astrophysics*, **5**, 49

Mirabel, I. F. & Rodríguez, L. F., 1999, *ARA&A*, **37**, 409

Mitsuda, K., Inoue, H., Koyama, K., Makishima, K., Matsuoka, M., Ogawara, Y., Suzuki, K., Tanaka, Y., Shibazaki, N., & Hirano, T., 1984, *PASJ*, **36**, 741

Mizuno, T., Ohnishi, T., Kubota, A., Makishima, K., & Tashiro, M., 1999, *Astronomische Nachrichten*, **320**, 356

Morgan, E. H., Remillard, R. A., & Greiner, J., 1997, *ApJ*, **482**, 993

Mucciarelli, P., Casella, P., Belloni, T., Zampieri, L., & Ranalli, P., 2006, *MNRAS*, **365**, 1123

Mucciarelli, P., Zampieri, L., Falomo, R., Turolla, R., & Treves, A., 2005, *ApJ*, **633**, L101

Mucciarelli, P., Zampieri, L., Treves, A., Turolla, R., & Falomo, R., 2007, *ApJ*, **658**, 999

Mukai, K., Pence, W. D., Snowden, S. L., & Kuntz, K. D., 2003, *ApJ*, **582**, 184

Mushotzky, R., 2004, *Progress of Theoretical Physics Supplement*, **155**, 27

Niemeyer, J. C. & Jedamzik, K., 1999, *Phys. Rev. D*, **59(12)**, 124013

Origlia, L., Ranalli, P., Comastri, A., & Maiolino, R., 2004, *ApJ*, **606**, 862

Pakull, M. W., Grisé, F., & Motch, C., 2006, in E. J. A. Meurs and G. Fabbiano (eds.), *IAU Symposium*, pp 293–297

Pakull, M. W. & Mirioni, L., 2002, astro-ph/0202488

Pakull, M. W. & Mirioni, L., 2003, in J. Arthur and W. J. Henney (eds.), *Revista Mexicana de Astronomia y Astrofisica Conference Series*, pp 197–199

Palumbo, G. G. C., Maccacaro, T., Zamorani, G., Panagia, N., & Vettolani, G., 1981, *ApJ*, **247**, 484

Patat, F., 2003, *A&A*, **400**, 1183

Patruno, A., Portegies Zwart, S., Dewi, J., & Hopman, C., 2006, *MNRAS*, **370**, L6

Perna, R. & Stella, L., 2004, *ApJ*, **615**, 222

Peterson, B. M., 1997, *An Introduction to Active Galactic Nuclei*, An introduction to active galactic nuclei, Publisher: Cambridge, New York Cambridge University Press, 1997 Physical description xvi, 238 p. ISBN 0521473489

Petre, R., Okada, K., Mihara, T., Makishima, K., & Colbert, E. J. M., 1994, *PASJ*, **46**, L115

Portegies Zwart, S. F., Baumgardt, H., Hut, P., Makino, J., & McMillan, S. L. W., 2004, *Nature*, **428**, 724

Portegies Zwart, S. F., Makino, J., McMillan, S. L. W., & Hut, P., 1999, *A&A*, **348**, 117

Portegies Zwart, S. F. & McMillan, S. L. W., 2002, *ApJ*, **576**, 899

Quinlan, G. D. & Shapiro, S. L., 1987, *ApJ*, **321**, 199

Ramsey, C. J., Williams, R. M., Gruendl, R. A., Chen, C.-H. R., Chu, Y.-H., & Wang, Q. D., 2006, *ApJ*, **641**, 241

Ranalli, P., Comastri, A., Origlia, L., & Maiolino, R., 2008, *MNRAS*, **386**, 1464

Remillard, R. A., Muno, M. P., McClintock, J. E., & Orosz, J. A., 2002a, *ApJ*, **580**, 1030

Remillard, R. A., Sobczak, G. J., Muno, M. P., & McClintock, J. E., 2002b, *ApJ*, **564**, 962

Roberts, T. P. & Colbert, E. J. M., 2003, *MNRAS*, **341**, L49

Roberts, T. P., Goad, M. R., Ward, M. J., Warwick, R. S., & Lira, P., 2002, astro-ph/0202017

Roberts, T. P., Goad, M. R., Ward, M. J., Warwick, R. S., O'Brien, P. T., Lira, P., & Hands, A. D. P., 2001, *MNRAS*, **325**, L7

Roberts, T. P., Kilgard, R. E., Warwick, R. S., Goad, M. R., & Ward, M. J., 2006, *MNRAS*, **371**, 1877

Roberts, T. P. & Warwick, R. S., 2000, *MNRAS*, **315**, 98

Ryder, S., Staveley-Smith, L., Dopita, M., Petre, R., Colbert, E., Malin, D., & Schlegel, E., 1993, *ApJ*, **416**, 167

Sakai, S. & Madore, B. F., 1999, *ApJ*, **526**, 599

Sánchez-Sutil, J. R., Muñoz-Arjonilla, A. J., Martí, J., Garrido, J. L., Pérez-Ramírez, D., & Luque-Escamilla, P., 2006, *A&A*, **452**, 739

Sarazin, C. L., Irwin, J. A., & Bregman, J. N., 2000, *ApJ*, **544**, L101

Schlegel, E. M., Petre, R., Colbert, E. J. M., & Miller, S., 2000, *AJ*, **120**, 2373

Schwarzschild, M. & Härm, R., 1959, *ApJ*, **129**, 637

Shakura, N. I. & Sunyaev, R. A., 1973, *A&A*, **24**, 337

Shimura, T. & Takahara, F., 1995, *ApJ*, **445**, 780

Sirianni, M., Jee, M. J., Benítez, N., Blakeslee, J. P., Martel, A. R., Meurer, G., Clampin, M., De Marchi, G., Ford, H. C., Gilliland, R., Hartig, G. F., Illingworth, G. D., Mack, J., & McCann, W. J., 2005, *PASP*, **117**, 1049

Snowden, S. L., 2002, astro-ph/0203311

Soria, R., 2007, in V. Karas and G. Matt (eds.), *IAU Symposium*, Vol. 238 of *IAU Symposium*, pp 235–240

Soria, R., Cropper, M., Pakull, M., Mushotzky, R., & Wu, K., 2005, *MNRAS*, **356**, 12

Soria, R. & Kong, A. K. H., 2002, *ApJ*, **572**, L33

Soria, R., Kuncic, Z., Broderick, J. W., & Ryder, S. D., 2006, *MNRAS*, **370**, 1666

Soria, R. & Wu, K., 2003, *A&A*, **410**, 53

Stevens, I. R., Read, A. M., & Bravo-Guerrero, J., 2003, *MNRAS*, **343**, L47

Stobbart, A.-M., Roberts, T. P., & Wilms, J., 2006, *MNRAS*, **368**, 397

Stocke, J. T., Wang, Q. D., Perlman, E. S., Donahue, M. E., & Schachter, J. F., 1995, *AJ*, **109**, 1199

Strickland, D. K., Colbert, E. J. M., Heckman, T. M., Weaver, K. A., Dahlem, M., & Stevens, I. R., 2001, *ApJ*, **560**, 707

Strohmayer, T. E., 2001a, *ApJ*, **552**, L49

Strohmayer, T. E., 2001b, *ApJ*, **554**, L169

Strohmayer, T. E. & Mushotzky, R. F., 2003, *ApJ*, **586**, L61

Strohmayer, T. E., Mushotzky, R. F., Winter, L., Soria, R., Uttley, P., & Cropper, M., 2007, *ApJ*, **660**, 580

Swartz, D. A., Ghosh, K. K., McCollough, M. L., Pannuti, T. G., Tennant, A. F., & Wu, K., 2003, *ApJS*, **144**, 213

Swartz, D. A., Ghosh, K. K., Tennant, A. F., & Wu, K., 2004, *ApJS*, **154**, 519

Terashima, Y. & Wilson, A. S., 2004, *ApJ*, **601**, 735

Tully, R. B., 1988, *Science*, **242**, 310

Turolla, R., Mucciarelli, P., Zampieri, L., Falomo, R., Kaaret, P., di Stefano, R., Chieregato, M., & Treves, A., 2004, in *35th COSPAR Scientific Assembly*, p. 3749

van der Klis, M., 1998, in R. Buccheri, J. van Paradijs, and A. Alpar (eds.), *NATO ASIC Proc. 515: The Many Faces of Neutron Stars.*, p. 337

van der Klis, M., 2006, *Rapid X-ray Variability*, pp 39–112, Compact stellar X-ray sources. Edited by Walter Lewin & Michiel van der Klis. Cambridge Astrophysics Series, No. 39. Cambridge, UK: Cambridge University Press, ISBN 978-0-521-82659-4, ISBN 0-521-82659-4, DOI: 10.2277/0521826594, 2006, p. 39 - 112

van der Marel, R. P., 2004, in L. C. Ho (ed.), *Coevolution of Black Holes and Galaxies*, p. 37

Vignarca, F., Migliari, S., Belloni, T., Psaltis, D., & van der Klis, M., 2003, *A&A*, **397**, 729

Watarai, K.-y., Mizuno, T., & Mineshige, S., 2001, *ApJ*, **549**, L77

Winter, L. M., R. F. Mushotzky Collaboration, & C. S. Reynolds Collaboration, 2005, in *Bulletin of the American Astronomical Society*, p. 1318

Wolter, A. & Trinchieri, G., 2004, *A&A*, **426**, 787

Wood, K. S., Meekins, J. F., Yentis, D. J., Smathers, H. W., McNutt, D. P., Bleach, R. D., Friedman, H., Byram, E. T., Chubb, T. A., & Meidav, M., 1984, *ApJS*, **56**, 507

Woosley, S. E. & Weaver, T. A., 1995, *ApJS*, **101**, 181

Wu, H., Xue, S. J., Xia, X. Y., Deng, Z. G., & Mao, S., 2002, *ApJ*, **576**, 738

Zampieri, L., Mucciarelli, P., Falomo, R., Kaaret, P., Di Stefano, R., Turolla, R., Chieregato, M., & Treves, A., 2004, *ApJ*, **603**, 523

Zampieri, L., Mucciarelli, P., Pastorello, A., Turatto, M., Cappellaro, E., & Benetti, S., 2005, *MNRAS*, **364**, 1419

Zampieri, L., Turolla, R., & Szuszkiewicz, E., 2001, *MNRAS*, **325**, 1266

Zaritsky, D., Kennicutt, Jr., R. C., & Huchra, J. P., 1994, *ApJ*, **420**, 87

Zdziarski, A. A., Johnson, W. N., & Magdziarz, P., 1996, *MNRAS*, **283**, 193

Zezas, A. & Fabbiano, G., 2002, *ApJ*, **577**, 726

Życki, P. T., Done, C., & Smith, D. A., 1999, *MNRAS*, **309**, 561

Acknowledgement

This Thesis is based on observations obtained with:

ROSAT, ASCA and RossiXTE satellites. The data were obtained from the High Energy Astrophysics Science Archive Research Center (HEASARC), provided by NASA's Goddard Space Flight Center;

XMM-Newton , an ESA science mission with instruments and contributions directly funded by ESA Member States and NASA;

NASA/ESA Hubble Space Telescope . The data were obtained from the data archive at the Space Telescope Institute. STScI is operated by the association of Universities for Research in Astronomy, Inc. under the NASA contract NAS 5-26555;

ESO 3.6m telescope at the La Silla Observatories under programme ID 68.B-0083;

ESO VLT telescope at the Paranal Observatories (archival data).

I analyzed the X-ray and optical data using dedicated software:

XMM-SAS XMM-Newton Science Analysis System;

Xspec an X-Ray Spectral Fitting Package;

CIAO Chandra Interactive Analysis of Observations. This software is provided by the Chandra X-ray Center (CXC);

IRAF is distributed by the National Optical Astronomy Observatories, which are operated by the Association of Universities for Research in Astronomy, Inc., under cooperative agreement with the National Science Foundation.

I would like to thank all the people that supported and collaborated with me during the PhD years:

- my supervisors: Luca Zampieri, for his constant support and his constant patience; Roberto Turolla for his precious collaboration; Alberto Franceschini, for following my PhD path;

- the referee of my Thesis, Professor Pepi Fabbiano, for useful comments that improved the robustness of the analysis;

- Aldo Treves for useful discussion and suggestion in all our collaboration;

- Marina Orio, for giving me the opportunity of a wonderful research period in Madison (WI) and Roberto that lent me his room;

- Jay Gallagher for the courage to put a telescope in my hands;

- Renato Falomo for helping an X-ray astronomer to understand optical data;

- the Padova-Asiago Supernova Group (in particular Andrea Pastorello) for providing us the ESO image of SN 1978K;

- Phil Kaaret and Rosanne di Stefano for providing us the *Chandra* position of NGC 1313 X-2.

The first thank is due to Ste, that lived with me all my crises, the second to Morgan that endured all them from his first second in this world (poor baby!!!).

A special hug to my family, unfortunately far away, Piero and in particular Marty (+Gabriele), that made to us the wonderful gift of the new life of Brando.

Thanks to Angela and Gian Luigi: they always said that they want to spend their time with Morgan, giving to me a very practical help.

To all my friends that meet me only once a year because of: thesis, moving, family and so on. I'M BACK (in Garching ;))))!

CURRICULUM VITAE ET STUDIORUM

Personal Information

First-Name:	Paola
Family Name:	Mucciarelli
Place of birth:	Montepulciano (Italy)
Date of birth:	03/03/1972
Nationality:	Italian
Affiliation:	Department of Astronomy, University of Padova
	INAF-Astronomical Observatory of Padova, Italy
Address:	Rathausplatz 15
	85748 Garching bei Muenchen
	Germany
E-mail:	paola.mucciarelli@oapd.inaf.it
	paola.mucciarelli@gmail.com

Education and Career Path:

2004–07/2008

PhD course at Astronomy Department of Padova (XIX cycle). Supervisors Prof. A. Franceschini and Dott. L. Zampieri (admission competition based on qualifications and oral examination).

22/07/2002

Graduate degree in Astronomy. Title of Laurea thesis: "X-ray cosmic background and absorbed AGN: tests and observational models". Supervisor Prof. A. Franceschini: 101/110

Languages

Italian: mother tongue;
English: good (reading, writing, speaking);
French: very basic (reading, speaking).

Research Grants

October 2006 - September 2007

Research grant on "**X-ray data analysis of ultraluminous sources**" at the Department of Astronomy, University of Padova, Italy. Supervisors Dott. L. Zampieri

February 2006 - August 2006

Research grant on "**X-ray source populations at optical and X-ray**" at the Department of Astronomy, University of Wisconsin (Madison WI, US). Supervisors Prof. J.S. III Gallagher and Dott.ssa M. Orio

June. 2005 - January 2006

Research grant on "**Observational properties of Ultraluminous sources**" at the Department of Physics, University of Padova (PRIN-2004-023189, research program "New vistas on the Astrophysics of Neutron Stars and Black Holes"). Supervisor Prof. R. Turolla and Dott. L. Zampieri

Nov. 2003 - Dec. 2004

Research grant on "**Astrophysics of X-ray compact sources**" at the INAF-Astronomical Observatory of Padova (COFIN-2002-027145, research program "Spectral properties and variability of Black Holes and Neutron Stars"). Supervisor Dott. L. Zampieri

Sept. - Dec. 2002

Research grant on "**Multiband data reduction and spectral analysis of X-ray point-like sources in nearby galaxies**" at the INAF-Astronomical Observatory of Padova and SISSA of Trieste (COFIN-2000-MM02C71842, research program "Astrophysics of Neutron Stars and Black Holes"). Supervisor Dott. L. Zampieri

Data reduction expertise

- Cleaning and extraction of X-ray data, images, spectra and light curves, of data from XMM-Newton, Chandra, ASCA and ROSAT X-ray observatories using the dedicated software (XMM-SAS, CIAO and Ftools respectively).

- Analysis of X-ray spectra of extragalactic sources (Lockman Hole field) observed with XMM-Newton. Brief analysis of spectral energy distributions (SEDs) extended from IR to X-ray.

- Analysis of X-ray archival data, images, spectra and lightcurves (timing), of Ultraluminous X-ray Sources (ULXs) observed with Chandra, XMM-Newton, ASCA and ROSAT. The analysis was performed using the XANADU packages, mainly XSPEC and XRONOS.

- Analysis of X-ray data, spectra and lightcurves, of Supernovae interacting with the circumstellar medium, observed in X-rays.

- Reduction and analysis of optical broad band images and spectra (ESO 3.6m, VLT and HST) of the faint optical counterparts of ULXs. I worked on both proprietary and archival data using standard IRAF (or PyRAF) tasks.

- Cross-correlation of X-ray, radio and optical catalogs. Implementation of procedures to obtain accurate astrometric calibration of optical images using IRAF and the Terapix software (in particular the packages SExtractor, SCAMP and SWarp).

Observational experience

I have used some of the facilities hosted at the Kitt Peak National Observatory (AZ, US) to observe dwarf and nearby galaxies, in order to study their stellar population and evolution. In particular I have observed with:

- 2.1m+GoldCam Spectrometer (slit spectroscopy);

- WIYN 3.5m(Bench Spectrograph)+SparsePak (multifiber spectroscopy);

- WIYN 0.9m+S2KB (imaging).

Informatics knowledge

Operating systems
UNIX, Linux and Windows

X-ray Astronomical Data reduction and analysis packages:
XMM-SAS, Ftools and XANADU, CIAO basics

Optical Astronomical Data reduction packages:
IRAF, PyRAF and Terapix

Programming languages
Super Mongo, basic Fortran and basic Python

Word processing
Latex, OpenOffice and Microsoft Word/PowerPoint

Workshops Participation

208 AAS meeting
Calgary, Canada, 4-8 June 2006. Poster presentation: "X-ray and optical variability of the ULX NGC 1313 X-2"

IV Italian Compact Objects Meeting
Padova, Italy, 23 - 25 November 2005. Oral presentation: "New results on the ULXs NGC1313 X-2 and M82 X-1"; participation as LOC member

MODEST6
Evanston, United States, 29 - 31 August 2005. Oral presentation: "The Ultraluminous X-ray source NGC 1313 X-2"

High Energies in the Highlands
Fort William, Scotland, 27 June - 1 July 2005. Oral presentation: "Ultraluminous X-ray sources: highlights on NGC1313 X-2 and M82 X-1"

1604 - 2004 Supernovae As Cosmological Lighthouses
Padova, Italy, 16 - 19 June 2004. Poster presentation: "XMM-Newton observation of SN 1995N"

III Italian Compact Objects Meeting
Roma, Italy, 9 - 11 December 2003. Oral presentation: "XMM-Newton, Chandra and optical observation of the ULX NGC1313 X-2: a luminous X-ray binary in NGC1313 with an intermediate mass black hole?"

XXI Symposium on Relativistic Astrophysics
>Firenze, Italy, 9 - 13 December 2002. Poster presentations: "The Nature of Ultraluminous X-ray sources: unveiling the mystery of NGC1313 X-2 (MS 0317.7-6647)";"Nature of X-ray Sources of the Lockman Hole Field"

5th Italian AGN Meeting
>Como, Italy, 11 - 14 June 2002. Poster presentation: "Nature of X-ray sources in the Lockman Hole Field: X-ray spectroscopy and analysis of the IR/optical/X-ray spectral energy distributions"

Schools Participation

RTN Winter School 2005: Supernova observations and data reduction
>7 - 11 February 2005, Asiago (Italy);

Cosmological Parameters - Extrasolar Planets
>IV Course of the Italian School of Astrophysics, Cycle VII, 2003-2004, 5 - 11 September 2004, Asiago (Italy);

3rd VILSPA SAS Workshop
>8 -10 October, Madrid (Spain);

Interstellar Medium - Pulsars and Compact Objects
>II Course of the Italian School of Astrophysics, Cycle VII, 2003-2004, 27 September - 3 October 2003, Cagliari (Italy);

Galaxies of the Local Group - New Generation Telescopes
>I Course of the Italian School of Astrophysics, Cycle VII, 2003-2004, 11 - 17 May 2003, Marciana Marina (Italy);

Cosmology - Relativistic Astrophysics
>IV Course of the Italian School of Astrophysics, Cycle VI, 2001-2002, 8 - 14 September 2002, Asiago (Italy).

LIST OF PUBLICATIONS

On Refereed Journals

[1] *The Ultraluminous X-ray source NGC 1313 X-2 (MS 0317.7-6647) and its environment*
Zampieri L., **Mucciarelli P.**, Falomo R., Kaaret P., Di Stefano R., Turolla R., Chieregato M. & Treves A., 2004, ApJ, 603, 523

[2] *Optical countepart of the Ultraluminous X-ray source NGC 1313 X-2*
Zampieri L., **Mucciarelli P.**, Falomo R., Kaaret P., Di Stefano R., Turolla R., Chieregato M. & Treves A., 2004, NuPhS, 132, 387

[3] *VLT Observations of the Ultraluminous X-ray source NGC 1313 X-2*
Mucciarelli P., Zampieri L., Falomo R., Turolla R. & Treves A., 2005, ApJL, 633, 101

[4] *Simultaneous XMM-Newton and ESO VLT observations of supernova 1995N: probing the wind-ejecta interaction*
Zampieri L., **Mucciarelli P.**, Pastorello A., Turatto M., Cappellaro E, & Benetti S., 2005, MNRAS, 364, 1419

[5] *The Ultraluminous X-ray Sources NGC1313 X-1 and X-2*
Turolla, R., **Mucciarelli P.**, Zampieri, L., Falomo, R., Chieregato M. & Treves A., 2006, AdSpR, 38, 1374

[6] *A variable Quasi-Periodic Oscillation in M82 X-1. Timing and spectral analysis of XMM-Newton and RossiXTE observations*
Mucciarelli P., Casella P., Belloni T., Zampieri L. & Ranalli P., 2006, MNRAS, 365, 1123

[7] *X-ray and optical variability of the ultraluminous X-ray source NGC 1313 X-2*
Mucciarelli P., Zampieri L., Treves A., Turolla R. & Falomo R., 2006, ApJ, 658, 999

[8] *X-ray Spectroscopy of the 2006 Outburst of RS Oph*
Nelson T., Orio M., Cassinelli J.P., Still M., Leibowitz E. & **Mucciarelli P.**, 2008, ApJ, 673, 1097

On Proceedings

[1] *Nature of X-ray sources in the Lockman Hole field: X-ray spectroscopy and analysis of the IR/optical/X-ray spectral energy distribution*
Mucciarelli P., Braito V., Franceschini A. & Fadda D., in "Inflows, outflows, and reprocessing around black holes", proceedings of the 5th Italian AGN Meeting, Como, June 11-14, 2002. Edited by I. Cagnoni. http://www.unico.it/ilaria/AGNS/proceedings.html

[2] *X-ray Emission Lines in ULXs:?*
Mucciarelli P., Zampieri, L., Turolla, R., & Treves, A., in prooceedings of "48 Congress of Italian Astronomical Society: The colors of the Univers - Italian Astronomy from ground and from space" (19 - 23 April 2004), electronic published proceedings in MSAIS, Ed. A. Wolter, G. Israel and F. Bacciotti

[3] *XMM-Newton XMM-Newton Detects the Beginning of the X-ray Decline of SN 1995N*
Mucciarelli P., Zampieri L., Pastorello A.,in proceedings of the International Conference "1604 - 2004 Supernovae As Cosmological Lighthouses" (16-19 June 2004, Padova), Ed. Turatto, Zampieri, Benetti & Shea, ASP Conf. Series

[4] *Spectroscopic and photometric observations of SN IIn 1995N and energy estimates*
Pastorello A., Aretxaga I., Zampieri L.,**Mucciarelli P.** & Benetti S., in proceedings of the International Conference "1604 - 2004 Supernovae As Cosmological Lighthouses" (16-19 June 2004, Padova), Ed. Turatto, Zampieri, Benetti & Shea, ASP Conf. Series

[5] *XMM-Newton and VLT observations of SN 1995N*
Mucciarelli P., Zampieri, L., Pastorello A., Turatto M., Cappellaro E., & Benetti S., in prooceedings of "49 Congress of Italian Astronomical Society" (2-7 May 2005, Catania, Italy), 2006, MSAIS, 9, 391

[6] *Ultraluminous X-ray sources in nearby galaxies: clues on their nature from X-ray timing and new optical data*
Zampieri, L.,**Mucciarelli**, P., Falomo, R., Casella, P., Belloni, T., Turolla, R., Treves, A., Ranalli, P., in proceedings of the "The X-ray Universe 2005", 26-30 September 2005, El Escorial, Madrid, Spain. Ed. by A. Wilson. ESA SP-604, Volume 1, Noordwijk: ESA Publications Division, 2006, p.189

[7] *X-ray And Optical Variability Of The Ultraluminous X-ray Source NGC 1313 X-2*
Mucciarelli, P., Zampieri, L., Treves, A., Turolla, R. & Falomo, R. 2006, AAS, 208, #50.04

[8] *A Deep HST Survey of the Prototypical Spiral Galaxy M81*
Zezas A., Gallagher J.S.III & **Mucciarelli**, P., 2006, AAS, 209, #04.01

[9] *X-ray grating spectra of RS Ophiuchi in outburst*
Orio M., Nelson T., Leibowitz E., Gonzalez-Riestra R. & **Mucciarelli P.**, in "The multicolored landscape of compact objects and their explosive origins" AIP Conference Proceedings, Volume 924, pp. 540-545 (2007)